Report Prepared by:
Dr. Francisco J. Presuel–Moreno
With
Ingrid Santillan

Final Report

Investigation into the Contributing Factors to the Corrosion of Steel Reinforced Concrete Structures at Elevations Greater than 12 Feet above the Mean High-Water Line

BDV27–977–18

Submitted to
Florida Department of Transportation
Research Center
605 Suwannee Street
Tallahassee, Florida 32399

Submitted by
Francisco Presuel–Moreno
Principal Investigator
Department of Ocean and Mechanical Engineering
Center for Marine Materials
Florida Atlantic University – Sea Tech

101 North Beach Road
Dania Beach, Florida 33004

January 2023

Disclaimer

The opinions, findings, and conclusions expressed in this publication are those of the author and not necessarily those of the State of Florida Department of Transportation.

Units Conversion Page

APPROXIMATE CONVERSIONS TO SI UNITS				
Symbol	**When You Know**	**Multiply By**	**To Find**	**Symbol**
		LENGTH		
in	inches	25.4	millimeters	mm
ft	feet	0.305	meters	m
yd	yards	0.914	meters	m
mi	miles	1.61	kilometers	km
		AREA		
in^2	square inches	645.2	square millimeters	mm^2
ft^2	square feet	0.093	square meters	m^2
yd^2	square yard	0.836	square meters	m^2
ac	acres	0.405	hectares	ha
mi^2	square miles	2.59	square kilometers	km^2
		VOLUME		
fl oz	fluid ounces	29.57	milliliters	mL
gal	gallons	3.785	liters	L
ft^3	cubic feet	0.028	cubic meters	m^3
yd^3	cubic yards	0.765	cubic meters	m^3
		NOTE: volumes greater than 1000 L shall be shown in m^3		
		MASS		
oz	ounces	28.35	grams	g
lb	pounds	0.454	kilograms	kg
T	short tons (2000 lb)	0.907	megagrams (or "metric ton")	Mg (or "t")
		TEMPERATURE (exact degrees)		
^oF	Fahrenheit	5 (F-32)/9 or (F-32)/1.8	Celsius	^oC
		ILLUMINATION		
fc	foot-candles	10.76	lux	lx
fl	foot-Lamberts	3.426	$candela/m^2$	cd/m^2
		FORCE and PRESSURE or STRESS		
lbf	poundforce	4.45	newtons	N
lbf/in^2	poundforce per square inch	6.89	kilopascals	kPa

APPROXIMATE CONVERSIONS FROM SI UNITS				
Symbol	**When You Know**	**Multiply By**	**To Find**	**Symbol**
		LENGTH		
mm	millimeters	0.039	inches	in
m	meters	3.28	feet	ft
m	meters	1.09	yards	yd
km	kilometers	0.621	miles	mi
		AREA		
mm^2	square millimeters	0.0016	square inches	in^2
m^2	square meters	10.764	square feet	ft^2
m^2	square meters	1.195	square yards	yd^2
ha	hectares	2.47	acres	ac
km^2	square kilometers	0.386	square miles	mi^2
		VOLUME		
mL	milliliters	0.034	fluid ounces	fl oz
L	liters	0.264	gallons	gal
m^3	cubic meters	35.314	cubic feet	ft^3
m^3	cubic meters	1.307	cubic yards	yd^3
		MASS		
g	grams	0.035	ounces	oz
kg	kilograms	2.202	pounds	lb
Mg (or "t")	megagrams (or "metric ton")	1.103	short tons (2000 lb)	T
		TEMPERATURE (exact degrees)		
^oC	Celsius	1.8C+32	Fahrenheit	^oF
		ILLUMINATION		
lx	lux	0.0929	foot-candles	fc
cd/m^2	$candela/m^2$	0.2919	foot-Lamberts	fl
		FORCE and PRESSURE or STRESS		
N	newtons	0.225	poundforce	lbf
kPa	kilopascals	0.145	poundforce per square inch	lbf/in^2

*SI is the symbol for the International System of Units. Appropriate rounding should be made to comply with Section 4 of ASTM E380.
(Revised March 2003)

Technical Report Documentation Page

1. Report No.	2. Government Accession No.	3. Recipient's Catalog No.
4. Title and Subtitle Investigation into the Contributing Factors to the Corrosion of Steel Reinforced Concrete Structures at Elevations Greater than 12 Feet above the Mean High-Water Line		5. Report Date January 2023 6. Performing Organization Code FAU–OE-cmM–08–3
7. Author(s) Francisco J. Presuel–Moreno, Ingrid Santillan.		8. Performing Organization Report No. BDV27–977–18
9. Performing Organization Name and Address Center for Marine Materials Florida Atlantic University – SeaTech 101 North Beach Road Dania Beach, Florida 33004		10. Work Unit No. (TRAIS) 11. Contract or Grant No. BDV27–977–18
12. Sponsoring Agency Name and Address Florida Department of Transportation 605 Suwannee Street, MS 30 Tallahassee, FL 32399		13. Type of Report and Period Covered Final Report February 21, 2020 – January 25, 2023 14. Sponsoring Agency Code
15. Supplementary Notes		

16. Abstract

The main objective of this project was to gain a better understanding and insight as to why corrosion takes place at elevations higher than 12 feet above the mean high-water line (>MHWL+12) for tall components that are part of the substructure (piles, columns, footers) of bridges that are partially immersed. There are several factors that influence corrosion initiation at these elevations.

Proximity to the ocean, the predominant wind direction, and wind speed affect the amount of ocean spray that reaches the structure at these elevations. The duration of wind events with wind speed greater than or equal to 3 m/s has been reported (by Meira and others) as an important parameter that varies by location and season (and from year to year). For example, during the monitored period, there were a few instances in which the measured chloride deposition was significantly larger, and the magnitude of the chloride deposition measured was different from year to year, as well as during a given year. The months in which the deposition was larger appear to coincide with the months that had the larger number of hours per month in which the wind was ≥ 3 m/s based on measurements made at weather stations close to the sites where the wet candles were deployed.

The geometry and orientation of the structure, as well as the surrounding detailing of the structure, can also play a significant role, particularly when the wind reaches a turbulent flow. The chlorides could reach inner columns that later are not wetted during rain events, but still exposed to high humidity for extended periods of time. The wind direction and rain intensity during rain events would dictate when and how much of the chlorides are washed out from the surface of outer elements.

Regarding whether similar corrosion damage can be anticipated on similar structures around the state, the answer is yes, particularly for older structures with no supplementary cementitious materials, with geometry and environments that allow a macroclimate where chloride deposition can be expected at high elevations. (The microclimate surrounding these structures is also important). For structures with supplementary cementitious materials in the concrete composition, the time to corrosion initiation is expected that to be longer than for structures built with ordinary portland cement (OPC) only, based on the apparent diffusion coefficient (D_{app}) values observed from profiles obtained on the outdoor samples and profiles corresponding to field cores. However, given enough time, corrosion could take place at elevations higher than 12 ft above the mean high-water line (>MHWL+12) when the chloride concentration at rebar depth exceeds the chloride threshold. Corrosion is still expected to initiate first at the splash zone.

17. Key Word	18. Distribution Statement		
Reinforced Concrete, Chloride Diffusion, Chloride Deposition, Mean High Water Line, Exposure Time.			
19. Security Classif. (of this report) Unclassified	20. Security Classif. (of this page) Unclassified	21. No. of Pages 142	22. Price

Form DOT F 1700.7 (8–72) Reproduction of completed page authorized

Acknowledgments

The author is indebted to the FDOT State Materials Office (SMO) for assistance during the field visits for this study, in particular, Mr. Rodrigo Antunes, Mr. Shannon Deese and Mr. Ronald Simmons, and several other SMO staff (Dennis Baldi, Kye Dittman). The author also acknowledges the assistance of several students who worked as graduate/undergraduate research assistants at FAU–SeaTech marine materials and corrosion lab during the duration of this project.

Executive Summary

The main objective of the project was to gain a better understanding and insight as to why corrosion takes place at elevations higher than 12 feet above the mean high-water line for tall components that are part of the substructure (piles, columns, footers) of bridges that are partially immersed. There are several factors that influence corrosion initiation at these elevations.

Proximity to the ocean, the predominant wind directions and wind speed (as well as for persistent periods of time) affect the amount of ocean spray that reach the structure at these elevations. The duration of wind events with wind speeds greater or equal than 3 m/s has been reported (by Meira and others) as an important parameter that varies by location and season (and from year to year). For example, during the monitored period, there were a few instances in which the measured chloride deposition was significantly larger, and the magnitude of the chloride deposition measured was different from year to year, as well as during a given year. The months in which the deposition was larger appear to coincide with the months that had the larger number of hours per month in which the wind was ≥ 3 m/s based on measurements made at weather stations close to the sites where the wet candles were deployed.

The geometry and orientation of the structure as well as the surrounding detailing of the structure can also play a significant role, particularly when the wind reaches a turbulent flow. The chlorides could reach inner columns that are not wetted during rain events, but still exposed to high humidity for extended periods of time. The direction of the wind driving the rain varies in intensity for each storm. These events will dictate the location and quantity of chlorides washed from the surface of the structure. Freshly wet concrete due to rain following a dry season could change the direction in which the chlorides move (from going into the concrete to going towards the concrete surface due to moisture gradient).

In several cases, the visited bridges had a cover that was less than one inch (e.g., a ½" stirrup was found with 0.65" cover, and in another a little less than one inch). In other cases, the cover ranged between 1.7" and 3". The above covers are examples in which the reinforcement was reached while coring, noting that the sites cored were those with larger cover or lower signal as measured by a reinforcement locator. Thinner cover affects when corrosion initiates, i.e., at an earlier time.

Several cores were obtained from Bridge #880005 from areas with cracks, and upon examining the cores, it was confirmed that the cracks were due to corrosion of the reinforcement. For Bridge #100585 (Gandy Bridge), cores were obtained from areas with surface cracks, but no evidence of corrosion of the reinforcement was found. In this case, the cracks could have been due to shrinkage or during placing of the elements. The cracks did enhance the chloride transport.

A requirement in the scope was to determine what the corrosion processes are at these higher locations. It appears that the corrosion processes at atmospherically exposed zones (higher elevations) are similar to those observed at the splash zone, in the sense that at the rebar depth, a certain chloride concentration was exceeded for corrosion to initiate and that there was water and

oxygen in the area surrounding reinforcement, plus conditions persisted that allowed the corrosion to propagate. Although measurements of moisture level at rebar depth were not made, it is speculated that, at least seasonally, there was moisture at the rebar depth where corrosion started and propagated. It is possible that during the dry season, the moisture content could be low, allowing the corrosion products to reach an oxide state. The rust red or brown coloring observed on the samples with cracks soon after obtaining the core appeared to confirm this (see, for example, Figures 67- 68). Locations where the cover depth is greater than 3 inches might contain moisture (assuming that porosity is low and that the concrete is not dry at those depths). The time for corrosion to initiate at these elevations can be considerably longer than for the splash zone, as the chloride at the surface was observed to be lower and would take longer to reach a stable high value at the surface and later at the rebar depth. In fact, in several cases, the chloride surface concentration (Cs) from cores obtained close to the top of the columns was low and the maximum chloride concentration was observed at a certain depth into the concrete (the position varied from 0.5 to more than one inch). See profiles for columns 13 and 11 from Bridge #880005.

Regarding whether similar corrosion damage can be anticipated on similar structures around the state, the answer is yes, particularly for older structures with no supplementary cementitious materials, with geometry and environments that allow a macroclimate where chloride deposition can be expected at high elevations. (The microclimate surrounding these structures is also important.) For structures with supplementary cementitious materials in the concrete composition, the time to corrosion initiation is expected to be longer than for structures built with OPC only, based on the apparent diffusion coefficient (D_{app}) values observed from profiles obtained on the outdoor samples and profiles corresponding to field cores. However, corrosion could take place at elevations higher than 12 ft above the mean high-water line (>MHWL+12) when the chloride concentration at the rebar depth exceeds the chloride threshold. Besides the concrete composition and cover thickness, the structure location, the surrounding macroclimate, and microclimate will influence the rate of chloride deposition and moisture levels within the concrete and at the reinforcement depth. Corrosion is still expected to initiate first at the splash zone.

Based on the wet candle measurements, it appears that chloride deposition can be significant several months in each year, but the magnitude can vary from year to year. Extreme weather events can enhance the chloride deposition on structures that are close to the ocean.

Table of Contents

List of Figures

List of Tables

Chapter 1 – Introduction and Literature Review

In the past, most of FDOT's (and other state departments of transportation with coastal bridges) focus has been directed to chlorides that are transported into the concrete on bridges exposed in the marine environment on partially immersed reinforced concrete elements, particularly the immersed, tidal, and splash zones. The splash zone is believed to be the region in which corrosion initiates first and then with time propagates at a faster rate (i.e., the region with the most aggressive conditions). Corrosion taking place on the immersed region is assumed to proceed at a lower corrosion rate due to oxygen concentration limitations.

Chlorides could reach higher elevations on bridges at locations subjected to direct marine spray (e.g., the bridges in the Tampa Bay area, Sebastian Inlet, and other locations along the Florida coast, particularly at inlets). These locations are considered extremely aggressive marine environments. Chloride deposition from marine spray could reach elevations higher than a 12 ft mean high-water line (>MHWL+12). Marine spray can include both ocean-produced aerosols and surf-produced aerosols. The build-up of chlorides at the concrete surface and the transport of chlorides into concrete at locations >MHWL+12 will depend on the environmental conditions as well as concrete properties. The microclimate and geometry of the element and surrounding elements could influence how much of the deposited chlorides penetrate into the concrete. There are instances in which chlorides from other sources could reach the concrete at these higher elevations. This chapter includes both intrinsic and extrinsic factors and how the synergy of these factors could cause a faster chloride transport.

The title of this project is "Investigation into the contributing factors to the corrosion of steel reinforced concrete structures at elevations greater than 12 feet above the mean high-water line". Hence the interest is on sections of bridges that have reinforced concrete elements at these elevations: e.g., beams, pile caps, and higher sections of the pile and column elements. Reinforced concrete elements at these elevations are part of what is known as the atmospheric exposure zone (for most locations in Florida). Based on the reviewed papers and reports, corrosion of the reinforcing steel can sometimes occur on older bridges exposed at sites in direct contact with marine spray at elevations >MHWL+12, particularly at bridges with poor drainage, and/or faulty joints, for which alternative chloride sources will be able to reach steel reinforcement. The alternative chloride source can be worsened if a boat ramp is near the bridge. But even if no alternative chloride source is present, the chloride ions deposited from constant and persistent marine spray can eventually allow enough chlorides (i.e., exceed the critical threshold) to reach the reinforcing steel of beams and pile caps even if located at high elevations >MHWL+12, when exposed to continuous marine spray for a long time. The splash and tidal regions of a partially immersed bridge substructure (piles/columns) are known to be prone to corrosion of the reinforcing steel as well. If the combination of concrete cover (expected to be thicker: 3 to 4 inches) and concrete chloride diffusivity are such that the critical concentration is reached first in these areas, then corrosion will initiate and propagate in these areas. It is expected that corrosion will initiate first at the splash zone, particularly on older bridges with higher apparent chloride diffusivity. No additional mention of corrosion of the steel at the immersed, splash, and tidal zones will be included in this report. The corrosion initiation of the reinforcing steel embedded in piles' and columns' higher sections, beams and pile caps located more than 12 ft above mean high tide depends on the environmental factors (macro- and microclimate), concrete cover, concrete chloride diffusivity, concrete moisture distribution (geometry could affect), and other factors

described below. Reinforcing steel corrosion can sometimes take place at locations >MHWL+12, if the exposure time is long enough and an aggressive marine environment surrounds the bridge. The time to corrosion initiation at these locations can initiate sooner if defects in the concrete are present combined with alternative chloride sources that enhance chloride penetration.

Intrinsic factors include: concrete properties, concrete cover thickness, moisture content and moisture distribution of the concrete cover, reinforcement, attack on the concrete (other than chlorides), and damaged concrete. Extrinsic factors include environmental parameters, distance from the coast (global environment), height (local environment), and microclimate (recently referred to as i.e., detailing and environment interaction in [1]).

At a given location, the terrain topography, predominant wind direction, wind speed, duration at a given wind speed, temperature and relative humidity tend to affect the surf spray and hence the chloride concentration that is in the surf spray/aerosols. Ocean-produced aerosols are due to breaking waves. Spume from breaking-wave whitecaps in the ocean-produce airborne chloride particles (ocean spray). It has been reported that the amount of ocean aerosol produced depends on the whitecap activity and wind velocity offshore (where the breaking waves take place). Locations at high north or south latitude experience higher wind speed [2]. Depending on the wind conditions, the marine spray at a height >MHWL+12 can be a mix of surf spray and ocean spray. The chloride deposited from marine spray can be considered a natural chloride source. Other sources could be due to chlorides washed out from the deck area during rain events when the drainage is poor and hence chlorides can reach the reinforced concrete elements below. Other chloride sources are described below. In some cases, synergy exists between internal and external factors which combine to allow corrosion to initiate after a given period of exposure. However, in many other cases, the chlorides deposited at elevations >MHWL+12 could be low and not reach the critical chloride threshold at the rebar depth within the service life of the structure.

1.1. – Intrinsic Factors

This section describes the intrinsic factors.

1.1.1 – Concrete Properties

Curing, proper compaction, cement/cementitious content, concrete composition (including the presence of supplementary cementitious materials), aggregate type, water to cementitious ratio are some factors that will dictate concrete properties, as for example, the concrete chloride diffusion coefficient at elevations >MHWL+12. The cement and/or cementitious content determine the initial concrete pore solution pH. A historical case mentioned that the pile caps (called crosshead in that paper) of a coastal bridge contained lower cement amounts than the piles [3-6]. After a prolonged period of exposure, the piles did not show corrosion (or little), whereas the pile caps had several instances with rust stains and, in some cases, cracks. The pile caps (crossheads) were located at a higher elevation. The beams of the approach bridge, also made with a lower cement content, showed spalls. (See Figure 1 below [3,4]). Another case mentions [7] that, no compaction or poor compaction caused voids/gaps at the rebar to concrete interface; these defects were mentioned as the cause of corrosion when compared to a similar concrete mix with the same composition, but no voids. Precast elements nowadays might be less prone to poor curing or poor compaction.

Figure 1. Hornibrook approach bridge; south-facing underside of the bridge [3]

1.1.2 – Concrete Cover

Pile caps and beams at elevations higher than >MHWL+12 might not have as thick a concrete cover as that used for the partially immersed reinforced concrete elements. A thinner concrete cover could then allow chlorides to reach the rebar more quickly than if it were constructed with a thicker cover. It would take additional time compared to splash zone to exceed the chloride concentration that allows corrosion to initiate. The moisture content in the concrete at these elevations would be lower compared to that found at the splash and tidal regions, so there might be less pore solution to transport the chlorides (at least on the region close to the surface). The moisture content could change depending on the season and the geometry of the elements (e.g., sections that are protected from rain and chloride washout).

The specified concrete cover, for reinforced concrete elements with heights >MHWL+12, has evolved over the years and, depending on the country and code used, the environmental exposure could dictate the minimum cover. In some cases, it has been found upon inspection that the cover of the built reinforced concrete element did not meet the requirements. A cover thickness below the specified concrete cover can allow corrosion to initiate earlier. [1, 8].

Cast in place reinforced concrete elements, and in some cases, precast reinforced concrete elements have been reported to have a thinner cover than specified on some sections either due to inadequate

quality control, over high demand, and/or accidents that cause shifting of the reinforcement cage [1].

1.1.3 – Concrete Attack other than Chlorides or Damaged Concrete

Precast concrete elements can be damaged during transport or while putting the elements in place (e.g., cracks could develop while driving precast concrete piles due to overload). It has been reported that cracks due to shrinkage could sometimes develop [9,10]. Mechanical loads over time can also damage concrete decks and/or joints [6, 11]. Pape and Melchers [6,12] give us an example of road bridges without a bitumen wearing or riding course. Melchers states that "Detailed rather than cursory observations showed that motor vehicles and lorries often cause physical damage to the concrete cover of the bridge deck and that corrosion damage then followed, rather than the damage being the direct result of inward diffusion of chlorides from de-icing salts causing corrosion that then cracked the cover (e.g., [13,14])." Similarly, damage of the concrete matrix protecting the steel over many years in service after first construction may be caused by volume changes resulting from alkali aggregate reactions, with corrosion then following [15,16]. Sulfate attack (due to seawater exposure) could also cause chemical attack of the concrete that with time can develop into cracks. In summary, chemical and/or physical damage (as those described above) can later allow chlorides to reach the reinforcing steel, and once it exceeds a critical concentration, corrosion could then initiate.

1.3 – Extrinsic Factors

This section describes some of the extrinsic factors. The distance from the coast (shoreline) is an extrinsic factor; some authors refer to this as the global environment [1]. Some construction codes use the distance to the coast to assign how aggressive the environment is. In Florida, no single point of land is more than 60 miles from the coast, and with high coastal winds during the year it is possible for every bridge to be affected by chloride deposition, with those closer to the coast affected more. Another extrinsic factor is the height (local environment) within the bridge/structure for a given reinforced concrete element. The microclimate (recently referred to as detailing and environment interaction [1]) is an extrinsic factor. Chloride source (due to marine spray only and in some cases other chloride sources) is another extrinsic factor.

Environmental parameters surrounding the reinforced concrete structure are also considered extrinsic factors. Temperature (T) and relative humidity (RH) at the site of interest over time (during the day and over the seasons) can affect the amount of chlorides that are deposited on the concrete surface. Only a fraction of the chlorides deposited go into the concrete. For example, RH and T at sites close to the tropics usually causes an increase in the rate of evaporation and moisture retained in the atmosphere. Because of this, there is a drop in sea level; therefore, the salinity of the sea water is higher in the tropics. Consequently, the aerosols generated in the tropics have a higher saline content. [17]

The seasonal differences in prevailing wind directions, wind speed and durations imply seasonal differences on a reinforced concrete structure exposure to airborne chloride deposition. During periods of high wind speed, the generation of airborne chlorides will be expected to be high. As indicated above, when the wind speed is high, larger waves develop on the sea. These larger waves break to form white foam which is rich in salt. Rainfall and direction of the wind during rain events

can wash out some of the deposited chlorides. Depending on the wind velocity turbulence could allow ocean spray (marine aerosols) to reach inner columns and at higher elevations that are later not washed-out during rain events.

1.3.1 – Chloride Sources

Chlorides reaching a reinforced concrete structure at heights >MHWL+12 can be due to marine aerosols or due to other chloride sources. Chloride deposition from marine spray particulates might be the only source of chlorides at the higher elevations of a bridge close to the coast. The aggressiveness of an airborne chloride environment is influenced by multiple factors such as height within the structure, altitude, distance from the sea, land orography, land topography, wind direction, wind velocity and duration of prevailing winds.

An example of another chloride source: salt particles accumulated on the deck surface and then washed down during rain events via run-off water from poorly designed drainage discharge that allows it to wet the reinforced concrete elements below.

The total amount of chlorides in the atmosphere is the sum of the wet and dry chloride deposition. A wet candle [63,64] measures what is known as dry chloride deposition. The chlorides reaching the wet candle can be surf spray, ocean spray or combination of both sprays. There are devices that capture precipitation and measure the wet chloride deposition (other devices measure the total chloride e.g., global device [18]). Only a fraction of the chloride deposition measured using a wet candle is captured by the concrete ([19,20,21]). Note that in the case of concrete (as well as other metals) that are atmospherically exposed, the section/areas where rain reaches the concrete surface can cause washout of the chlorides at the surface section wet by the rain. However, inner portions of the reinforced concrete element could receive no rain, it has been found that sometimes the inner section shows more corrosion damage [1] and contains a higher chloride concentration.
The magnitude of the chloride deposition at a given location depends on the wind direction (from the ocean towards the structure), wind speed greater than a threshold (Meira [22], and Feliu and Morcillo [23] suggest that the threshold is 3 m/s) and the duration of the wind at speeds greater than the threshold (this duration is sometimes called residence time).

Alao [17] and others have indicated that the airborne chloride concentration must be studied (measured) to estimate the severity of the environmental loading in a specific location. Chlorides might be more or less abundant depending on location (characteristics) and environmental conditions surrounding the structure and what is in the vicinity of the structure. The inland topography and the presence of urban landscape and forests can reduce the amount of chlorides that can be transported. Hence two sites close to the coast (say 100 m from the shore) can have significantly different chlorides reaching it, even if the two locations have similar airborne chloride production. [24]

1.3.2 – Other Chloride Sources

It has been reported [11] that bridges with poor drainage can allow some of the reinforced concrete elements below it to be wet when rain events take place. In the cases in which the drainage is poor and there is accumulation of salt on the road, the washout water during rain events can reach the surface of reinforced concrete elements below as for example beams, pile caps.

Another example of other chloride source are chlorides that wash down from the deck, at joints where there is separation (due to corrosion or other mechanical damage) during rain events. These chlorides can then reach the reinforced concrete elements below the leaky joints. This is more critical for cases in which damaged joints are present and a boat ramp is close by, where seawater/brackish water is spilling from the boat. The seawater dripping from boats crossing the bridge after leaving a nearby boat ramp likely enhance chloride deposition to reinforced concrete elements below a leaky joint.

1.4 – Chloride Deposition at Coastal Sites due to Ocean Spray

There are several publications [19-23 and others] that describe how marine aerosol is generated in the ocean or in the surf zone. The reader is directed to these publications for a more in-depth description. Meira [22] indicates that surf-produced aerosol is predominant for the salt concentrations found at locations close to the coastline (shore), whereas the influence of ocean-produced aerosol is dominant at greater heights and at locations farther inland. Higher wind velocity allows the smaller aerosol particles to travel longer distances (compared to larger/coarser aerosol particles) without settling. The chloride concentration due to marine aerosols is expected to be highest along the coastline. At a given site, the winds from the ocean toward land carry the largest amount of marine spray. More chlorides become available for deposition when the wind speed is higher than a threshold value. [22,23] This increase in marine aerosols is affected by how long (duration) the wind speed is above the wind speed threshold. [22] During seasons/months with winds above the threshold conditions, the corresponding chloride deposition recorded is high. Higher wind speeds cause higher waves, and when these break, the spume formed causes the ocean spray. Wind speed >3 m/s and long residence time (duration) have been found to significantly increase amount of chloride ions that deposits on a wet candle. Others [25,26] have reported a higher wind velocity threshold.

Komar [27] describes how the wave height has increased over the last 30 years on the Atlantic Ocean (the paper used data from a buoy located in North Carolina but it could also apply to Florida). They separated the summer months and removed the waves < 3 m high; provided a clearer view of the increase in wave height with time. This is relevant in the sense that there is a connection of wind speed and wave height [28,29]. What is not included in Komar's publication are the residence times (duration of events for the waves with reported height).

Montgomery [30] indicates that the wet candles exposed at the Kennedy Space Center (KSC) beach site are placed at ~100 (98) feet from high tide line, which is ~30.4 m from the high tide line. The wave height was monitored in the Montgomery, et al., study, because of the relationship between wave height and concentration of marine aerosols, where increased wave height is generally related to an increase in chlorides in the air. Bubbles created from increased wave action are the main generator of marine aerosols and are generally related to wave height. The monthly average wave height for ocean water off the coast of Cape Canaveral and approximately twenty-five miles from the wet candle location was compared to the monthly average chloride concentration values. Figure 2 shows the monthly chloride deposition and the average monthly wave height compiled by NASA from May 2010 to December 2017 [31].

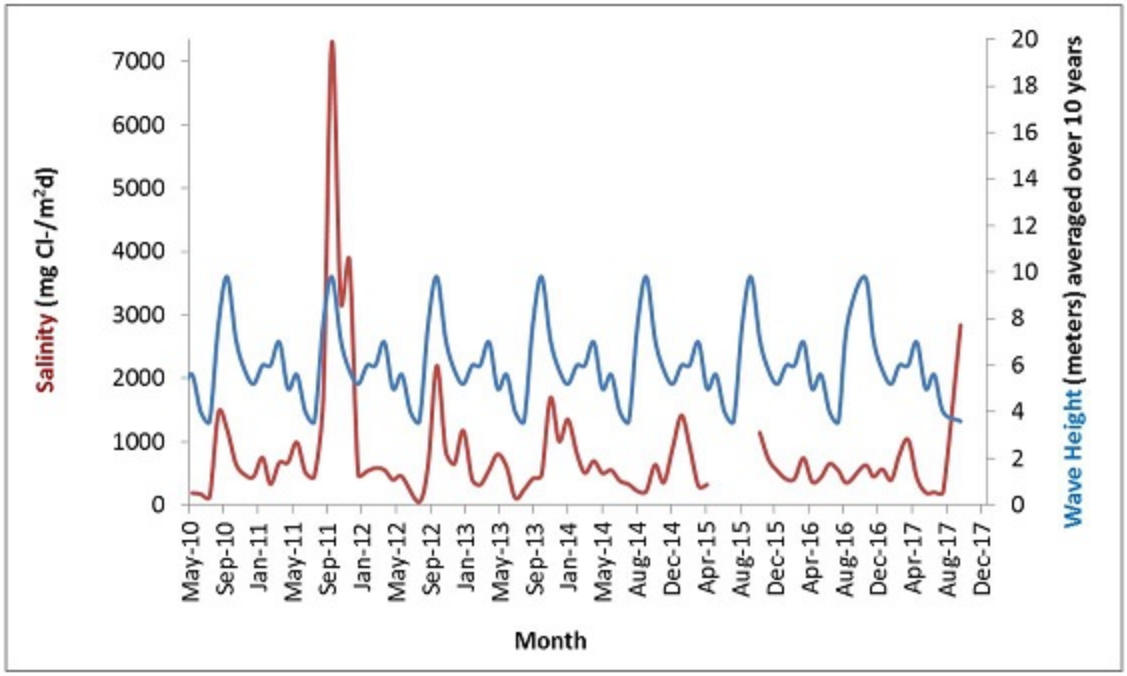

Figure 2. Chloride deposition and wave height vs. time (KSC Beach) [31]

The chloride deposition rate at KSC's beach atmospheric corrosion test site varies between 70 and 7300 mg/m^{2}d, with a weighted mean value of 983 mg/m^{2}d. An average value of 1044 mg/m^{2}d was reported in a previous study that included a somewhat shorter period. An average of 1000 mg/m^{2}d will be assumed for KSC site, when comparing deposition at other locations.

Corvo [32] reports an average salt deposition of 525 mg/m^{2}d at a distance of 1 m from the sea, Meira [19] reports 460 mg/m^{2}d at a site 10 m from the sea, and Alcántara [28,29] reports 1905 mg/m^{2}d at 300 m from the sea (this value seems a little high compared to others). Alao [17] reports 138.1 mg/m^{2}d at 50 m from the sea (South Africa) and Hossain [33] reports 54 mg/m^{2}d at 93 m from the sea at a site in Bangladesh. Cape Canaveral reports an average chloride deposition of 1000 mg/m^{2}d at a site ~30 m from the high tide line [31]. The Kure Beach, NC site [34] reports an average value of 400 mg/m^{2}d at a site 25 m from the shore. At FAU SeaTech [21], the east site is at about 100 m from the sea, and the average chloride deposition measured is 262.3 mg/m^{2}d with a maximum observed value of 810 mg/m^{2}d within the monitored period.

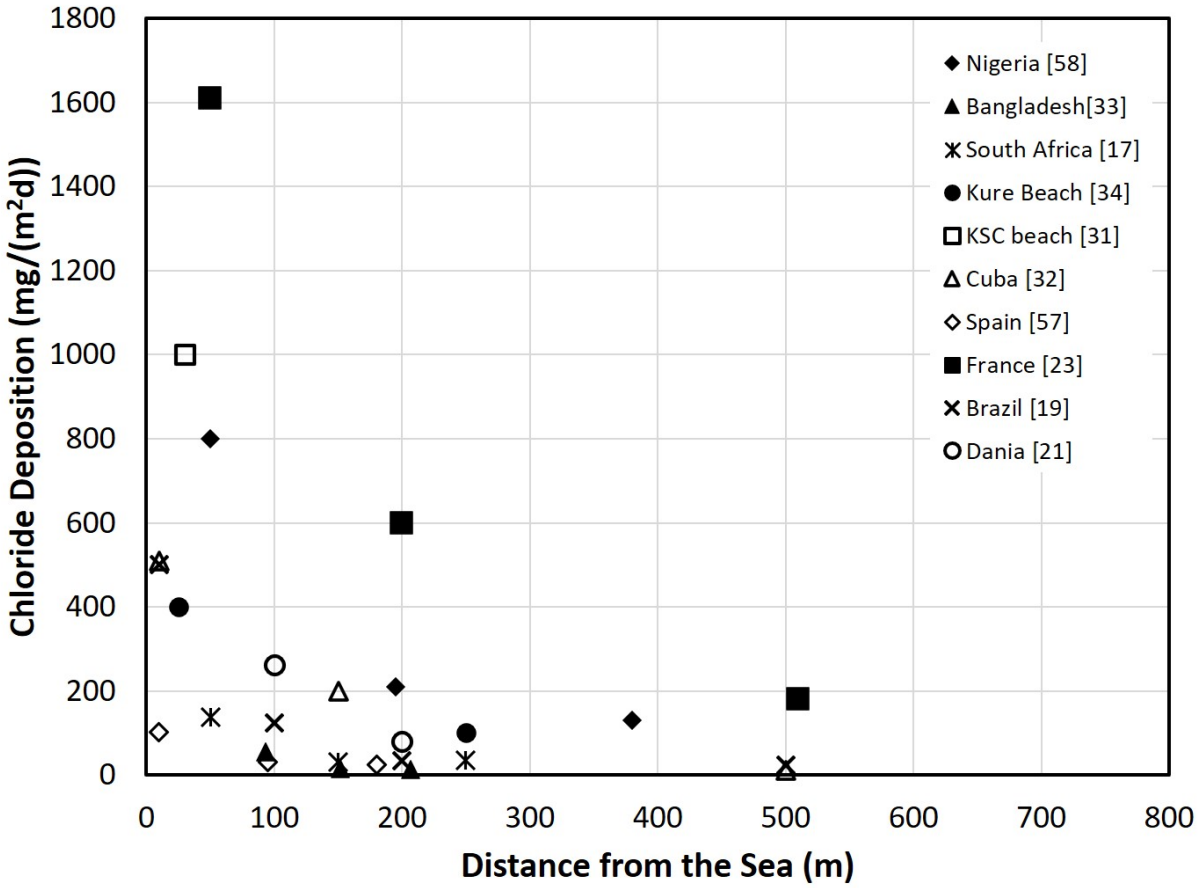

Figure 3. Chloride deposition as a function of distance from the coast.

1.4.1 – Chloride Deposition as a Function of Distance from the Coastline

There are several publications over the last couple of decades that report how the deposited amount of chloride decreases as a function of the distance from the coast [17, 19, 21, 28, 31-34]. There is an exponential decay on chlorides found as the distance from the coast increases. The exponential decay is affected by the local terrain of a given site and the predominant environmental conditions (wind direction, salinity, breaking waves, etc.). Figure 3 shows trends of how the chloride deposition changes as a function of distance from the sea for various locations around the world.

Akiyama, Frangopol and Suzuki [35] proposed a reliability-based durability design model that included the effects of airborne chlorides. Thirty-four stations are mentioned to have been deployed in the paper. Three years of airborne chloride samples were used. They proposed an equation that fitted to the experimental collected values. It included the ratio (fraction of time during one day) that wind flowed from the sea toward land, the average wind speed during the observed period, and the distance from the coastline. The authors mention the limited applicability of the equation; the example cannot be used for splash zone. The calculated values tended to be larger than the observed based on observation comparing model fitting to the experimental date reported. (Figure 3 in Akiyama ref [35]) The model applied from 0.1 km to 1.7 km and the values were reported in mdd. This study did not include wind threshold nor the duration of the events with winds faster than the threshold. The paper did indicate that a region with higher wind velocity was more prone to corrosion.

1.4.2 – Chloride Deposition as a Function of Elevation Near the Coastline.

There are similarities in how the amount of chloride changes between chloride found as a function of distance and chlorides found as a function of elevation at sites close to the coastline, in the sense that an exponential decrease in the amount in chlorides is observed. Meira [36] reports that the chlorides deposited decrease as the height increases (at least within the first 10 m).

Meira reports the results for a site 100 m from the shoreline [36]. Chloride depositions were measured at a height between 1.5 and 10 m. The area between the shoreline and the exposure site was free of obstacles in this study. The authors mentioned that this site was selected to prevent significant removal of salt particles by obstacles that could impact the measurements at four heights (1.5, 4, 7 and 10 m from the ground level). At this site, the maximum amount of chloride deposition was found at 1.5 m [36]. At 1.5 m the deposition ranged between 100 and 200 mg/m^2d, and at 4 m it ranged between 40 and 85 mg/m^2d. An exponential decrease in the amounts of chlorides deposited were found as the height increased. Meira and collaborators [36] report a decrease in marine aerosol salinity when increasing the height from the ground. This was attributed to the gravitational settlement of salt particles that makes salinity concentration at lower layer (heights) to be higher.

It is believed that at low elevations, e.g., 1.5 m, most of the chlorides are due to surf (wave breaking) aerosols, and as the height increases, most of the chlorides are attributed to ocean spray. However, there are situations where, at heights between 10 m (or less) and 130 m [37, 38], the chlorides found are due to a mix of surf and ocean spray. The marine aerosols made of a mix of surf aerosols and ocean aerosols are due to the terrain/topography, wind direction and wind speed and wind turbulence that allows surf-produced spray to mix with ocean-produced spray. [37,38]
A recent study of coastal bridges in Norway [1] reported that the chloride profile found on beams at 5.8 m above sea level was significantly greater than the chloride amounts found from chloride profiles on another bridge on beams at 12 m above sea level. There are other Scandinavian studies that report that chlorides deposited at a higher elevation will be lower for conditions in which atmospheric chloride deposition is the only chloride source and measured on bridges along the coast [39,40].

At locations right at the coast and depending on the wind speeds, it could be possible to find a significant amount of chlorides even at elevations of 10 m or more, particularly if the reinforced concrete bridge elements (at >MHWL+12) are in the path of high winds that could cause a mix of surf spray and ocean spray to be carried to higher elevations by turbulence.

Short tests, such as those reported in Hawaii [37] using a special kite that had steel wires to capture chlorides, suggest that the chloride concentration is higher at lower heights (lowest height was 10 m), then decrease, but it tends to slightly increase and remains almost constant after a certain height. This trend might have been influenced by the wind conditions during the experiment (which lasted about one hour – and it was repeated eleven times). This paper mentions turbulence as the reason for aerosol mixing and higher concentrations at higher elevations. At other runs the amounts of chlorides found was lower.

1.4.3 – Chloride Deposition as a Function of Elevation Farther Inland.

Farther inland, the amount of chlorides in greater amounts could be found at higher elevations. Indirect confirmation has been reported via wire on bolt corrosion experiments. In one case, at 500

m from the coast corrosion was found three times greater at a height of 20 m vs. 1.5 m [38]. LaQue [41] reports that the corrosion at 250 m was found at a higher elevation on steel piles (low alloy and regular carbon steel) compared to the greatest corrosion found on piles placed at 25 m from the coast. The corrosion was greater on the piles located 25 m from the shore compared to the corrosion found at 250 m from the shore. [41]

Pham et al. [42] presents a method that uses what the authors define as the effective wind power, which combines wind speed, its duration and wind direction adjusted to what fraction of the wind directly hit the structure. Pham et al. discusses how these wind parameters influence the atmospheric chloride deposition. Measurements were performed at elevations that ranged between 6.5 m and 7.5 m on four bridges; at one site the measurements were made at 27 m. Each wet candle deployment lasted seven days (one week). Pham et al. presents data collected at 5 bridges in Vietnam. Besides weekly sampling of the chlorides the wind speed, direction and duration was also considered. The distance from the east coast ranged from 2000 m to 3100, whereas the distance from the river mouth ranged from 10 to 7020 m. As indicated above, the elevation at which the wet candle apparatus was placed ranged between 27 and 6.5 m (from the water surface in high tide conditions). The bridge with the wet candle at 10 m from the river mouth and with the wet candle at 27 m from the water surface had the largest chloride deposition ranging from 18 to 48 mg/m^{2}day. The authors do not discuss what is the salinity of the water at the river mouth (or if at the discharge there is mix with ocean water). For the site at which the wet candle was exposed at a height of 27 m, the authors mentioned that the chloride deposition might have been larger if measured at 7 m from the water. But it could be that the ocean spray particles reached a higher concentration at the higher elevation. The elevation effect on chloride deposition was not discussed. It could also be that the deposited chlorides at the various locations tested are a combination of particulates from the river discharge (brackish water?) and ocean spray particulates. No values were reported regarding the chloride concentration at the coast.

1.5 – Alternative Methods to Measure Chloride Deposition

There are several studies that have used drilling of reinforced concrete structures to assess the chloride concentration close to the concrete surface as an indicator of the chloride that can potentially penetrate the concrete. It is important to note that if only one layer is obtained it might not be possible to distinguish cases in which skin effect is present (particularly for areas/regions that are subjected to wet/dry events with periodic/sporadic chloride deposition, i.e., cases with thick skin effect layer).

Liu et al., [43] used a drilling method to compare the chloride deposited into concrete structures located in coastal area. The chloride data obtained from drilling the structures was used to compare chloride deposition as a function of elevation and as a function of distance from the shore. Liu et al., reports elevation effect. However, it is not clear which structures were included for the chloride deposition as a function of elevation. The paper reported that the chloride increased with elevation from 0.4% at 10 m, to 0.51% (average) at 30 m. (The paper says absolute altitude). Structures were located at 3 areas within the city of Shenzhen in southeast China. The structures were drilled to obtain chloride surface concentrations. The structures were located at a range of distances (0 to 1000 m) from the coast (the paper refers to it as offshore distance) and elevation that ranged from -10 to 50 m The values shown in Liu, et al., paper does not separate distance and the elevation.

Figure 3 in the Liu et al. [43] paper shows the concentration as a function of distance from the coastline. It is possible that only values at locations less than 300 m from the coast were used to generate the chloride deposition with elevation plot (Figure 4 in Liu et al. [43]), but it is not stated. The authors indicate that they identified two zones. They mention, "It is well known that wind speed increases with the increasing height, which results in more airborne aerosol salt and higher chloride deposition." This could be seasonal and depend on the airborne salt amount present and the wind speed. As the distance from the shore increases the aerosol salt decreases.

A study performed in South Africa [17] conducted drilling concrete from various structures. The concrete powder was analyzed to determine chloride concentration. The amount of chloride as a function of distance from the coast is reported, but not as a function of elevation.

Phan, et al. [44] proposed a novel methodology to monitor chloride deposition, but the device (and its solution) needs to be replaced more frequently than for the wet candle test [44].

Santucci and collaborators [45] reported on the precision of salt deposition from measurements done using the wet candle. It included the bias that could occur when different technicians perform the test, and effects due to the location and duration of the test (interval duration varied). The wet candles were deployed at Key West, FL. The possible contamination from various protective equipment was also studied. The chlorides in this publication were all measured by ion chromatography by a single operator. The interval 2 weeks + 2 weeks was the one that captured the most chlorides vs. 4 weeks, 1 week × 4, and 3 weeks + 1 week.

Indirect methods involve examining the corrosive effects of airborne chloride on exposed metals, through an analysis of the exposed metal's loss of mass. This method can also be used to classify environmental severity [46]. Other methods used to measure chloride deposition include dry gauze [47] or the Doken [48] method. These two methods collect aerosol from only one wind direction.

Suzuki and Robertson [49] describe an alternative data collection system that used single chloride content measurements from roof beams of city bus shelters in Hawaii. One hundred and twenty-six (126) sheltered bus stops were tested.

A recent study [18] reports that the total chloride deposition (wet and dry) was investigated in French Guiana for locations 4 km to 14 km from the coast. A novel device was used to gather the total chlorides. The average chloride measured ranged from 22.4 mg/m^2d (at 4 k-m) to 15.7 mg/m^2d (14 km) over three years. The maximum monthly average was 42 mg/m^2d. The effect of seasonal wind directions and other parameters were also discussed by Gobinddas et al. [18].

A recent study by Bian et al. [50] describes characterization of chlorides from 200 m to 12 km. Vertical profiles of sea salt aerosol concentration and size distribution were measured in a NASA-funded Atmospheric Tomography Mission (Atom) over vast oceanic routes in different seasons. These heights don't apply for coastal bridges in Florida.

Wattanapornprom and Ishida [51] have reported and proposed on a model that uses airborne chloride data at a given location, environmental conditions, and concrete properties to predict the chloride ingress into concrete. Wattanapornprom and Ishida describe a model that uses chloride

deposition data as well as local conditions to estimate the amount of chlorides that adhere to the concrete surface, and then a second component of the model tackles the transport into the concrete. It does not seem to include effect as a function of elevation but does account for location (distance from the ocean) and if obstacles are present a correction factor is added. [51]

1.6 – Chloride Transport into Concrete at >MHWL+12

Chloride ingress in concrete occurs through a combination of mechanisms. These include permeation, diffusion, capillary absorption, migration, and convection. The pore structure, environmental conditions, and degree of saturation of a concrete structure strongly influence the rate of chloride ingress into concrete and the interaction between species [52]. In the case of atmospherically deposited chlorides (marine aerosols), chloride transport could be by capillary suction close to the surface and by diffusion through the partially saturated pore structure, and the degree of saturation can vary as a function of depth (seasonally or due to location). The transport is influenced by the chloride concentration at the concrete surface (or sometimes the maximum chloride concentration is farther in when skin effect is present) and influenced by the fraction of the chlorides deposited in the surface that actually goes into the concrete. The moisture content in the concrete will also dictate the depth at which diffusion starts to be the dominant transport mode. Seasonal conditions could prevail; for example, during the rainy season, the moisture content could be high in all the concrete covers and the chlorides then move via diffusion, whereas during the dry season, by capillary suction (or a more complex situation could be present).

1.7 – Reinforced Concrete Elements at >MHWL+12

Beams, pile caps and higher sections of the piles can be found at elevations >MHWL+12 on bridges that are tall. This section describes several field studies that report reinforcing steel corrosion on beams and pile caps. It also includes a study for beams exposed outdoors at a coastal site.

Precast elements, for example, prestressed beams and prestressed piles, contain high strength steel wires (as well as traditional steel reinforcements). Marine exposed prestressed beams containing these steel wires have been reported to corrode and, in some cases, show no cracks at the surface (particularly after modest cross-section loss), which might be difficult to identify via visual inspections. In other instances, the corrosion propagated and caused cracks and, in some cases, caused delamination and/or spalls.

1.7.1 – Reinforcing Steel Corrosion Observed on Field Exposed Samples

Otha [53] describes beams prepared with various concrete compositions and pre-crack after 20 years of exposure (the paper also includes results after 10 years). Monthly chloride deposition for 2 years is also included, although the units are in mg/10cm^2/day (mdd), the maximum value observed during that period was 6.5 mdd and the average was 3 mdd. The exposure site was located 30 to 40 m from the beach line in Rumoi, Japan. This beach site faces the Sea of Japan (East Sea). The beams were exposed at heights that range between 1 and 4 m. Otha [53] mentions that during the winter there is a strong seasonal wind. Most compositions contained OPC and a variety of parameters were investigated; two compositions contained fly ash blended cement (10 to 20% fly ash) and blast furnace slag blended cement (30 to 50% slag). The paper reports the D_{app} after 20 years, as well as the chloride profiles. The D_{app} was 4 times smaller on concrete prepared with blended cement: D_{app} was 1.81×10^{-12} m^2/s for concrete with only OPC, D_{app} was 0.59×10^{-12} m^2/s

for concrete with fly ash blended cement, and D_{app} was 0.49×10^{-12} m^2/s for concrete with blast furnace slag blended cement, the w/cm was 0.44 and 300 kg/m^3 cement. From the results it is not clear if corrosion took place on samples prepared with blended cements after 20 years of exposure. The results regarding corrosion are grouped based on cover, exposure time, and/or cross section loss. Most samples with 20 mm cover had longitudinal cracks and an average cross section loss of 7.7%. The paper also mentions average cross section losses of 3.25% and 2.68% for samples with 30- and 40-mm concrete cover, respectively.

A recent publication by Meira, et al., [54] describes reinforced concrete samples exposed at a beach site (10 m from the sea). The concrete mixes prepared contained 320 to 406 kg/m^3 of cement (two different cements were used) and w/cm that ranged from 0.65 (the mix with least cement) to 0.5 (the mix with the most cement). The samples were terminated shortly after corrosion initiated. The results were compared to the test on lab specimens prepared with the same compositions and exposed to wet/dry cycles. The chloride threshold values were determined; the chloride threshold was found to be lower in the samples exposed to the marine ocean spray (field exposure). Lab samples containing cement with 25% natural pozzolan, 420 kg/m^3 and 0.5 w/c required 87 to 230 days for corrosion to initiate with an average chloride threshold of 2.12 %c.w., whereas it took 1407 to 2418 days and an average of 1.47 %c.w for the field exposed samples.

1.7.2 – Reinforcing Steel Corrosion on Reinforced Concrete Elements at >MHWL+12

Most publications do not report the height with respect to MHWL. In this section, most described publications refer to reinforced concrete elements that showed corrosion or that reported chloride profiles for elements exposed to marine aerosols. A few of the cases described below correspond to bridges exposed to deicing salt during the wintertime. The joints on the superstructure on different types of bridges is where deterioration took place (either mechanical or corrosion). Bridges in northern states are subjected to de-icing salts, which can wash thru leaky joints and cause corrosion to the beams below (in some cases these were metal beams, in others reinforced concrete).

Fukuda, et al., [55] reports that salt damage (from marine aerosol) was observed on main girders, cross beams, piers, and abutments of eight bridges along the seashore of the Sea of Japan (East Sea), Mutsu Bay and the Pacific Ocean. The bridges along the Sea of Japan (East Sea) suffered the most serious deterioration. Fukuda, et al., [55] attributed this to the bridges being exposed to a severely cold climate with substantial amounts of suspended salt particles due to strong westwardly winds from the sea in the winters. The bridges were between 20 and 50 m from the seashore. One of the bridges 20 m from the shore was inspected in detail. Figure 4 shows a picture included in [55]. Corrosion of the rebars was found in the bottom of the main girders in the upstream side opposite to the sea. At the reinforcement depth (3 cm), 5 to 6 kg/m^3 of chlorides were measured.

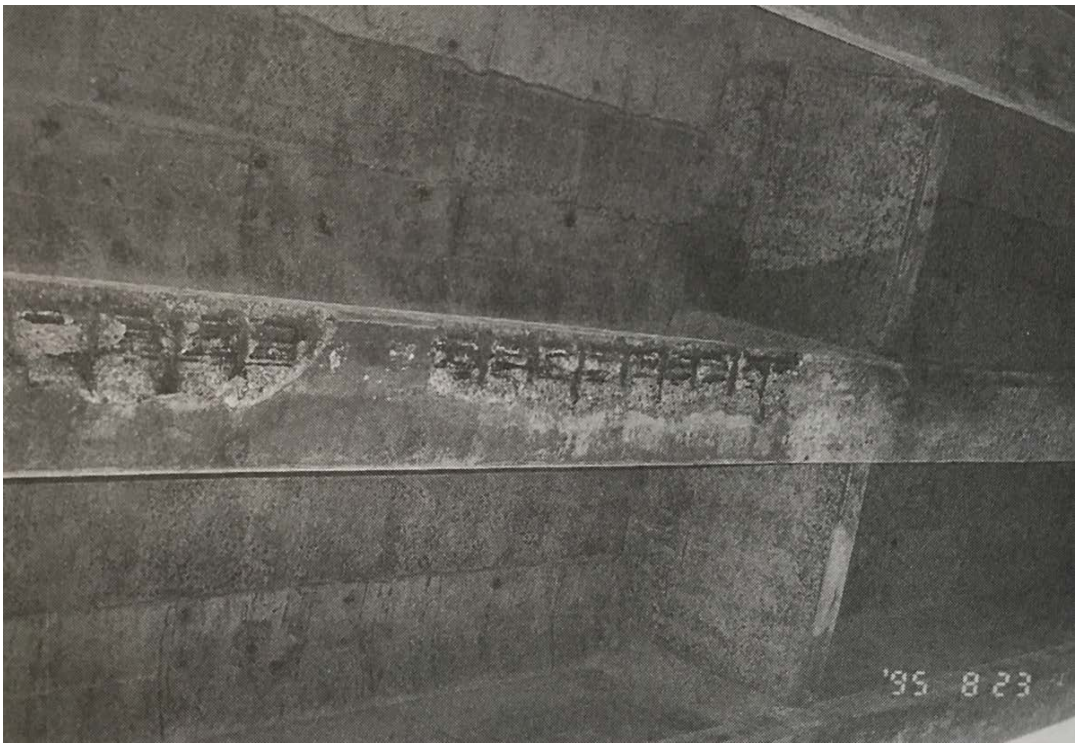

Figure 4. Corrosion damage on main girder on the bridge along the seashore of the Sea of Japan [55]

Balestra [56] presents the chloride profiles for structures that were between 40 and 60 years old of exposure to marine environment. Five profiles correspond to locations described as atmospheric zone, but no details of the elevations at which these cores were obtained is given. All profiles had skin zones. The paper also includes two different ways to fit D_{app} values.

Nagi and Whiting [11] reported findings of several field visits and field case studies. For pretensioned structures, they mention that "drainage details should ensure disposal of deicer solution without contact with the prestressed beams." On a different section in the same paper, Nagi and Whiting suggest a water-to-cement ratio of 0.45 or lower. The paper also states that when salt spray cannot be prevented to consider increasing the concrete cover. From the reviewed field evaluations, Nagi and Whiting found that the most common defects were deterioration of the joint sealer, lack of sealer, and cracking of concrete around joints. Corrosion of the steel reinforcement and the highest chloride concentration were found in the beams adjacent to the leaking joints. The authors also indicate that an adequate drainage system was found to be important in providing effective removal of storm water (other details were described). The case histories reviewed by Nagi and Whiting mentioned the leakage of salt water at defective joints. Although the pretensioned structures were in northern states or countries where de-icing salt is used, the presence of similar defects on marine exposed bridges also applies, with the alternate source of chlorides as described above.

Whiting [57] describes field inspections that took place in the early 1990s on the old Gandy and old Sunshine Skyway. Locations where corrosion took place were identified. The prestressed beam described at the Gandy was about 2 ft above mean high tide (Figure 5); whereas the prestressed

beam noted with damage at the old Sunshine Skyway was located at the abutment span and at a higher elevation (a reproduction of the picture is included in Figure 6). The authors state that the prevailing winds blew saltwater spray onto the pretensioned support beams. Whiting recommended the use of high-performance concrete, i.e., concrete with low w/c and containing fly ash and/or silica fume, or similar supplementary cementitious material. (The Whiting study was completed in 1993.) This presents additional evidence that in some situations after long-term exposure, enough chlorides may reach the prestressing steel wires (steel reinforcement) and allow corrosion to initiate.

Figure 5. Corrosion damage on post-tensioned beam on Gandy Bridge [57]

Figure 6. Spalled areas over pretension tendons on abutment span Old SSK bridge [57].

Whiting wrote “many of the members in both bridges received almost continuous exposure to direct saline spray under hot and humid conditions for most of the year.” Bridges in the Tampa Bay area, other bridges in the area, and bridges all around the Florida coast are also subjected to

the continuous ocean water spray. Whiting and Stejskal considered this exposure an extremely corrosive environment.

Pape and Melchers [12] present a description of three beams forensically analyzed for a bridge in Tasmania, but other beams also were observed to have corrosion (based on pictures and paper text). Figure 7 shows an image of a longitudinal crack along a beam. The bridge was built in 1957 and was found to have nitrate chlorides when the concrete was prepared; however, it is not clear if those chlorides were enough to cause corrosion or if additional chlorides penetrated and also played a role in the observed corrosion. In this case several longitudinal cracks were observed, starting in 1970. The bridge was demolished and replaced in early 2000. Three beams were selected for further study and that is what is reported in Pape and Melcher's paper [12]. Significant cross section loss was found on both the high strength steel wires as well as the conventional reinforcement. Other interesting points are made regarding the corrosion that took place via the corrosion products observed upon removing the concrete surrounding the strands or the conventional concrete. Cross section losses as large as 75% to 100% were observed on some of the wires, as well as on some of the conventional reinforcement. This reference is another example of corrosion taking place at heights relevant to the current study.

Figure 7. Typical longitudinal web crack along a beam [12]

Melchers [3-6] points out that an archeological approach to assessing older bridges has some advantages and disadvantages. Most relevant is the finding that the beams at the Hornibrook Bridge approach spans were found with cracks and spalls on the beams and the pile caps (crossheads). Melchers reports that there was considerable corrosion on some of the cast-in-place pile caps. Several elements of the reinforced concrete approach bridges showed considerable corrosion at beams and crossheads. Corrosion was evident on the underside beams and crossheads.

For the part of the bridge with little corrosion, i.e., the piles, it was found that the precast concrete piles were cast with a composition that contained more cement than the concrete used for the crosshead or the beams. It is not clear if the concrete cover was the same for the pile caps and the piles (60 mm cover).

Figure 8. Typical damage reported by Osmolska et al. [1]

A recent publication by Osmolska et al. [1] presents field inspection results of pretensioned Norwegian standard I-beams (NIB) girders in 227 coastal climate bridges. The authors found that about 51% of the bridges had corrosion damage (of the reinforcement in the NIB girders). A high percent of the bridges built with the thinner concrete cover showed corrosion. Seventy-four percent of the corrosion damage was found on bridges with the concrete cover was below the specified thickness (typically due to production faults). The authors explain that there was a period with a high rate of construction that might have caused high demand and lower quality. The number of bridges in what is considered harsh coastal zones is lower than the other coastal zones. Eighty-two percent of the NIB girder bridges in the harsh coastal zone registered corrosion. Corrosion was found in the inner NIB girders, particularly in the support zone and its vicinity. The authors hypothesize that this can be due to combined effects of geometry and exposure conditions (also known as microclimate). Higher chlorides deposited close to the support zones might be associated with wind flow affected by the vertical supports acting as barriers. Turbulent wind flow around pillars and abutments could cause accumulation of moisture and chlorides and therefore increased chloride ingress. [1] Figure 8 shows the type of damage observed on the NIB girders. In some cases, the concrete was removed to observe the corrosion.

1.7.3 – Bridge in Denmark

Gulikers [58] presents chloride profiles and D_{app} values for a structure that was cored at the elevations of interest. The chloride profiles and corresponding D_{app} appear to vary significantly, even though the structure was exposed to the same environment. The structure was visited after 18 and 30 years. Gulikers indicates that even though the chloride concentration might be high at the rebar depth (i.e., exceeding typical values assumed for chloride initiation), corrosion did not seem to have initiated. The concrete used in the structure described was concrete with 50% slag. The author suggests that concrete with 50% slag, with good compaction and initial curing contributed to the low D_{app}. Gulikers [58] reports that a good bonding was found between the reinforcement and concrete (i.e., no voids). It also suggests that slag cement used in the structure is known to bind more chlorides compared with cement with no slag.

This paper presents and discusses the findings and interpretation of the chloride profile measurements obtained in 2002 and 2016 on the wall of a bridge box girder facing the North Sea (windward side). Concrete used cement CEM III/B with w/c 0.44 and 325 kg/m^3. The precast elements were steam cured for 2 hours shortly after casting. The lowest part of the bridge is located at a level of +6 m above MWL, whereas the bridge deck is at a height of +11.75 m above MWL. The environment can be described as predominantly atmospheric with exposure to chlorides contained in aerosol, and occasionally seawater spray and incidental splash.

D_{app}, was found to range between 0.15×10^{-12} m^2/s and 0.78×10^{-12} m^2/s, respectively, with an average D_{app} of 0.35×10^{-12} m^2/s from cores obtained in 2002. From 2016 measurements, D_{app} ranged between a value 0.07×10^{-12} m^2/s and a maximum value of 0.47×10^{-12} m^2/s, whereas the average D_{app} value amounted to 0.23×10^{-12} m^2/s. The D_{app} was less than 1×10^{-12} m^2/s even for the largest value measured. The author mentioned that in 2016, cores were obtained at 3 different elevations, but no breakdown was provided in the paper. It was not indicated if the D_{app} was smaller at the higher elevations. The assumption described in the paper is that all surface exposed to similar environmental aggressive conditions might not hold. It is possible that lowest D_{app} corresponded to the highest elevation or the section of the structure that receives less marine spray, or to locations where there is not as much moisture or as much chloride being deposited.

Quote from the paper “However, the chloride profiles that have been measured show a significant scatter, despite the fact that both the quality of the concrete cover and the environmental load with respect to moisture and chlorides is considered quite uniform over the exposed concrete surface of the wall.”

Not included in the above is that the fitted surface concentration also ranged broadly during both visits. The obtained values were used to estimate remaining service life using a probabilistic approach. The results suggest that corrosion can be expected within next 10 yrs. The authors states that the owners will not follow the probabilistic approach but rather a pragmatic approach. The author indicates “Therefore, in the near future, no further investigations on site are envisaged but a pragmatic engineering approach based on common sense will be adopted.”

The following chapters will describe the experiments, results samples at SeaTech, results of samples obtained from the field visits, discussion, and conclusions for the research efforts carried as part of this project.

1.8 – Summary

The chloride deposition into the concrete at elevations >MHWL+12 can be high if the bridge is located at the ocean or a short distance (less than 50 m) from the coast, particularly if there are no buildings to obstruct the marine spray. A higher chloride deposition is expected when the environmental conditions include winds with speeds above a critical threshold and that last for long durations, with the wind direction from the sea toward the bridge. The presence of other chloride sources and intrinsic factors (e.g., leaks at joints, poor drainage design, $D_{app} > 1\times10^{-12}$ m^2/s) tend to reduce the time to corrosion initiation.

At elevations >MHWL+12, it is expected that it will take longer time to reach a critical chloride concentration at the reinforcement depth on bridge elements built with supplementary cementitious materials that have low D_{app} and no other damage on the cover concrete, and when there are no other chloride sources.

Chapter 2 – Experimental Methods and Methodology

2.1 – Samples Exposed Outdoors at FAU SeaTech

Eleven concrete compositions were prepared for the DCL samples in 2011. Table 1 shows the various compositions. Samples were deployed outdoors at FAU SeaTech in 2011. The east site is approximately 100 m from the ocean, and the west site is about 200 m from the ocean, but some of the samples are 10 to 20 m from the intercoastal. On the east site, one block per mix remained, and they had been cored twice; most samples were milled using the profiler device (a few specimens were cored and then milled). Figure 9 shows an image of these samples. On the west site of the property there were at least two samples per mix; one sample per mix has been cored once. The samples at the west site area are exposed facing up. Figure 10 shows an image of some of the samples on the west site at SeaTech. In addition, samples that were prepared earlier (see table 2) and placed outdoors in 2011 were also selected for testing; these samples had no mortar layer. The nominal density for the samples in Table 2 is 2276 kg/m^3. The composition of the older samples is described in Table 3. On the west property, some of the samples from this latter group are exposed in a vertical orientation, whereas other samples are exposed facing up. Figure 11 shows some of the 1CX samples. At the east site location, these older samples are being exposed as shown in Figure 12. The samples (both DCL and the older concrete samples) on the east site might on occasion have been exposed to seawater; these samples are placed next to the pump house, and there is an outlet that sometimes opens and discharges outside next to where the samples are located. This chloride exposure is in addition to the natural chloride deposition from the ocean spray.

Table 1. DCL specimens concrete mix detail

Mix	Cast Date	Cementitious Content (kg/m^3)	Cement Content (kg/m^3)	20% FA (kg/m^3)	8%SF (kg/m^3)	50% Slag (kg/m^3)	Fine agg. (kg/m^3)	Coarse agg. (kg/m^3)	w/cm ratio
DCL1	Dec. 7, 2011	390	312	78	0	0	653	1,062	0.35
DCL2	Sep. 22, 2011	390	312	78	0	0	721	949	0.41
DCL3	Oct. 19, 2011	390	312	78	0	0	697	918	0.47
DCL4	Dec. 21, 2011	390	312	78	31	0	653	1,062	0.35
DCL5	Dec. 21, 2011	390	312	78	31	0	721	949	0.41
DCL6	Oct. 26, 2011	390	312	78	31	0	697	918	0.47
DCL7	Dec. 14, 2011	390	195	0	0	195	653	1,062	0.35
DCL8	Nov. 22, 2011	390	195	0	0	195	721	949	0.41
DCL9	Nov. 2, 2011	390	195	0	0	195	697	918	0.47
DCL10	Sep. 28, 2011	335	268	67	0	0	765	1,007	0.41
DCL10a	Oct. 12, 2011	335	268	67	0	0	765	1,007	0.41
DCL10b	Nov. 16, 2011	335	268	67	0	0	765	1,007	0.41
DCL11	Nov. 9, 2011	279	223	56	0	0	765	1,009	0.41

Table 2. List of older samples selected for testing (cored then milled)

Cast Date	Mix	Sample ID	Location, and Sample Direction
3/3/2008	1C1 (OPC only)	1A1B-H	West- Horizontal-Up - 1C
		1A2B-VF	Fence-Vertical
		1A3B-V	West-Vertical
8/19/2008		2C2B-E	East - H but facing the ocean - (with thin layer of FA mortar) - West
		2C1A-V	Fence Vertical OPC only (with thin layer of FA mortar) -West
6/2/2008	1C2 (with Fly Ash)	1E2B-FV	20% FA, Fence Vertical
		1E4A-H	20% FA, West Horizontal-up
8/19/2008		2A1A-V	20% FA, West Vertical (with thin layer of OPC only mortar)
		2A1B-E	20% fly Ash - East (with thin layer of OPC only mortar)
10/26/2009	1C3 (with Fly Ash and Silica Fume)	3A1B-H	West Horizontal-up
		3A4B-E	East-Horizontal but facing the ocean

Table 3. Composition of older concrete (samples prepared between 2007 and 2009 see Table 2)

Mix No.	Cement	Coarse agg.	Cement (kg/m^3)	FA (kg/m^3)	SF (kg/m^3)	Water (kg/m^3)	Fine agg. SSD (kg/m^3)	Coarse agg. SSD (kg/m^3)
1C1	type I/II	Limestone	390	-		156	734	996
1C2	type I/II	Limestone	312	78		156	734	996
1C3	type I/II	Limestone	281	78	31	156	734	996

Figure 9. DCL samples exposed at the east site

Figure 10. DCL samples exposed at the west site

Figure 11. Older samples exposed at the west site (left examples of horizontally oriented)

Figure 12. Older samples exposed at the east site – horizontal facing the ocean

Each sample on the east property was milled using the profiler device (except for DC3-F which was repeated by coring then milling). Similarly, one sample per mix of the DCX-C samples on the west property was cored and milled or milled using the profiler device. Chloride analyses were then performed on the concrete powders for each layer. The layer thickness for samples milled with the profiler was 0.5 mm. Table 4 lists the number of samples per composition tested for the DC samples. The table also lists the density corresponding to each mix.

Table 4. Number of samples per mix and exposure site to be tested after 108 months

Sample	Cast Date	Density kg/m^3	West	East
DC1	12/7/2011	2242.29	1	1
DC2	9/22/2011	2220.54	1	1
DC3	10/19/2011	2186.97	1	1*
DC4	12/21/2011	2232.56	1**	1
DC5	12/21/2011	2210.05	1	1
DC6	10/26/2011	2178.45	1	1
DC7	12/14/2011	2246.90	1**	1
DC8	11/22/2011	2224.00	1**	1
DC9	11/2/2011	2191.10	1**	1
DC10	9/28/2011	2246.21	1**	1
DC10a	10/12/2011	2246.24	1**	1
DC10b	11/16/2011	2244.46	1	1
DC11	11/9/2011	2248.84	1**	1

* repeated by coring and then milling

** cored then milled samples

2.2 – Wet Candles

This section describes the wet candles, where they deployed and how the chloride concentration was determined from the solution. The procedure used in here combines ISO 9225 [63] (solution in the flask) and ASTM [64] (geometry), and the chloride was determined via titration using a modified FDOT [65] method to measure low chloride concentrations.

2.2.1 – Frames

Frames were prepared with different geometries to hold the wet candles in place, the geometry is somewhat different from what is indicated in the ASTM standard. This section describes the four different geometries (the two setups deployed at Sebastian Inlet Bridge State Park are identical). The material used was obtained from HDPE blocks. Figure 13 shows the geometry of the frame deployed on the east site (approximately 100 m from the ocean and 20 m from the intercoastal/marina and an elevation of 12 ft above the MHWL with relation to the waterline observed at the dock), Figure 14 shows the setup prepared and deployed at the rail (higher elevation) facing the ocean. (Approximately 110 m from the ocean and at height of 6.6 m / 21’ 8” above the MHWL).

Figure 13. Wet candle setup deployed on the east site, at approximately 12 ft above MHWL.

Figure 14. Wet candle setup deployed on the railing at SeaTech (21 ft 8” above MHWL). Left drawing, center front view, right deployed.

2.2.2 – Frame for Deployment Next to Bridges or Close to Bridges of Interest.

Frames were prepared for deployment at two bridges. Figure 15 shows a picture of the frame used to deploy the wet candle on the palm tree, note the round geometry on one side. This palm tree is close to bridge #860160. The wet candle was deployed at an elevation approximately 13 ft to 14 ft above MHWL. Figure 16 shows the frame prepared for deployment at the Sebastian Inlet Bridge (A1A state park). The height is approximately 21 ft above MHWL for the candle deployed above an electrical box (see next section).

Figure 15. Setup for wet candle deployed on the palm tree next to bridge #860160.

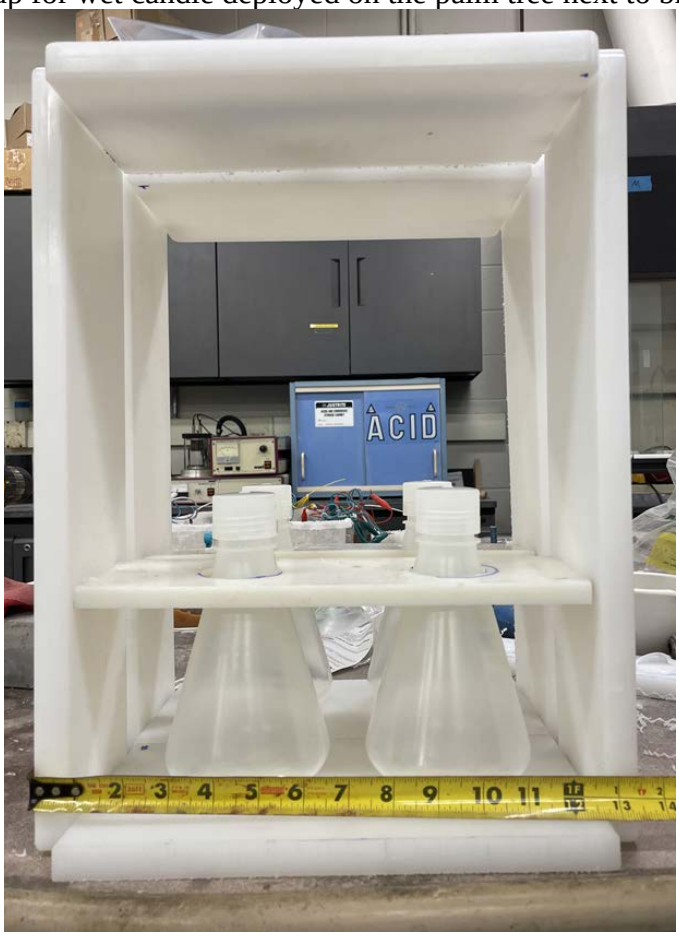

Figure 16. Wet candle setups deployed at Sebastian Inlet Bridge

2.2.3 – Solution used in the Wet Candles

The solution used in the wet candles consists of 400 ml of DI and 100 ml of glycerol [$CHOH(CH_2OH)_2$]. About 200 ml of the solution are added to each flask. One ml of octanoic acid [$CH_3(CH_2)_6COOH$] is added to each volumetric flask (part of the solution). A titration method based on the FDOT [65] method was used to measure chlorides. It is slightly modified to measure the chlorides in the solution upon retrieving the samples. This was done for consistency to the approach used in a previous project. [21]

2.2.4 – Deployed Setups

This section presents images of the wet candles either being deployed or while deployed. Figure 17 and Figure 18 show images of the two setups deployed at bridge #880005 called in here the Sebastian Inlet Bridge (on A1A – State Park). The wet candles shown in Figure 17 are at of about 24’ to 30’ above MHWL. Figure 19 shows a couple of images of the setup deployed on a palm next to Bridge #860160. Figure 20 shows the two wet candles deployed on the east site at FAU SeaTech.

Figure 17. Wet candle setup installed on the top rail of the bridge (Eastward facing)

Figure 18. Wet candle setup installed on top of electric box, fishing area (elevation approx. 21 ft MHWL). (Core – fresh patch – was obtained at 22 ft MHWL)

Figure 19. Pictures of the wet candle setup next to bridge #860160. Left closer view of the setup, right with bridge in the image

Figure 20. Picture of the two wet candle setups on the east site at SeaTech

An initial deployment took place for the setup hanging from the rail from February 20, 2020, to March 12, 2020, and the average chloride deposition was 1200 mg/m^{2}day, but due to Covid-19 no additional deployments took place during 2020. Once students were allowed back to FAU during Spring 2021, the setups described above were completed. The wet candle setups at SeaTech and the setup next to Bridge #860160 were first deployed on March 30, 2021. The two setups at Sebastian inlet bridge were first deployed on August 30, 2021. Twelve deployments have occurred, and the titrations have taken place eleven times.

2.3 – Field Visits

A visit to the Sebastian Inlet Bridge (Bridge #880005) took place June 15, 2021; cores were obtained from Bent 7 and Bent 8. The columns of Bent 7 are not immersed in water, but cores were obtained at elevations similar to those obtained in Bent 8. A second trip took place on August 2021 to Bridge #880005 to obtain cores at higher elevations at the Sebastian Inlet Bridge.

The bridge adjacent to FAU SeaTech (Bridge #860160) is suffering similar corrosion issues as the Sebastian Inlet Bridge (#880005) and was selected for coring. In the results section pictures are included that show the type of damage observed. The piles selected for coring did not suffer from cracks or spalls. The visit to Bridge #860160 took place during November 2021. The third bridge

identified was the Gandy Bridge in Tampa Bay westbound (#100585). Two bents were visited (one column from each was cored). Both cored columns showed cracks, but as it will be described later in one column the crack was only close to the surface. No other columns were found to have cracks from the visual inspection conducted from the boat. Support for all field visits was provided by FDOT-SMO, both for access to, and performing of the coring. The obtained cores were milled and then titration performed as per FDOT's method (but adjusted in some cases for the smaller mass per layer).

The obtained cores were in most instances milled, with thinner layers close to the exposed concrete surface. In some cases, the cores that showed cracks had to be sliced and then the concrete pulverized. The mass of each layer (after subtracting zip-lock bag mass) was recorded and used to estimate the layer thickness, assuming a nominal value for the concrete density. Not reflected in this report is the fact that in some cases not all concrete particles were recovered. Chloride analyses were then performed on the concrete powders for each layer. The total chloride amount was measured. The procedure used followed FDOT method [65], with two changes: the mass was reduced to 2 grams, and it was performed in duplicate. The results section shows in the plot the average concentration of the two measured values for each layer.

Chapter 3 – Results: Samples Exposed Outdoors at FAU SeaTech and from the Field

3.1 – Profiles of Samples Exposed at SeaTech

The profile plots show on the left axis the concentration in lb/yd^3 and on the right in kg/m^3, for Figure 21 to Figure 44 the x-axis is in cm, and for Figure 45 to Figure 57 the x-axis is in inches. Figure 21 to Figure 57 show the profiles of the tested samples. Figure 45 to Figure 57 shows also the profiles obtained at 28 months and 43 months. In general, most profiles showed that the concentration decreased as a function of depth (as would be expected for diffusion), but there were a few exceptions that will be discussed in sub-sections 3.1.1, 3.1.2,and 3.1.3. Several samples had more complex profile shapes, for the region closest to the exposed surface. In some profiles, the chloride concentration of the layers closest to the surface was significantly smaller than the concentration measured on subsequent layers. This is known as the skin effect.

3.1.1 – Profiles of 1CX Specimens (up to 110 Months)

The profiles of the 1CX mix samples (i.e., older samples with cross-section showing the aggregates during exposure, i.e., with no mortar layer) will be described first. The profiles of these samples include the concentration obtained at more than 5 cm (the core was cut approximately in half and a layer milled at this depth was used to estimate the Co value).

Figures 21 to 25 show profiles for mix 1C1 samples which contain only OPC and a w/cm of 0.41; Figures 26 to 29 show profiles for mix 1C2 samples, and Figures 30 and 31 show profiles for mix 1C3 samples. Figure 25 shows the profile of the sample that showed the largest chloride concentration (10 lb/yd^3), and this took place on layer 9. This sample was located on the east site (location closest to the ocean). The next largest concentration was observed on sample 1A2B-VF, which was close to the fence (on the west site), and during year one of exposure, the sample was immersed in brackish water during a storm. This immersion took place during the high tide and storm surge. The samples were moved farther from the fence several years ago. This sample showed a chloride concentration close to 6 lb/yd^3 on all layers (except for Co). The other samples showed smaller concentration, but the concentration changed modestly from those in layers 2 and 3 to the inner layers obtained (layers 10 to 12); see Figure 23 and Figure 24. The most pronounced chloride monotonic decay as a function of depth was observed on the sample that was exposed on the west site, in the horizontal position facing up; this profile can be observed in Figure 21. The maximum chloride concentration observed on mix 1C2 sample was close to 12 lb/yd^3 (Figure 10); a similar maximum concentration was also observed on the mix 1C3 sample (contains fly ash and silica fume); see Figure 31. Both samples were exposed at the east site. The profile shapes are quite different as can be observed from Figure 29 (FA) and Figure 31 (FA+SF). The other three 1C2 samples (Figures 26 to Figure 28) had profiles in which the maximum chloride concentration was observed close to the surface and was between 4 and 5 lb/yd^3.

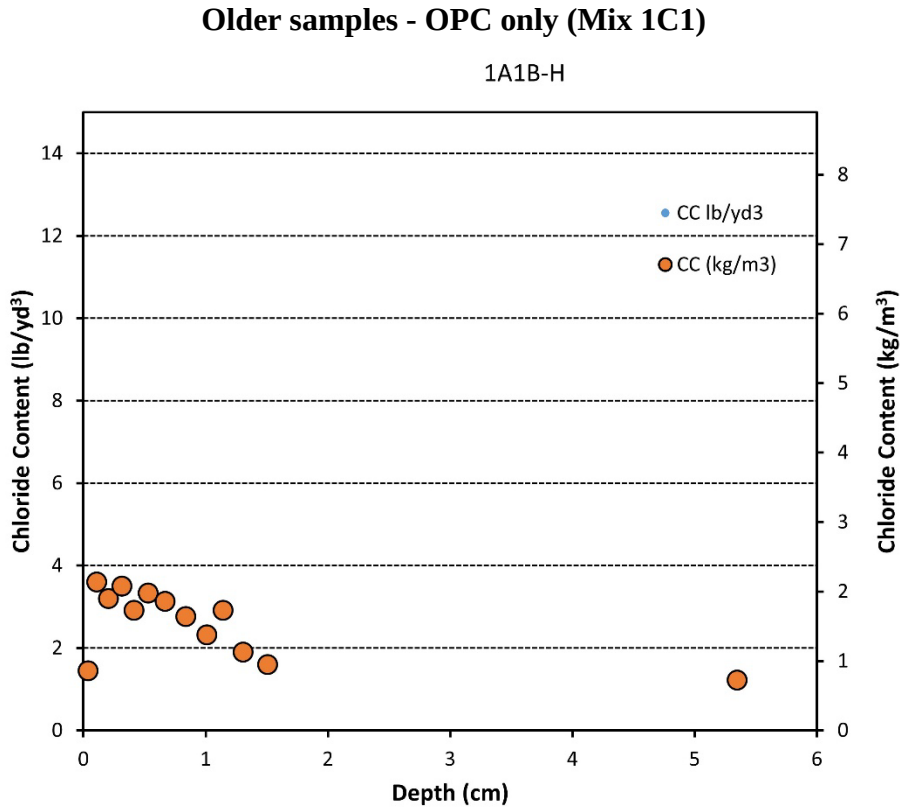

Figure 21. Chloride profile sample exposed at west site – horizontal facing up (mix 1C1)

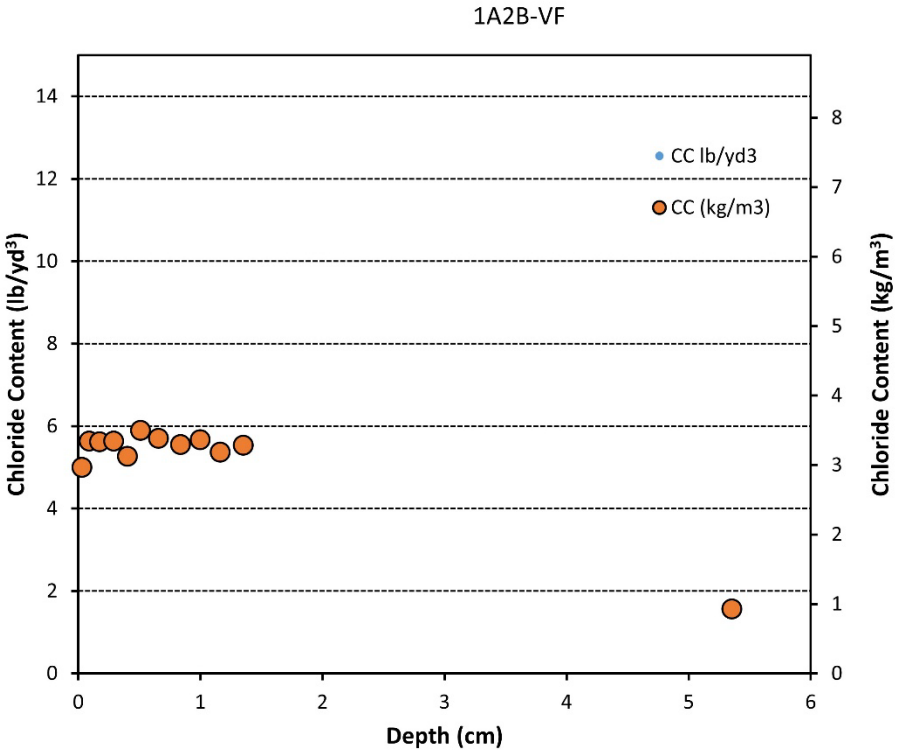

Figure 22. Chloride profile sample exposed next to fence at west site – vertical (mix 1C1)

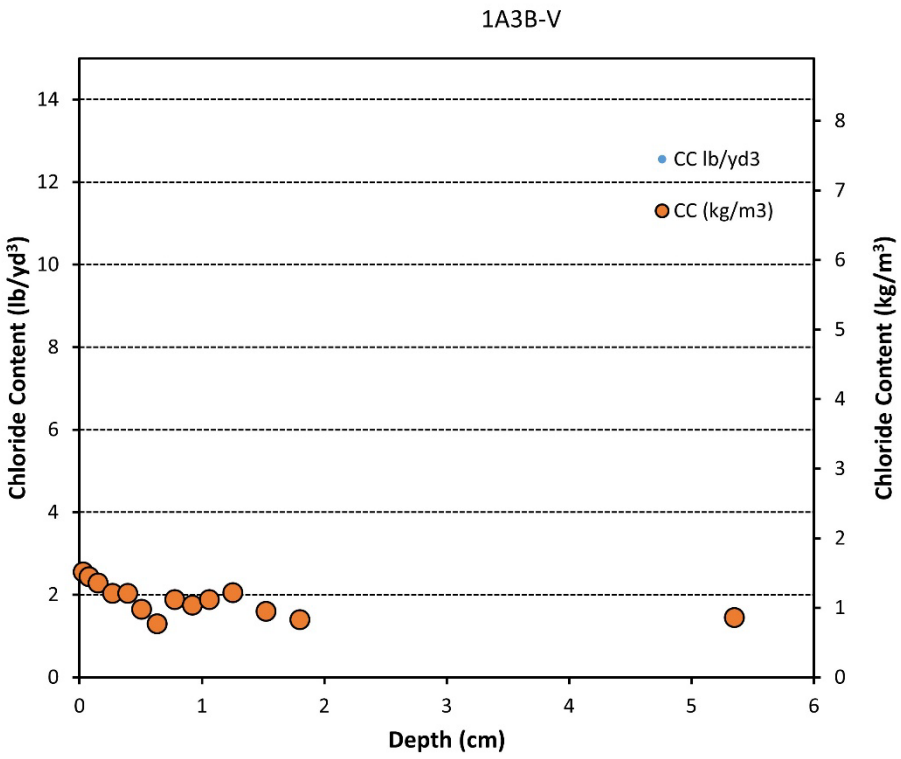

Figure 23. Chloride profile sample exposed at west site – vertical (mix 1C1)

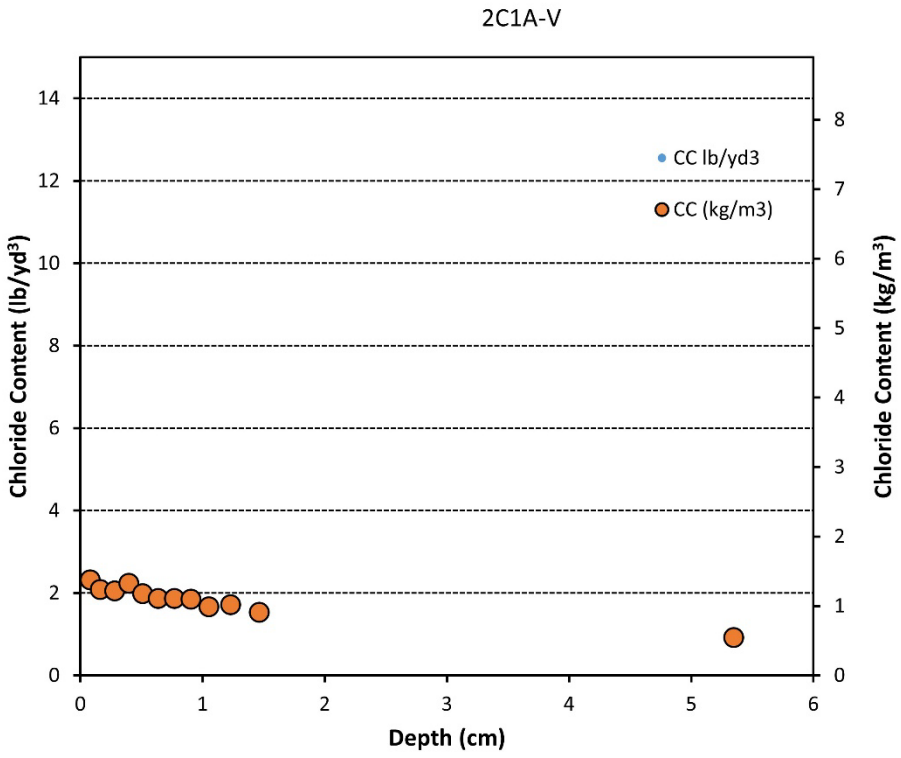

Figure 24. Chloride profile sample exposed next to fence at west site – vertical (mix 1C1)

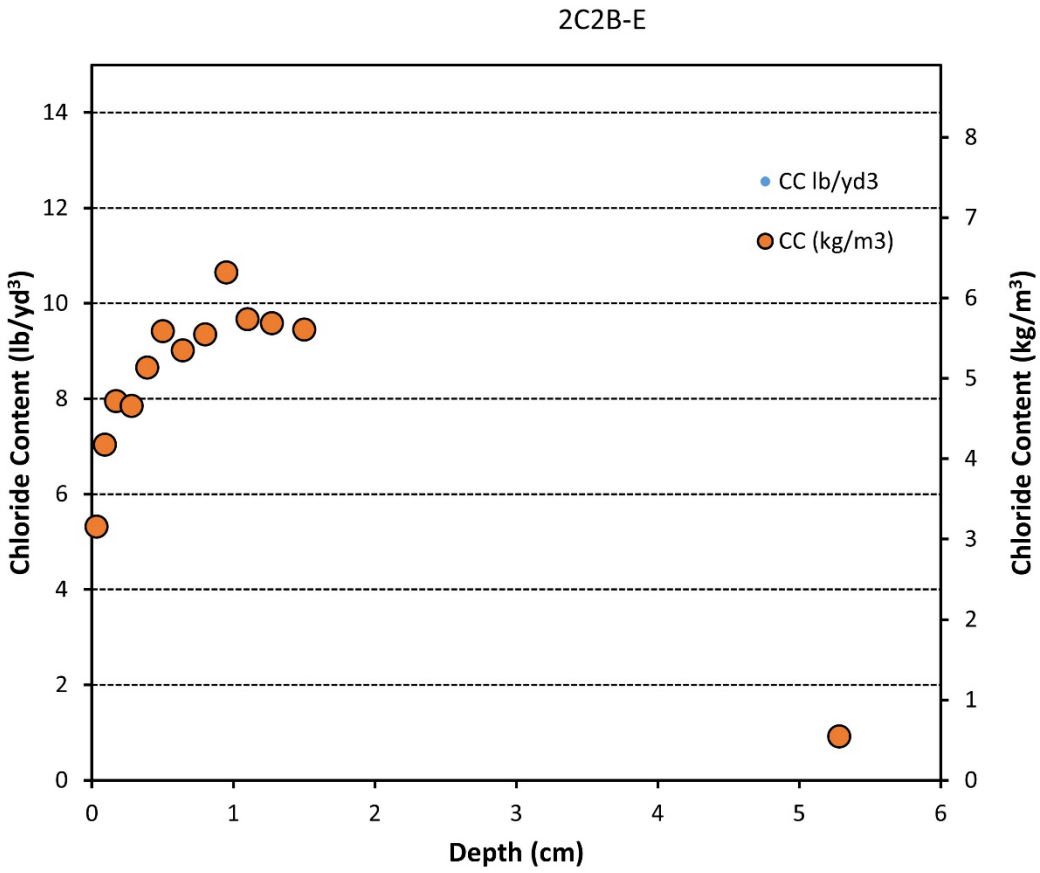

Figure 25. Chloride profile sample exposed at east site – horizontal (mix 1C1) facing the ocean

Older samples – OPC and 20%Fly ash (Mix 1C2)

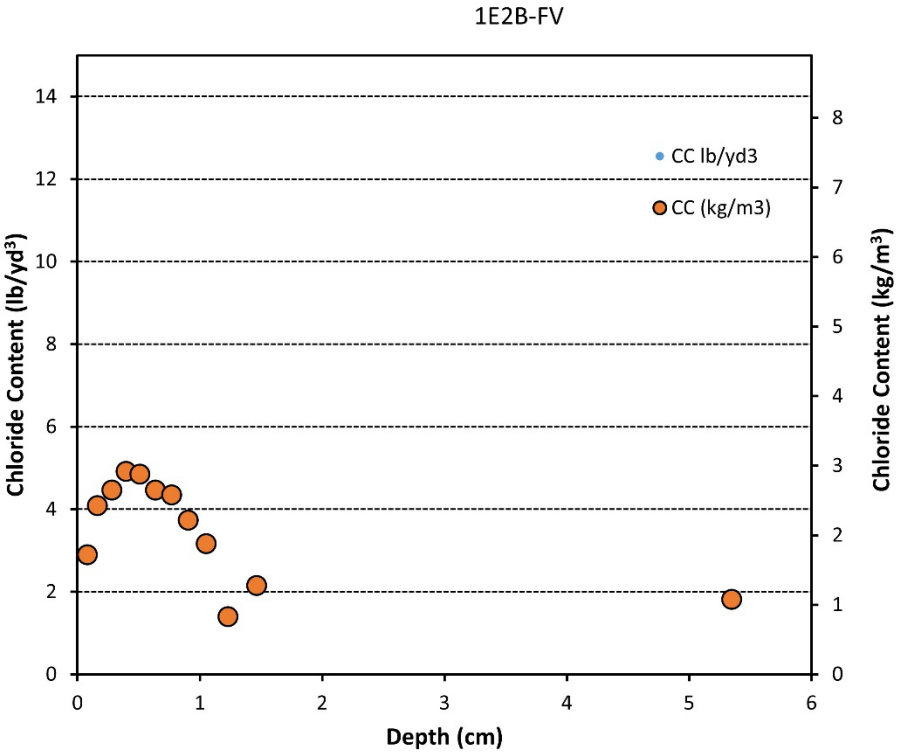

Figure 26. Chloride profile sample exposed next to fence at west site – vertical (mix 1C2)

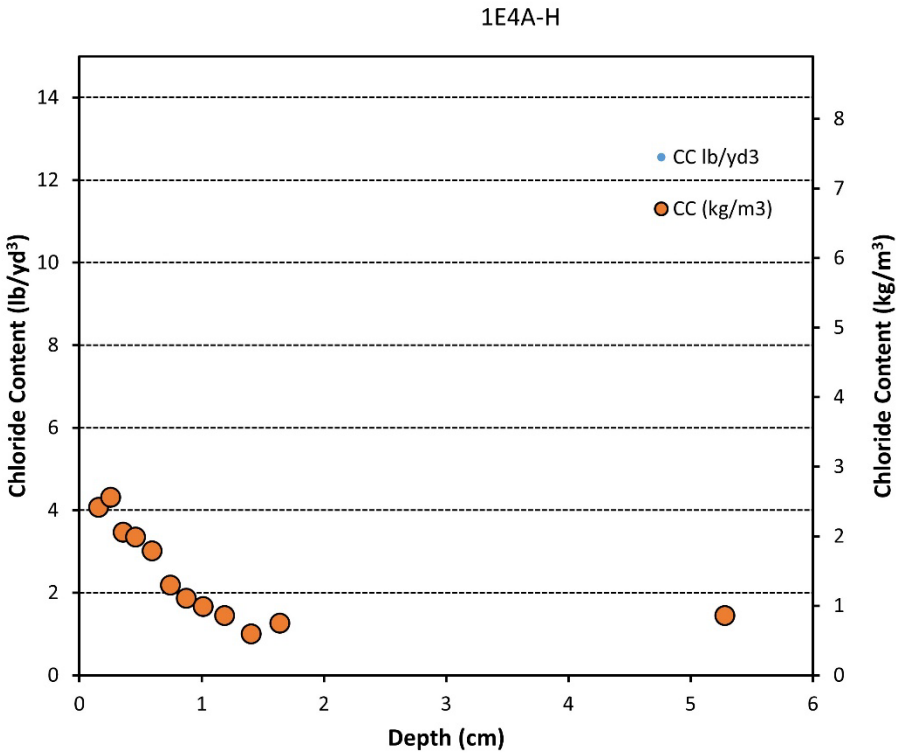

Figure 27. Chloride profile sample exposed at west site; horizontal – facing up (mix 1C2)

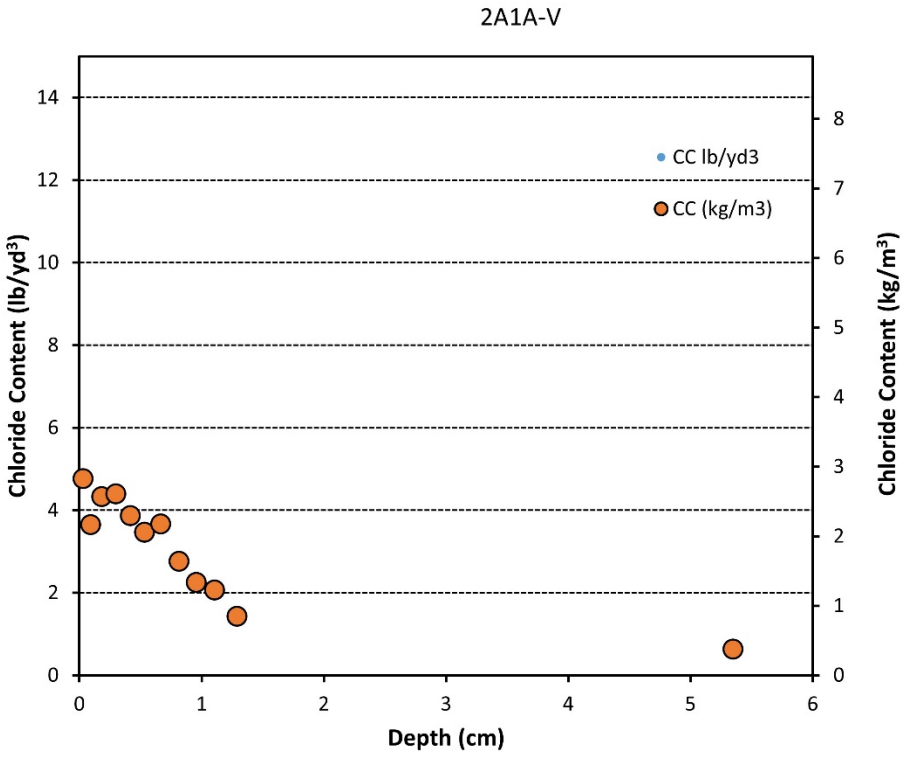

Figure 28. Chloride profile sample exposed at west site – vertical (mix 1C2)

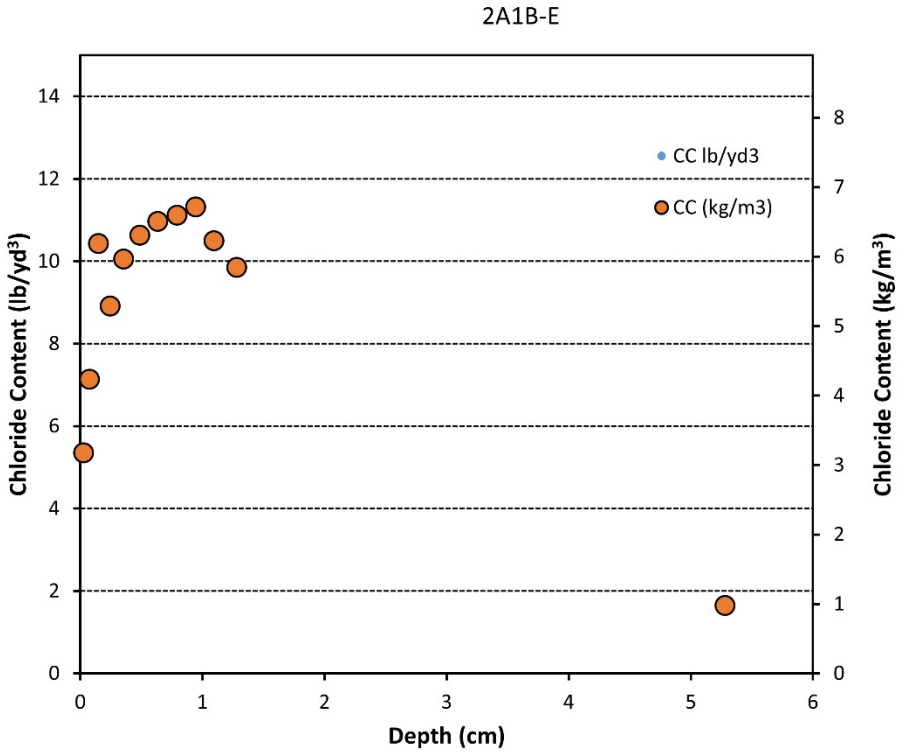

Figure 29. Chloride profile sample exposed at east site (mix 1C2), facing the ocean.

Older samples – OPC and 20%Fly ash and 8% silica fume (Mix 1C3)

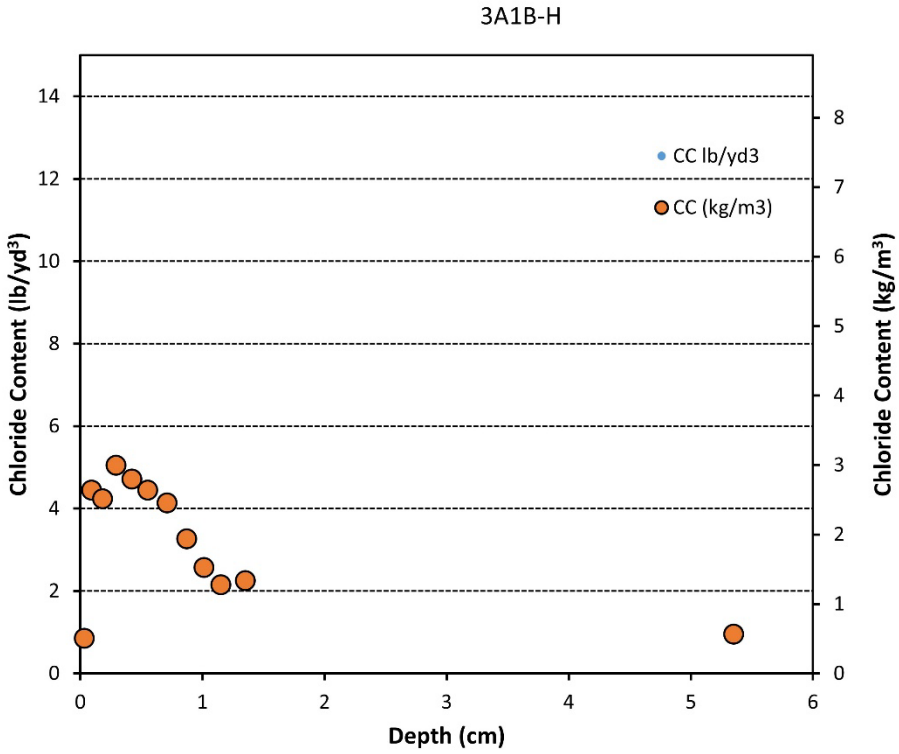

Figure 30. Chloride profile sample exposed at west site – horizontal facing up (mix 1C3)

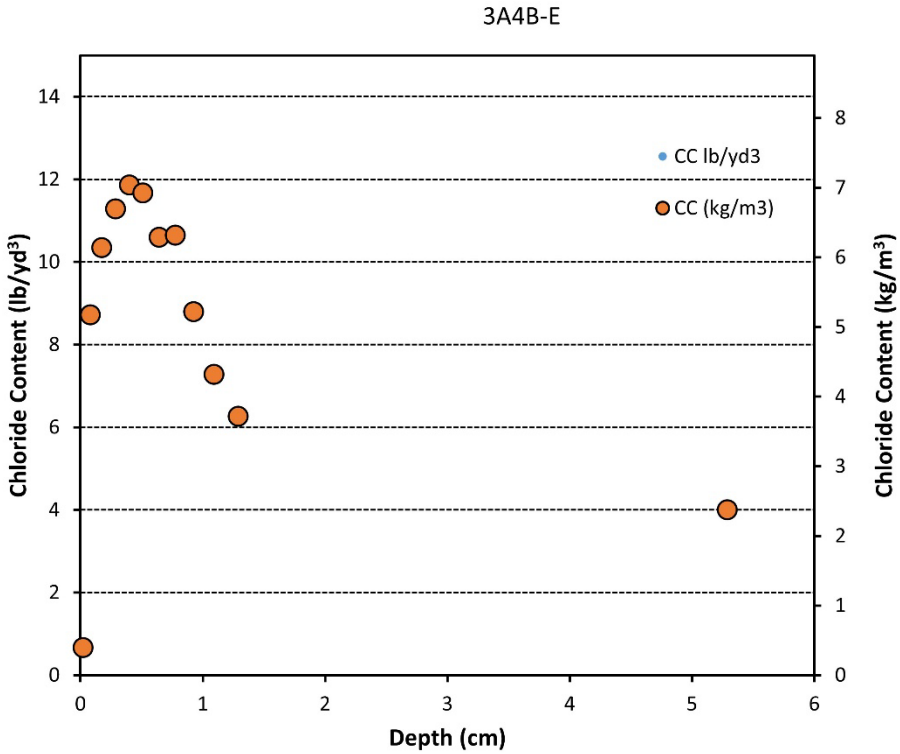

Figure 31. Chloride profile sample exposed at east site – horizontal facing the ocean (mix 1C3)

3.1.2 – Profiles of DCL Specimens Exposed at the West Site (up to 108 months)

These samples were exposed with surface facing up**.** Figures 32-44 show the chloride profiles corresponding to the DCL samples exposed at the west site. The maximum chloride concentration was observed on samples DCL1-C (Figure 32) and DCL7-C (Figure 38) and was observed in layers close to the surface. In the case of DCL1-C the maximum chloride was 8 lb/yd^3, and on sample DCL7-C, it was approximately 7.5 lb/yd^3. Rain events might wash off some of the chloride close to the surface. The horizontal position (facing up) of the samples might also have allowed these samples to dry faster and be exposed to the sun for longer periods of time than samples in the vertical orientation. Lower moisture content on the section closest to the exposed surface might have limited the amount of chloride that penetrated. Most profiles show that the chloride concentration at the inner layer was less than 0.5 lb/yd^3 (in some cases this is layer 22 for those milled in 0.5-mm increments, but in others is layer 12-14 for those milled at 1-mm increments). In a few cases, the measured concentration at the inner layer was close to 2 lb/yd^3, e.g., DCL-2 (Figure 33) and DCL-3 (Figure 34).

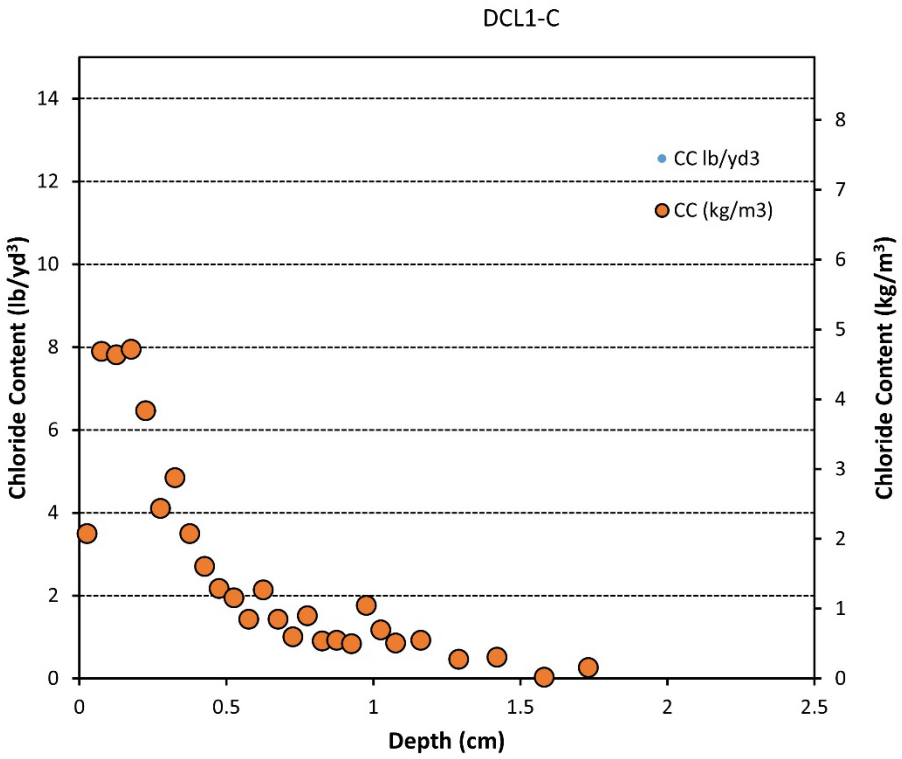

Figure 32. Chloride profile for sample DCL1-C

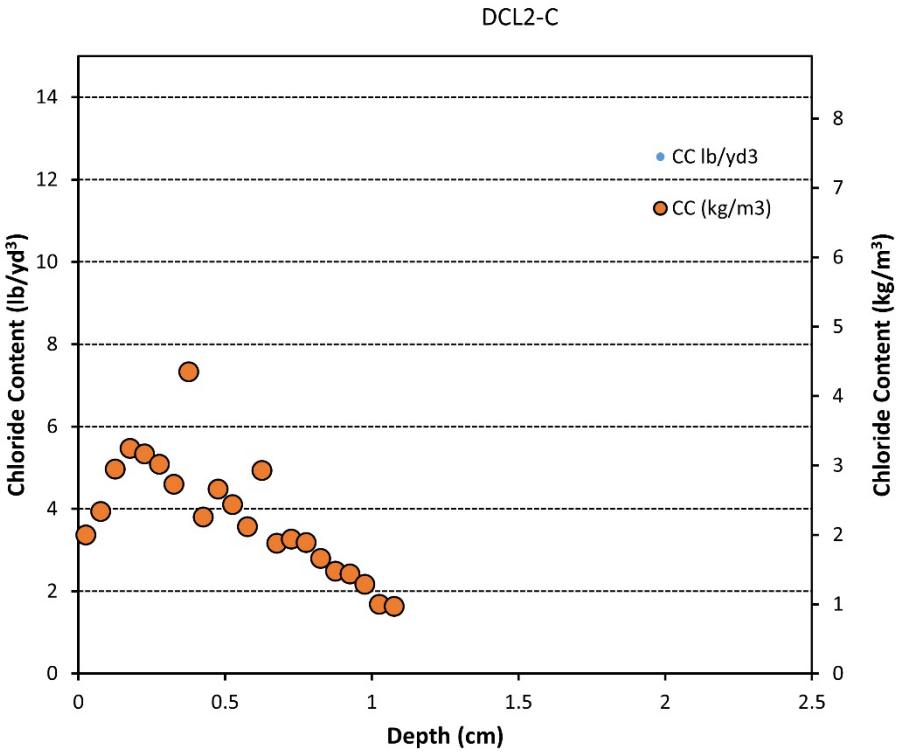

Figure 33. Chloride profile for sample DCL2-C

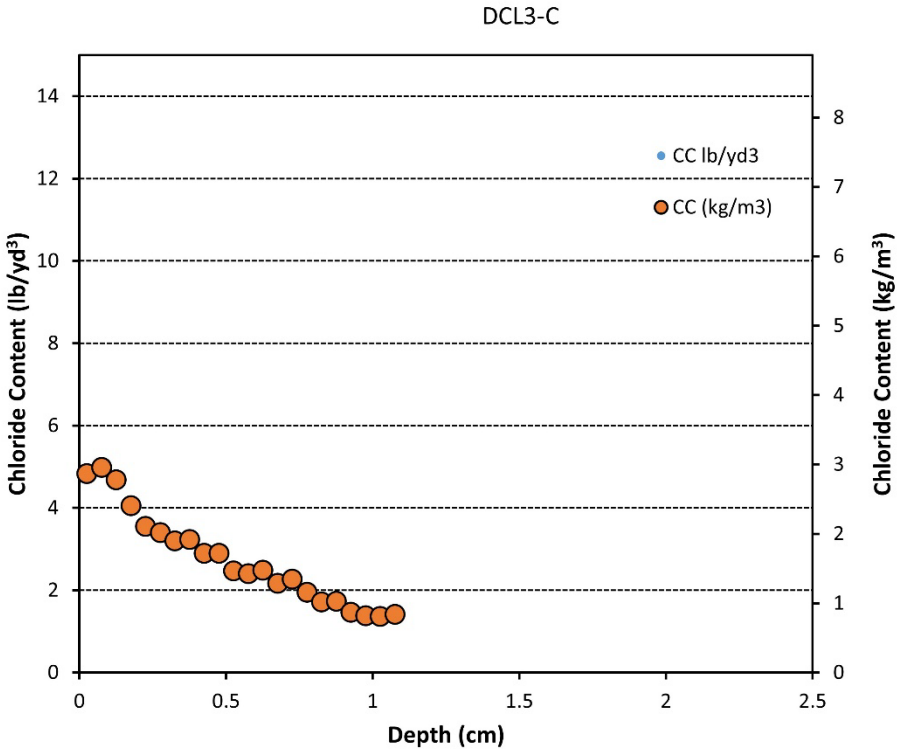

Figure 34. Chloride profile for sample DCL3-C

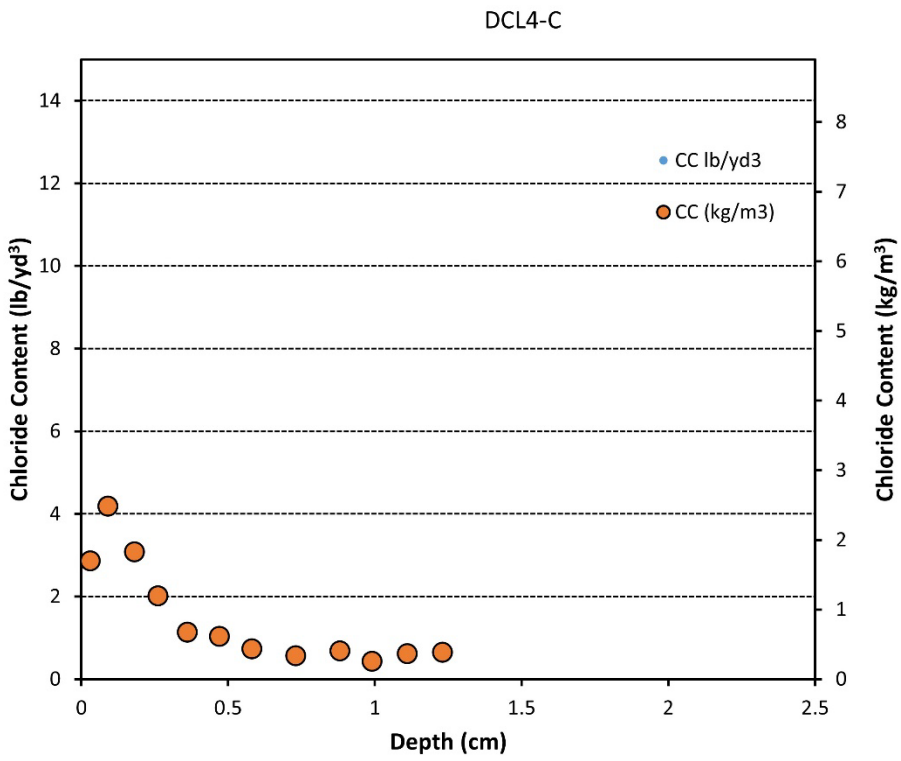

Figure 35. Chloride profile for sample DCL4-C

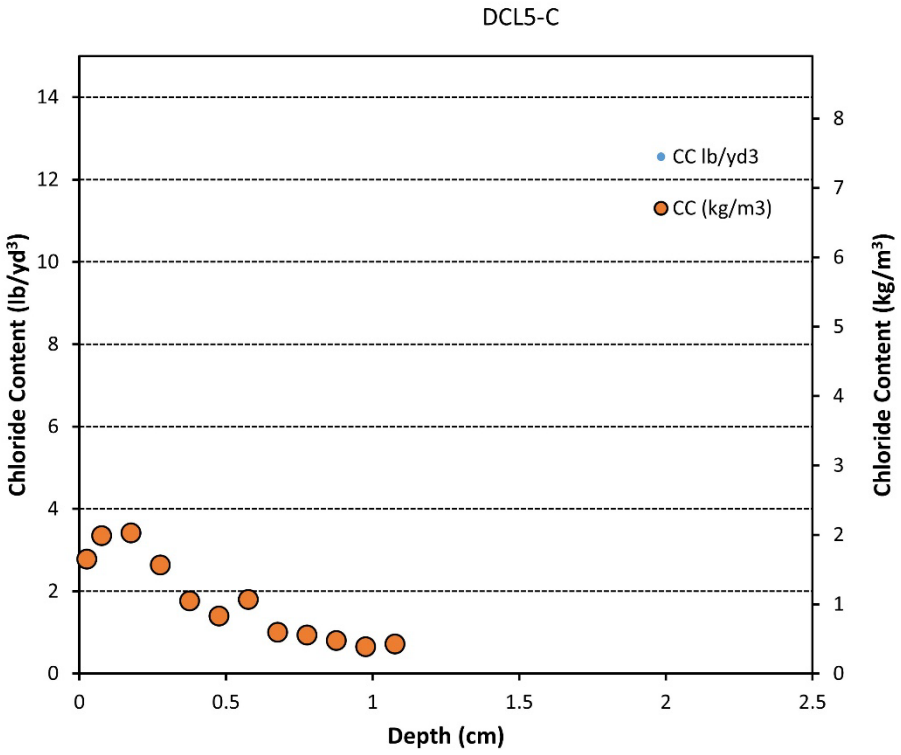

Figure 36. Chloride profile for sample DCL5-C

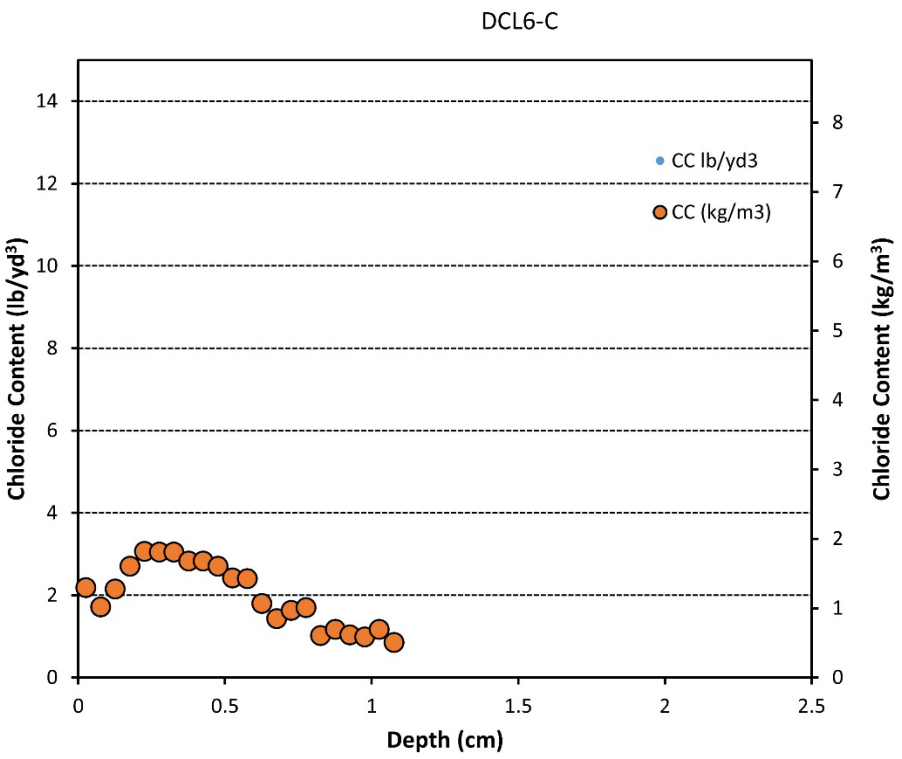

Figure 37. Chloride profile for sample DCL6-C

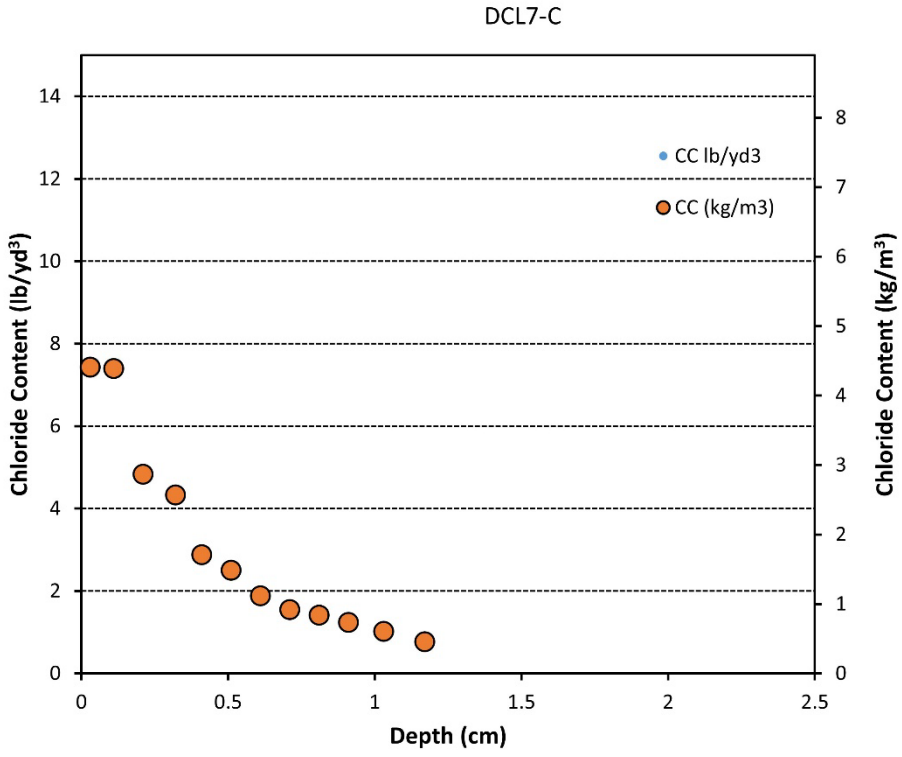

Figure 38. Chloride profile for sample DCL7-C

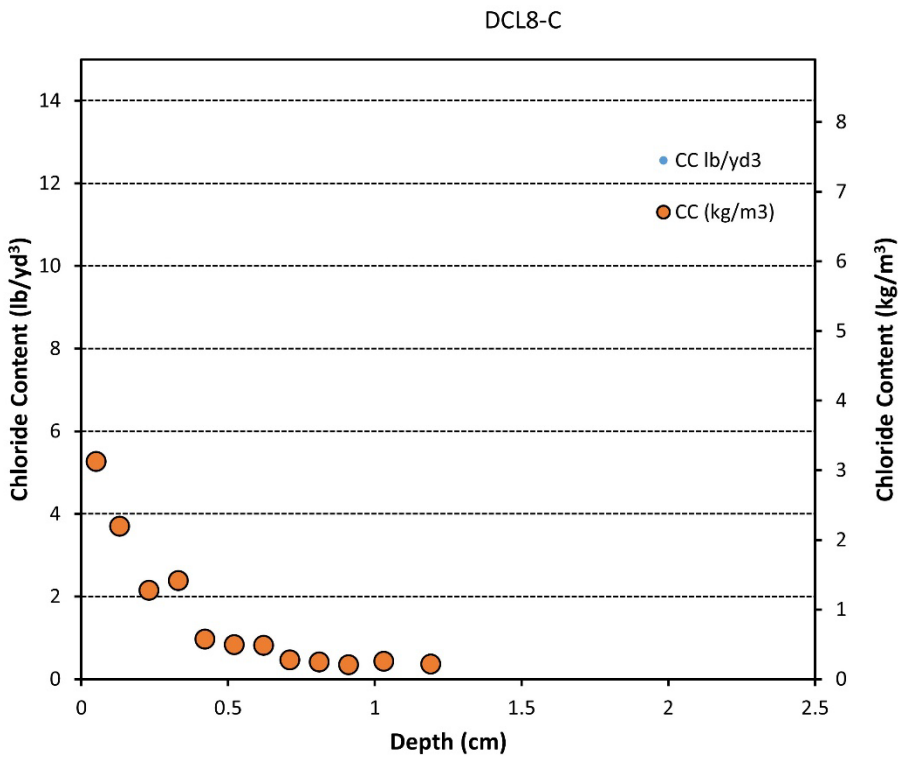

Figure 39. Chloride profile for sample DCL8-C

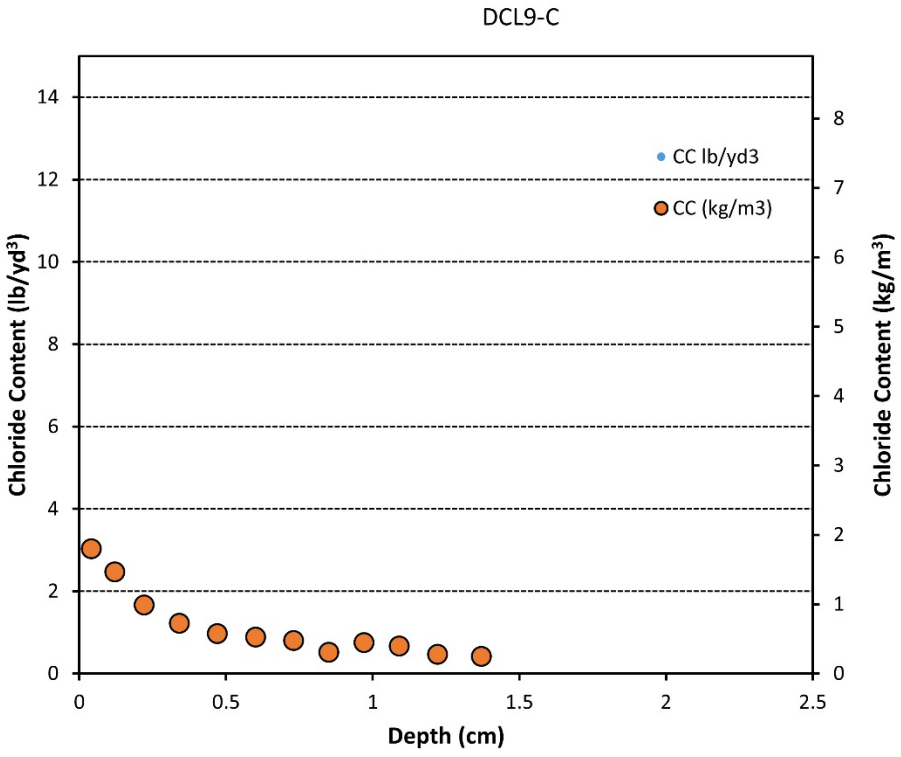

Figure 40. Chloride profile for sample DCL9-C

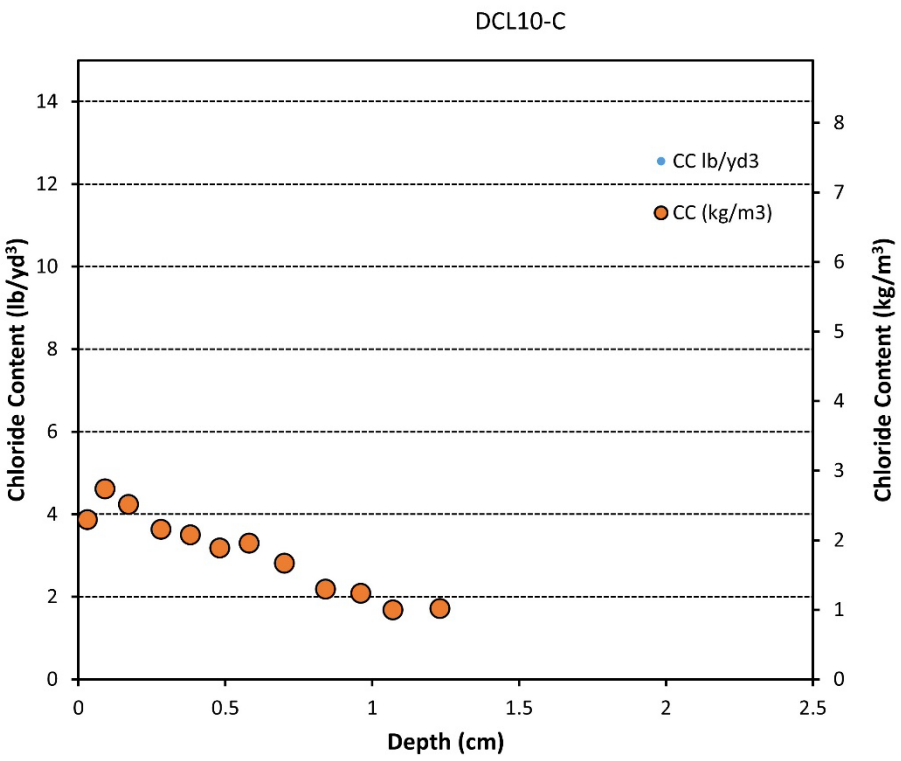

Figure 41. Chloride profile for sample DCL10-C

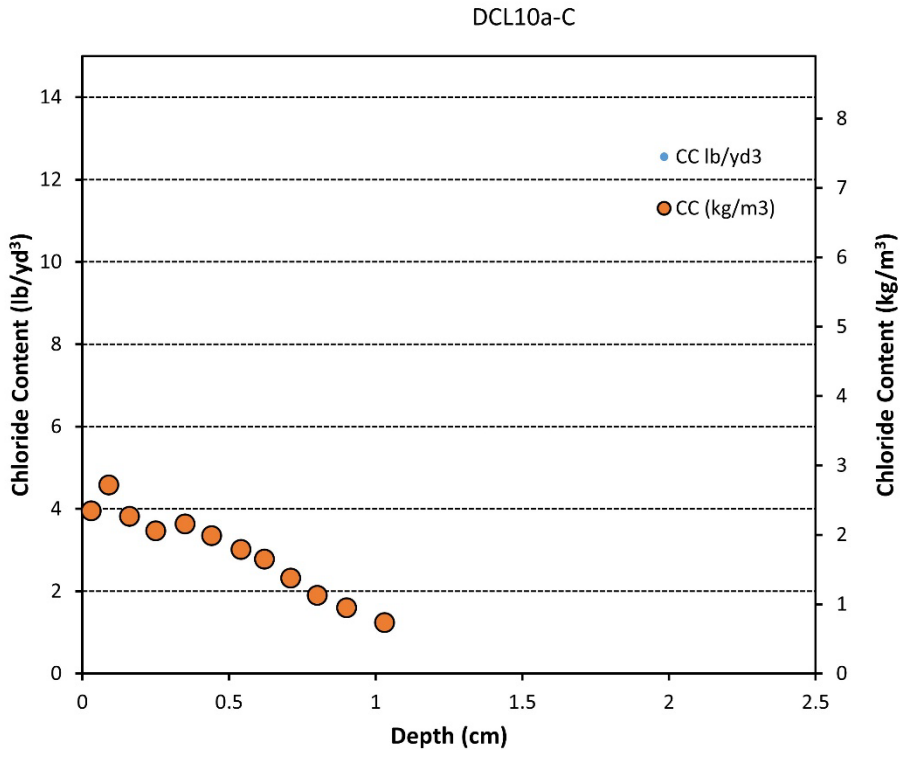

Figure 42. Chloride profile for sample DCL10a-C

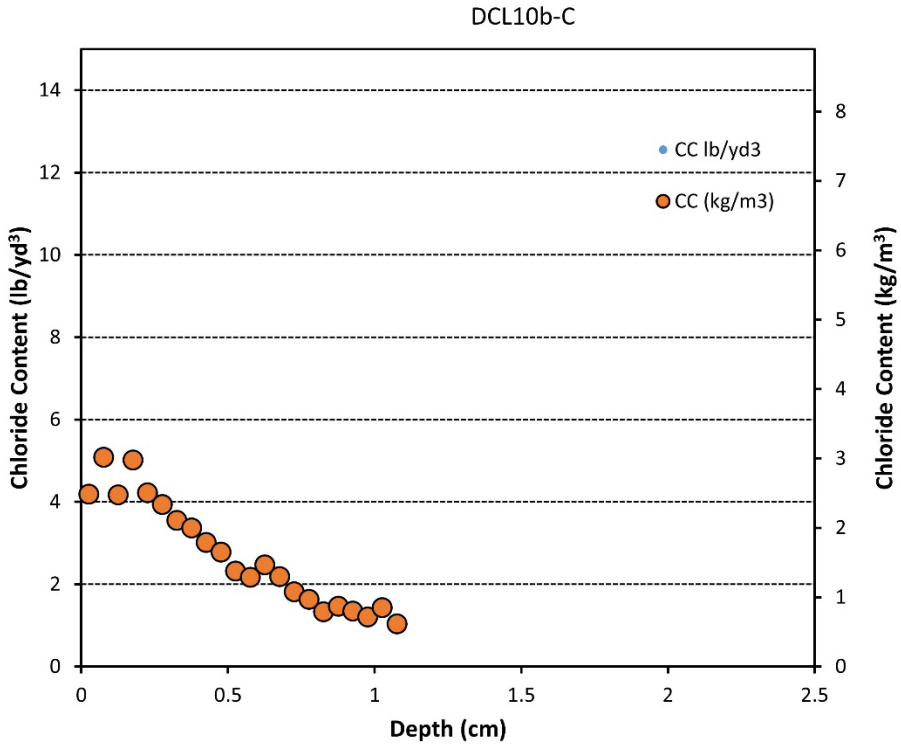

Figure 43. Chloride profile for sample DCL10b-C

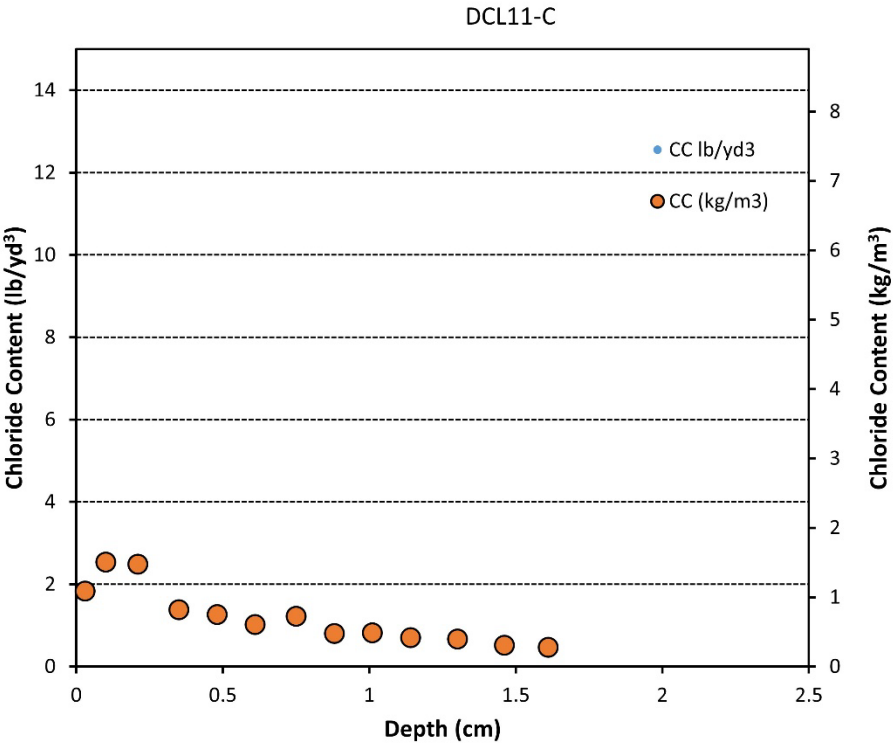

Figure 44. Chloride profile for sample DCL11-C

3.1.3 – Profiles of DCL Specimens Exposed at the East Site (up to 108 months)

This section shows profile plots for the samples exposed at the east side. These samples had the exposed surface facing the ocean. Each plots shows the profiles after 28 (24) months, 43 months, and 108 months. The x-axis shows the depth in inches. Most figures show that the chloride that penetrated increased with time. The profiles suggest that more chlorides penetrated into these samples when compared to corresponding samples exposed at the west site. The closer proximity to the ocean likely allowed a higher loading of chlorides when the ocean spray particles reached these samples. The maximum chloride concentration (14 lb/yd^3) was observed on the profile of sample DCL-3F. The profile for sample DCL10a appears not to follow typical diffusion. It is not clear why this happened (it is possible that electrode failure took place, or operator error occurred, or the sample suffered to seawater spray). In a few cases the deeper layers appear to have a higher concentration; it is believed that for the samples that were observed there was an error (these layers were not included on the D_{app} calculations). It is possible that when a sample had to be setup again to obtain additional layers, these layers might have been contaminated if the profiler was not placed exactly above the initial center.

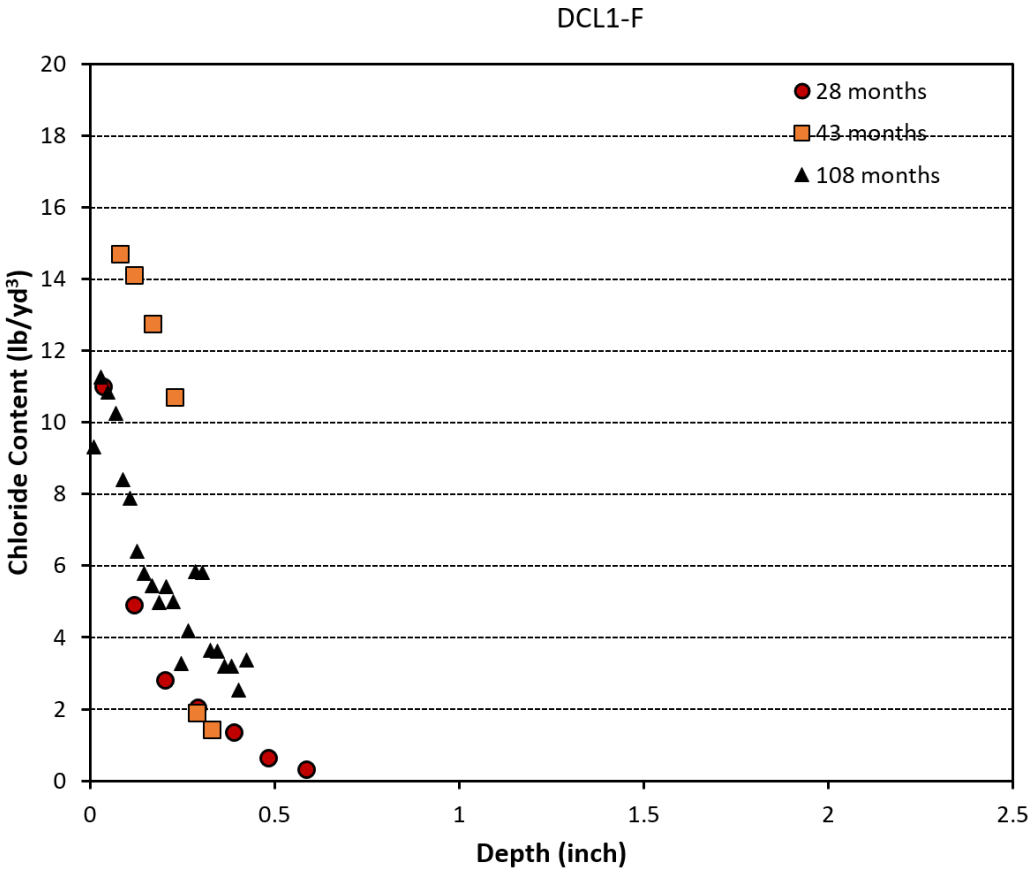

Figure 45. Chloride profile for sample DCL1-F

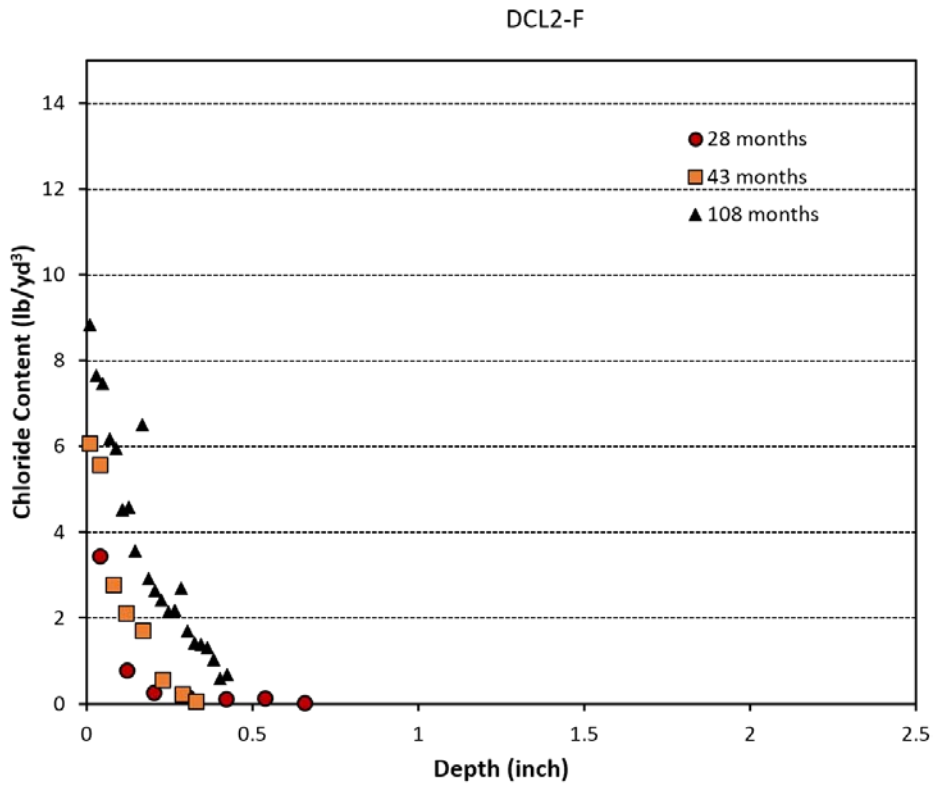

Figure 46. Chloride profile for sample DCL2-F

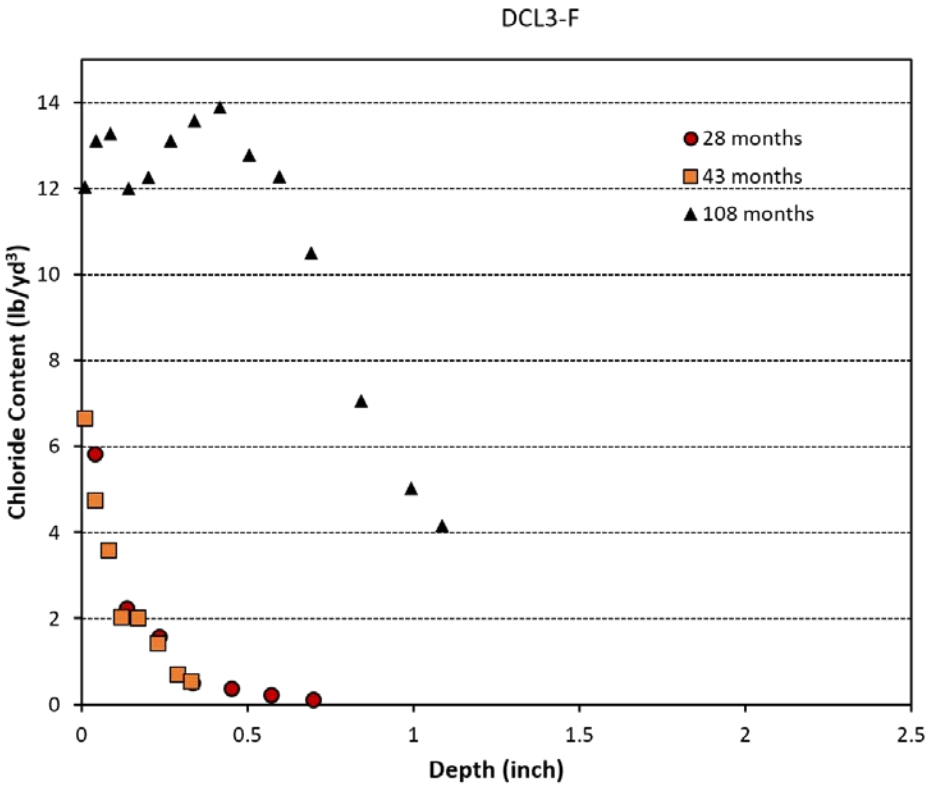

Figure 47. Chloride profile for sample DCL3-F

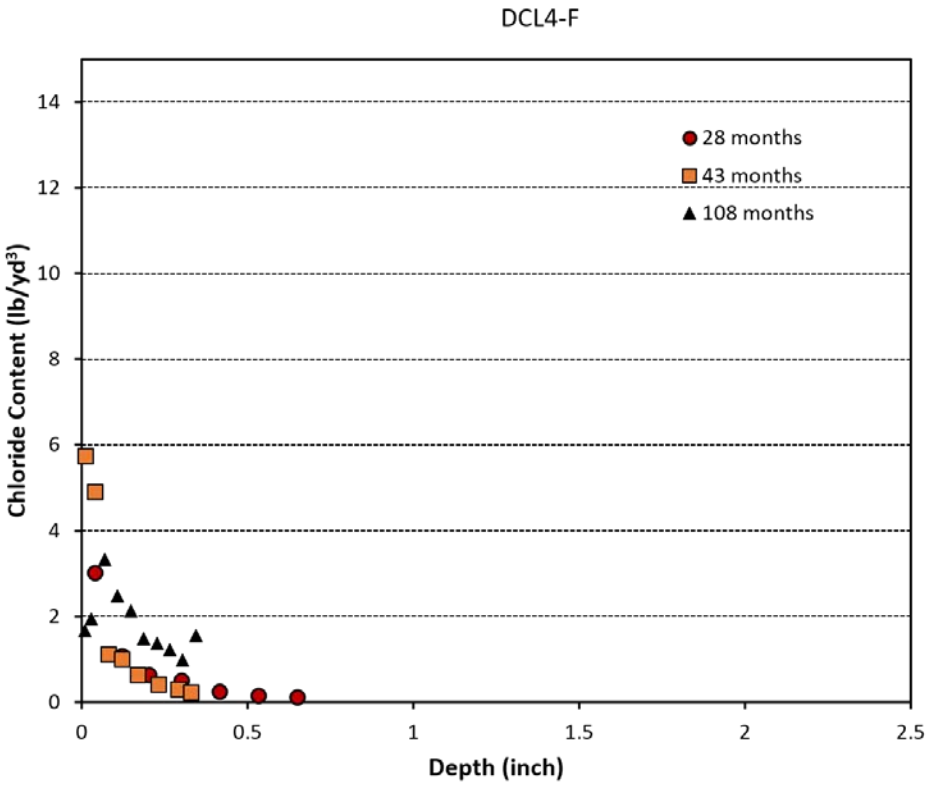

Figure 48. Chloride profile for sample DCL4-F

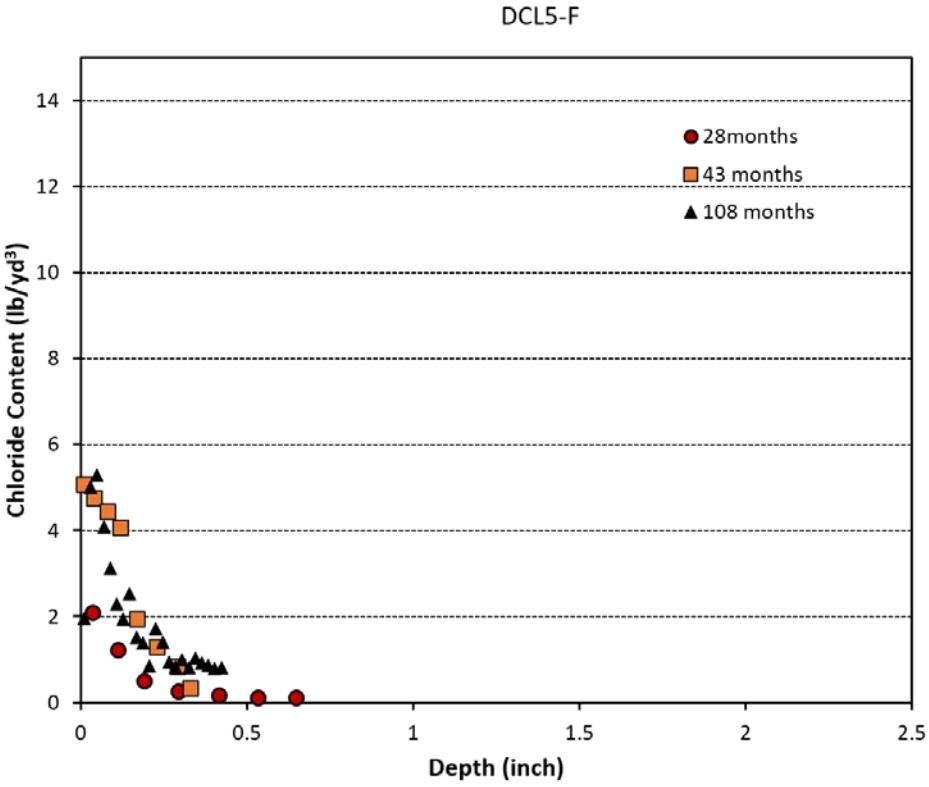

Figure 49. Chloride profile for sample DCL5-F

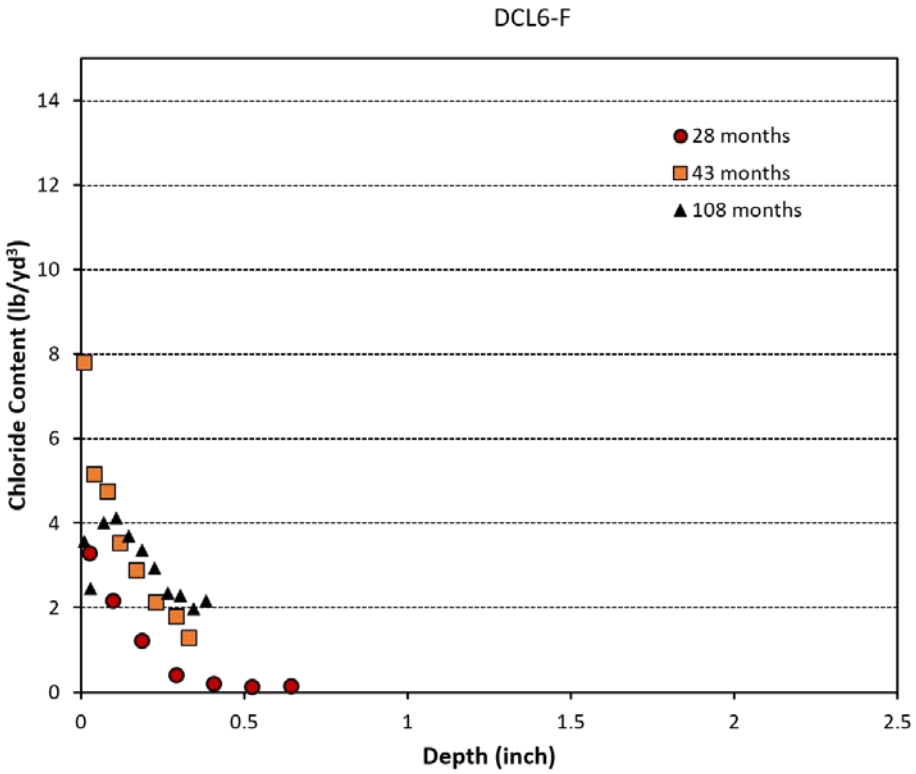

Figure 50. Chloride profile for sample DCL6-F

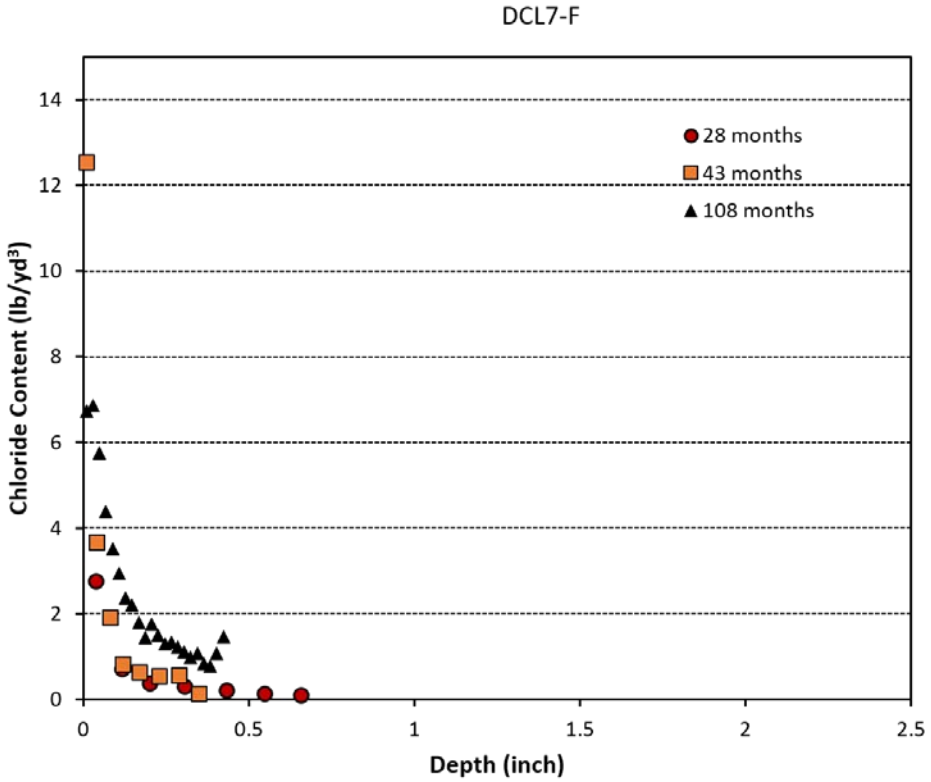

Figure 51. Chloride profile for sample DCL7-F

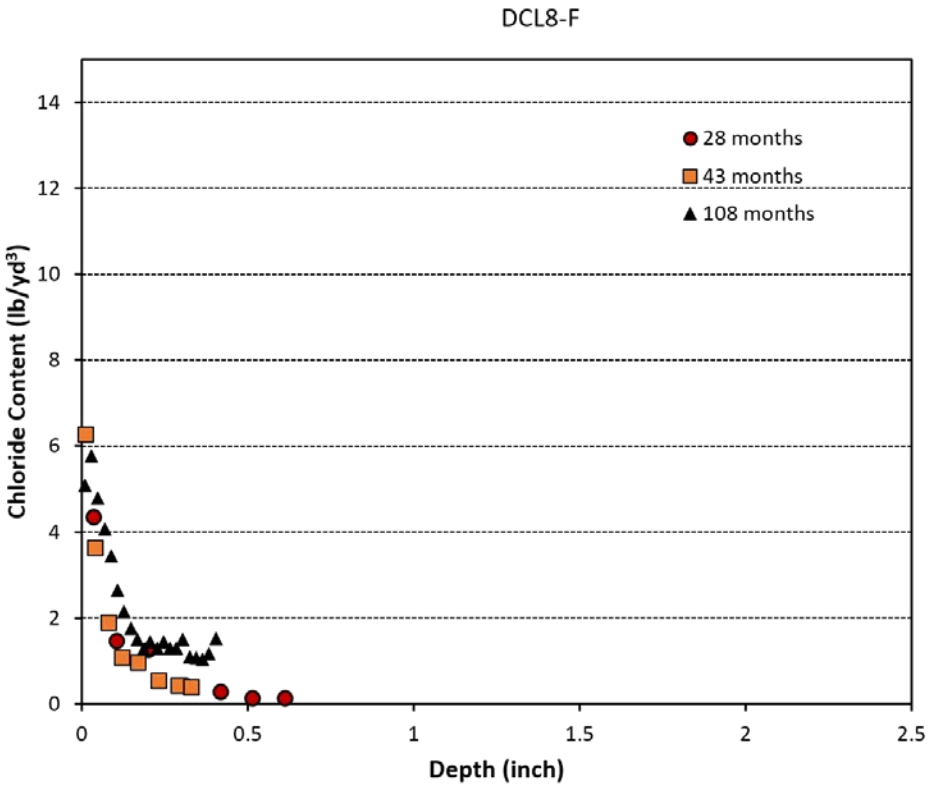

Figure 52. Chloride profile for sample DCL8-F

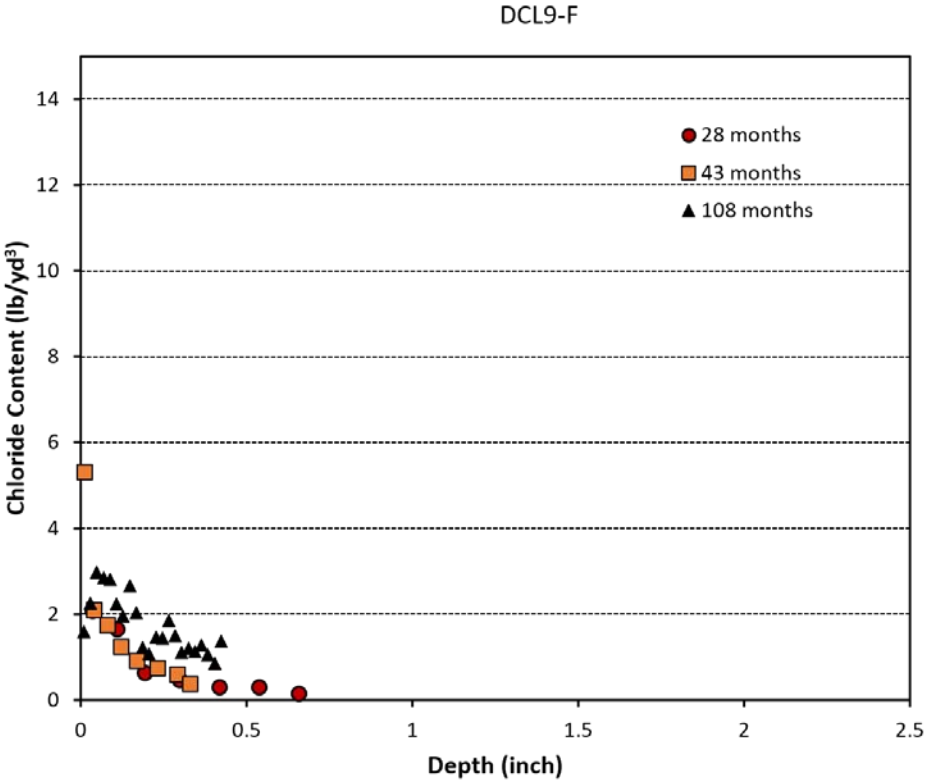

Figure 53. Chloride profile for sample DCL9-F

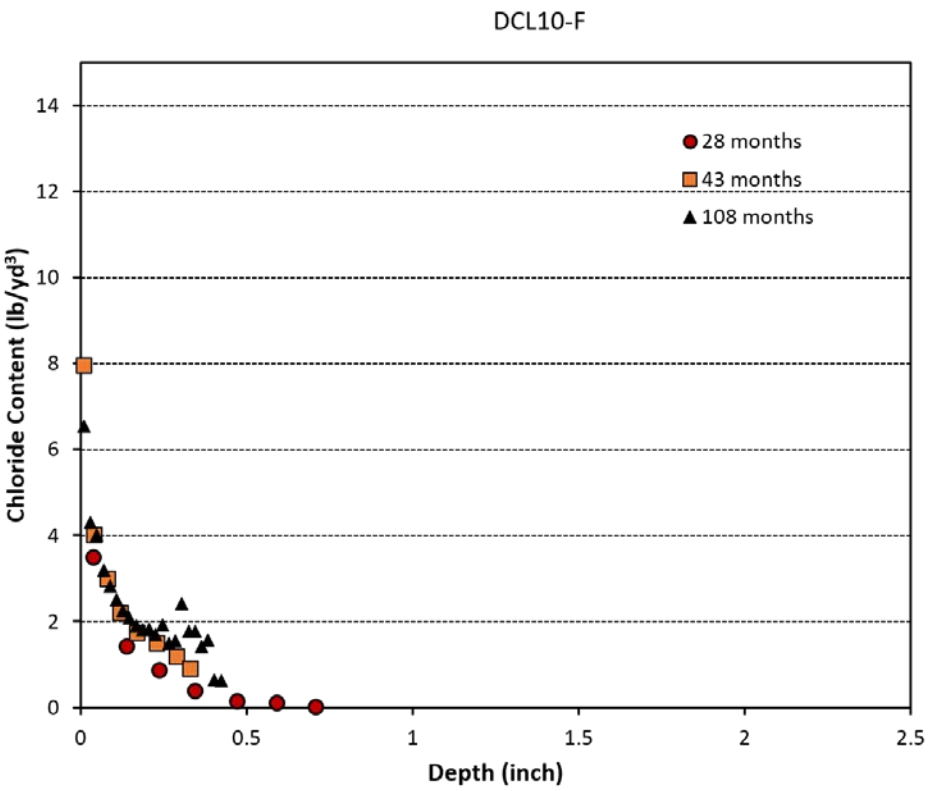

Figure 54. Chloride profile for sample DCL10-F

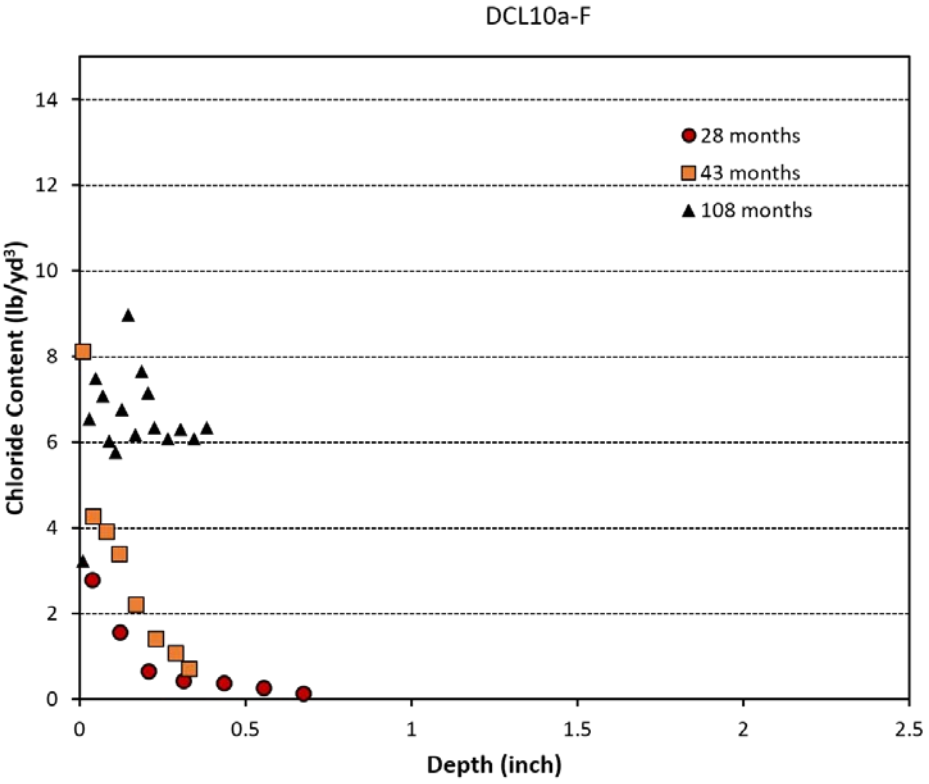

Figure 55. Chloride profile for sample DCL10a-F

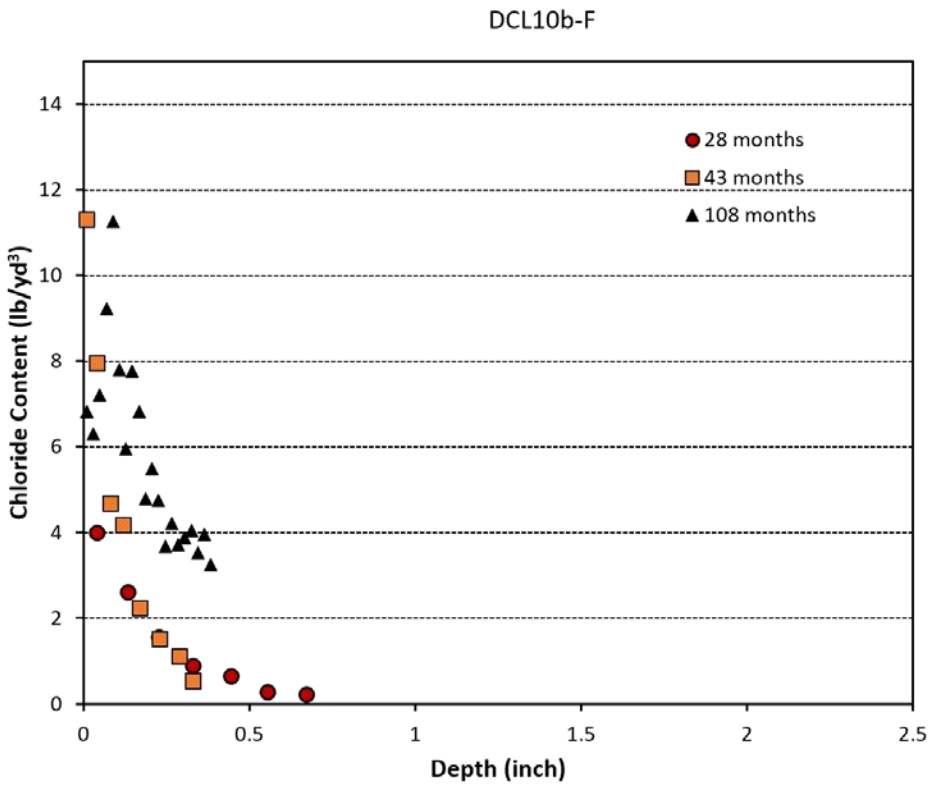

Figure 56. Chloride profile for sample DCL10b-F

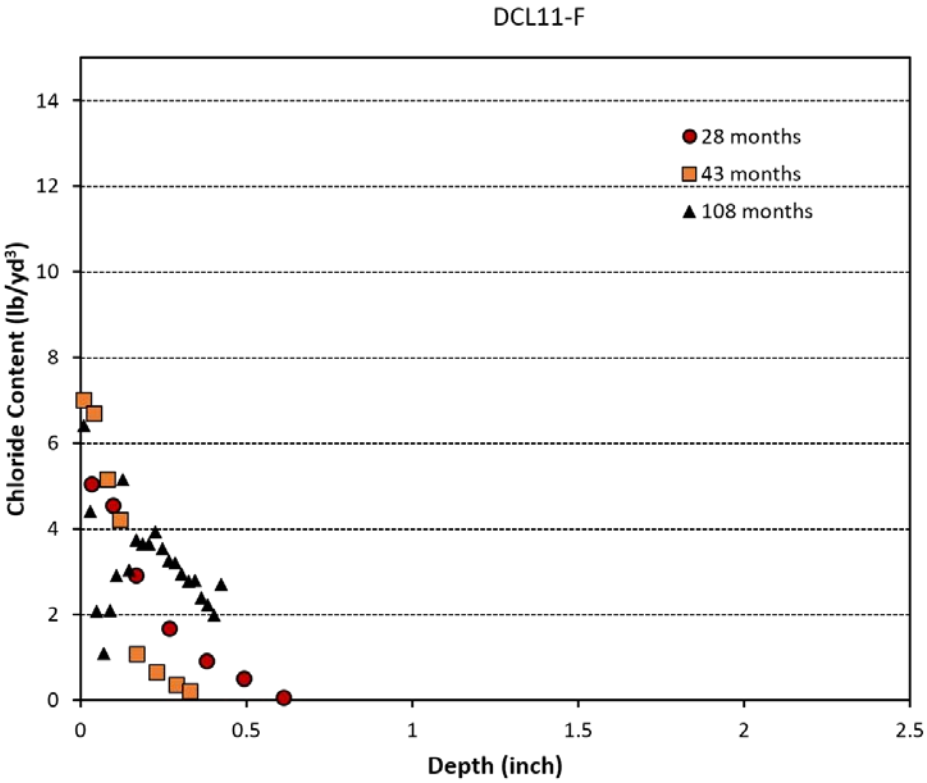

Figure 57. Chloride profile for sample DCL11-F

3.2 – Field Visits

3.2.1 – Coring

As indicated in the experimental section, two visits were made to the Sebastian Inlet Bridge (State Park) along A1-A. This Bridge #880005 was visited in June 2021, and cores were obtained up to 20’ above MHWL during the first trip. Figure 1 shows selected images taken during the first visit.

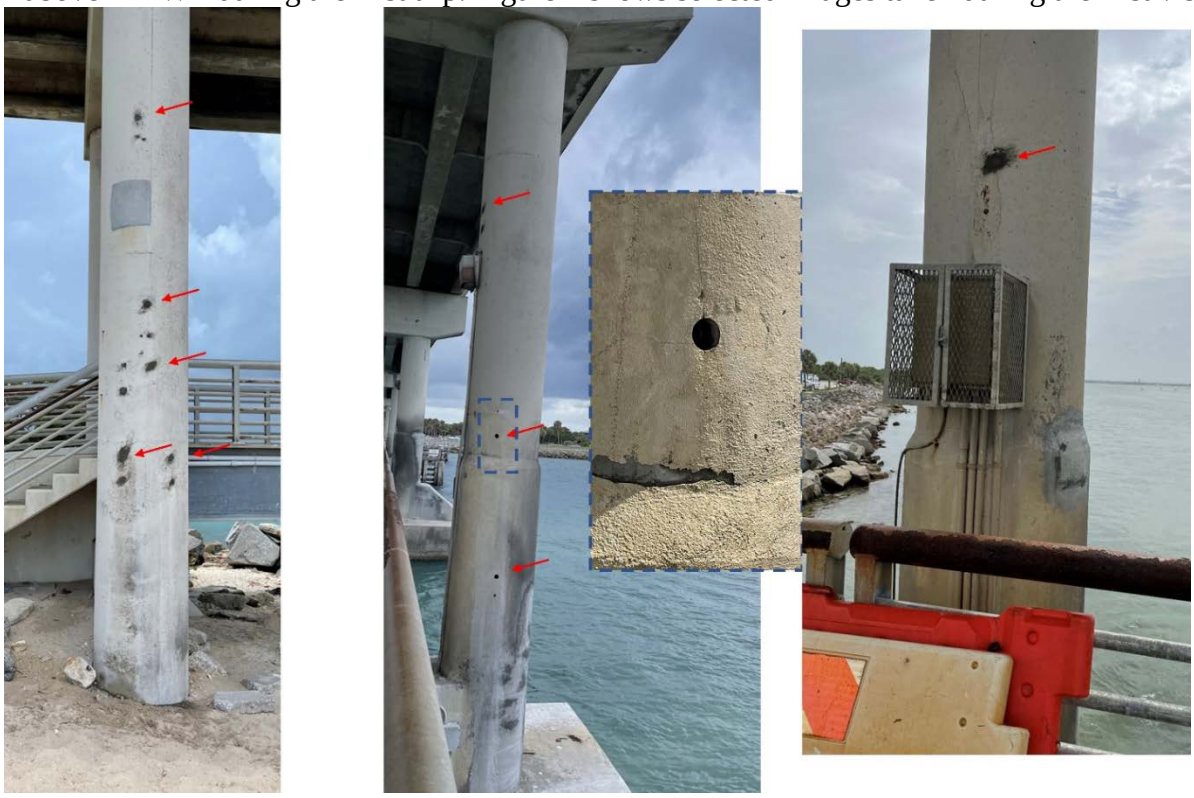

Figure 58. Figures shows the locations at which cores were obtained during trip 1.

The red arrows in Figure 1 show the sites where the cores were obtained. Bent 7 east column is shown on the picture on the left; five cores were obtained. Two cores were obtained at 11’ above MHWL, one along a crack and the second with no crack. Four cores were obtained from Bent 8. Three cores were obtained from the east column and one core from the west. A cathodic protection jacket is present on the region where the core at the lower location was obtained. In this case the core had two sections one for the outer jacket and one for the original concrete. Figure 2 shows a picture of this core. Figure 3 shows the view after removing the cores on Bent 8; whereas Figure 4 shows a view after removing the cores on the cored column in Bent 7. Note that in Figure 3 two of the cored locations had cracks that reach farther in, similarly in Figure 4 one of the cores in Bent 7 showed a crack (at 11’ above MHWL), left image.

Figure 59. Shows a core obtained on bent 8 east column at 12 ft above MHWL (with CP jacket)

Figure 60. Pictures after removing cores in bent 8, left two images from east column, right west column.

Figure 61. Pictures after removing cores in bent 7.

For the second visit to the Sebastian Inlet Bridge (bridge #880005) a snooper truck was used to access the upper part of the selected columns. The cores were taken as follows: “Two cores per column. The east side of column was cored (easier to access and is preferred). One core was taken near the cap and a second core approximately 5 feet lower. The coring was performed on 4 columns (Columns 8, 10, 11 & 13) for a total of 8 cores.” No pictures were taken during the second coring trip. No rebar was reached on these cores.

In November 2022, the bridge next to SeaTech was visited, Bridge #860160. The upper part of most piles in Bent 4 show spalls. Figure 5 shows a couple of images of Bent 4 Pile 4-1 to Pile 4-5 from the north and south. The cored pile in Bent 4 was Pile P-4-6 which is the eastern most pile and did not show any spalls. The north and south face were cored (two cores per face). Pile 3-6 was also cored, in this case along the east face. Figure 6 shows pictures after removing the cores on this bridge. The three images show that the reinforcement was reached in all cases. Cores were obtained from regions with the thicker cover.

Figure 62. Bent 4, left image shows north face (piles P4-5 to P4-1), right image south face (P4-5 to P4-1)

Figure 63. Pictures taken after removing the cores at the dridge in Dania Beach (bridge #860160).

During March 2022, the Gandy Bridge (westbound) #100585 was visited. Two columns were identified to have cracks from those inspected. Figure 7 shows the columns cored, on the left the south column in Bent 237 and on the right, the north column, in Bent 223. Figure 8 shows images after removing two cores in Bent 237. It shows that the reinforcement was reached, and in this case, epoxy coated rebars are the used reinforcement. Note the crack on the image on the left. Figure 9 shows two images of a site cored in Bent 223. In this case the image on the left show that there was a crack, but it was at most 0.5" deep.

Figure 64. Gandy bridge, images show the two columns that were cored at the Gandy Bridge.

Figure 65. Bridge #100585, pictures taken after removing the cores, showing that reinforcement was reached

Figure 66. Bridge #100585, images taken after removing core obtained about 5 ft above MHWL, crack was only close to the surface.

Typical Images of Cores.

This section shows pictures of selected cores; additional images of the obtained cores can be found in Appendix A. Figure 10 shows pictures of a core with cracks. This core was obtained from the Sebastian Inlet Bridge (Bridge #880005). The corrosion products are orange and brown. Figure 11 shows a core obtained from Bent 8 west column (Sebastian Inlet Bridge) and cored on the east face. This core also shows a crack along the length of the core. Most of the cores had no cracks.

Figure 67. Core obtained column 7 at 11 ft above MHWL

Figure 68. Core obtained bent 8 west column at 22 ft above MHWL

3.3 – Chloride Profiles of Cores from the Field Visits

3.3.1 – Profiles Sebastian Inlet Bridge (Bridge # 880005)

Figure 69 and Figure 70 show the chloride profiles obtained in column 7 and column 8 respectively, from the cores obtained during the first visit to Bridge #880005. Figure 71 and Figure 72 show the profiles obtained from cores taken close to the of the columns.

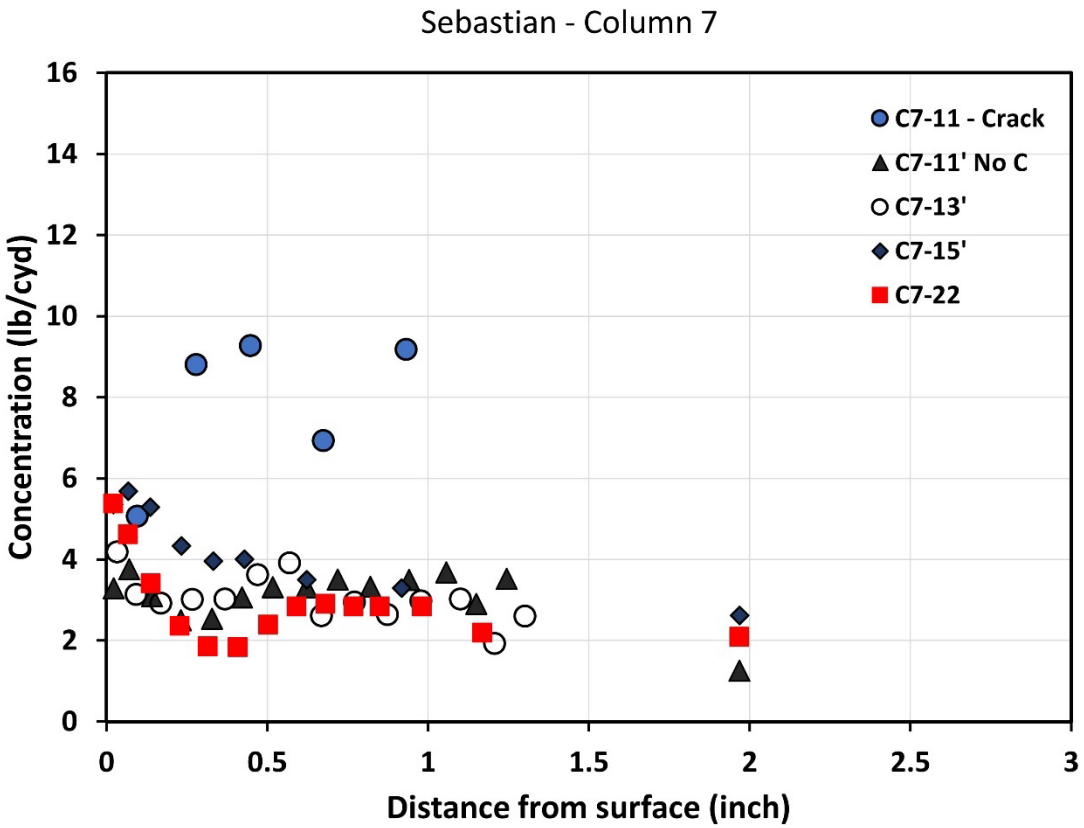

Figure 69. Chloride profiles – column 7 (Bridge # 880005)

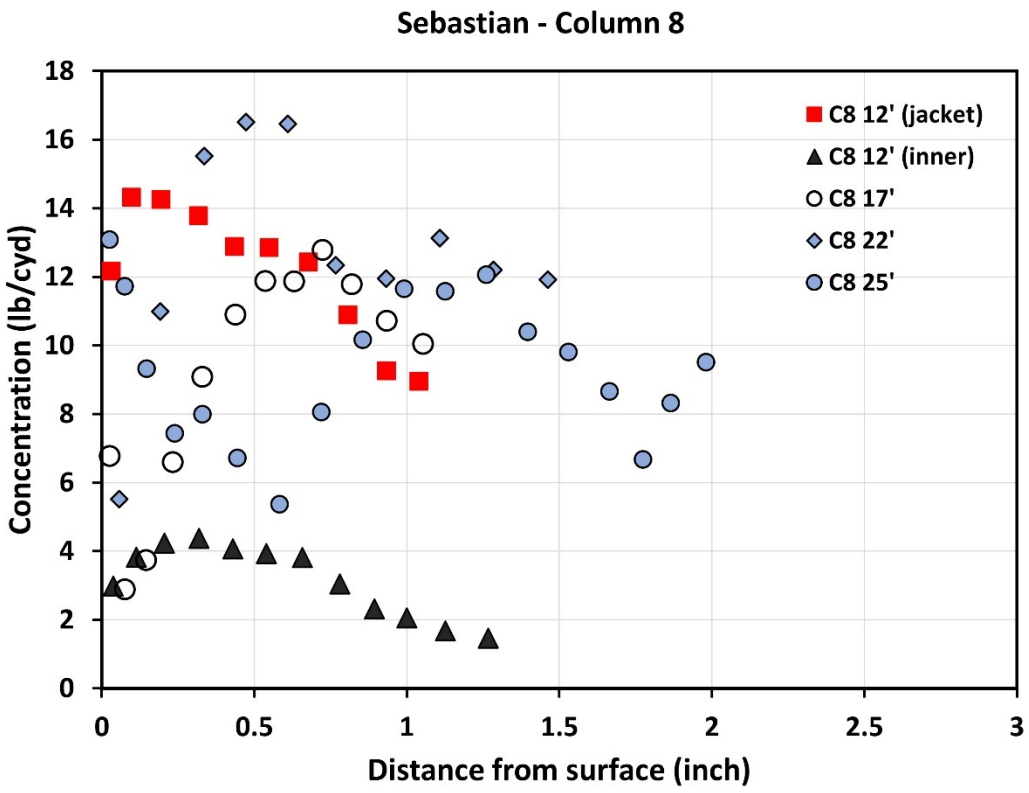

Figure 70. Chloride profiles – column 8 (Bridge # 880005)

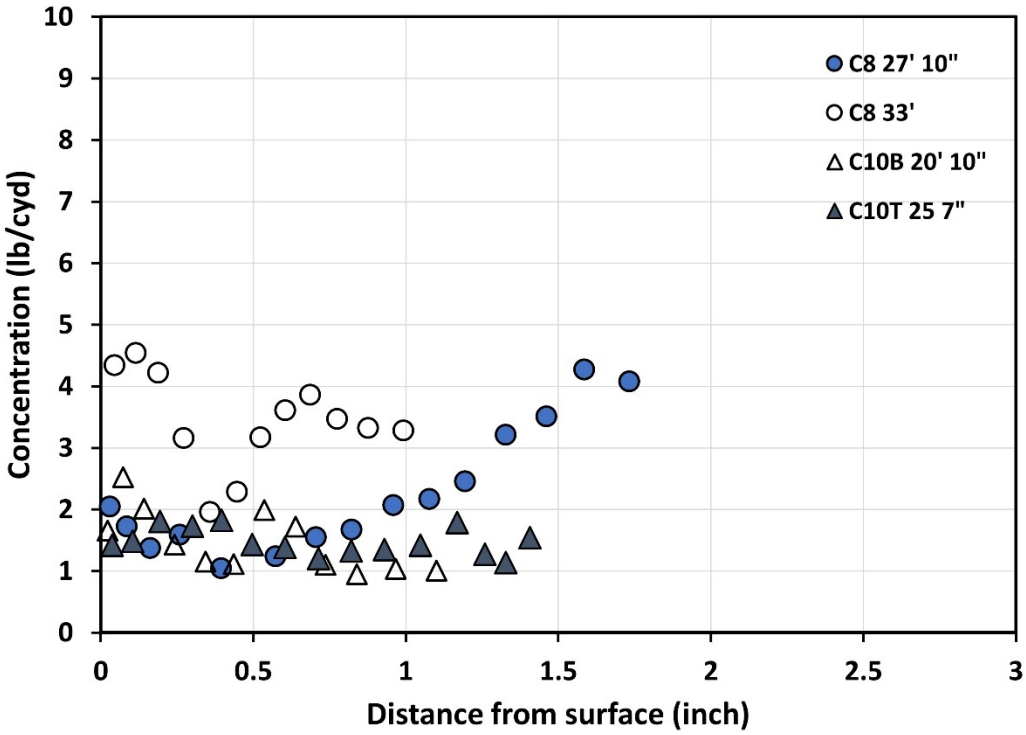

Figure 71. Chloride profiles – column 8 and 10 (Bridge # 880005)

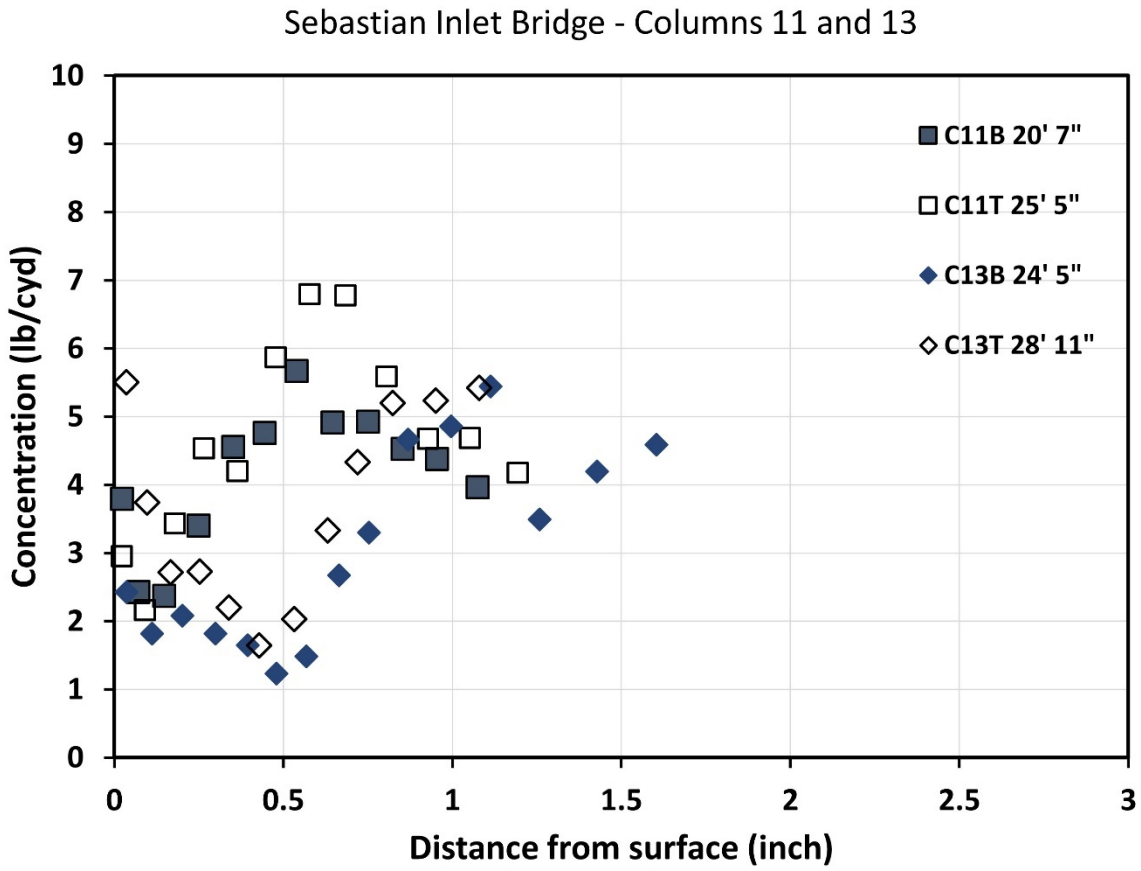

Figure 72. Chloride profiles – Column 11 and 13 (Bridge # 880005)

In Figure 69, the profile that corresponded to the cracked core showed significantly higher chloride concentrations than the profiles of the cores with no cracks obtained from Column 7 and the various elevations. All profiles show trends similar to those expected for chlorides diffusing into the concrete. The profiles in Figure 70 show that the chlorides profiles showed various trends and a transition (skin layer of various depths). The inner core obtained at 12 ft showed the smaller chloride concentration values (it is possible that some of the chlorides were transported into the concrete of the cathodic protection jacket, which was not energized/interconnected). Significant chloride amounts were observed at depth of one inch (in some cases deeper) even for the profile corresponding to the core obtained at 25 ft above the MHWL. The profiles shown in Figure 71 show more complicated (non-traditional) profiles for the cores obtained in column 8. More modest amounts of chlorides were observed for profiles obtained from column 10. Figure 72 shows that the profiles obtained in columns 11 and 13 had higher concentrations for the cores obtained closer to the top (i.e., higher elevations) and this might be in part due to less rain washing closer to the top (Cs higher at higher elevation). The profiles had complicated trends that showed a Cs value followed by decrease of chloride as a function of depth reaching a minimum and followed by a monotonic increase in chloride concentration (i.e., skin effect). The moisture as a function of depth might vary with elevation and also as a function of the season.

3.3.2 – Profiles Bridge (#860160)

The profiles from Bridge #860160 are labeled as Dania in the figures that follow. Two bents were visited. Pile 4-6 was cored on the south and north face (two cores per face), Pile 3-6 was also cored, but in this case on the East face, two cores were obtained. Figure 73 shows the profiles for the cores of P3-6 East. The profiles show that a greater Cs was observed at 11 ft 2.5" than at 12 ft 10", however the concentration at one inch suggest higher chloride penetration on the core obtained at 12 ft 10". A concentration higher than Cs was observed in layers three to five, with the largest concentration observed for layer five. Figure 74 shows the profiles corresponding to P4-6 North; a skin effect is observed in several layers on both profiles. Figure 75 shows the profiles corresponding to P4-6 South; the skin effect is also observed on both profiles shown. It is possible that the prevalent humidity closer to the top of the columns is due to pile cap; the beams and deck above the piles allow for a more humid environment. Piles 4-2 to 4-6, north faces showed spalls.

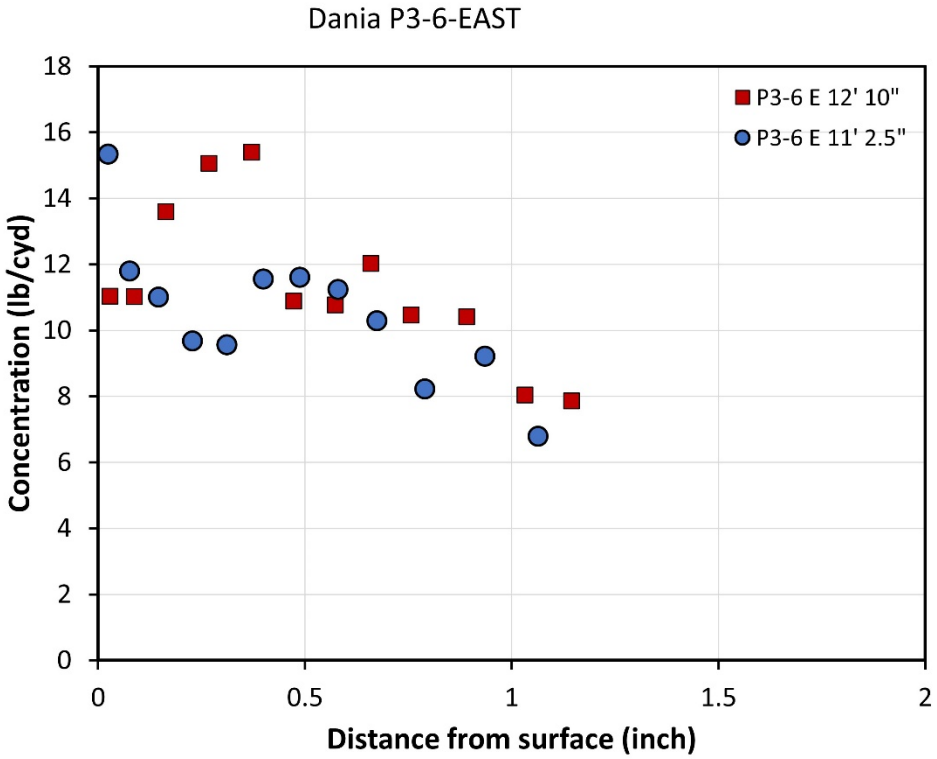

Figure 73. Profiles from cores pile 3-6 east (Bridge #860160)

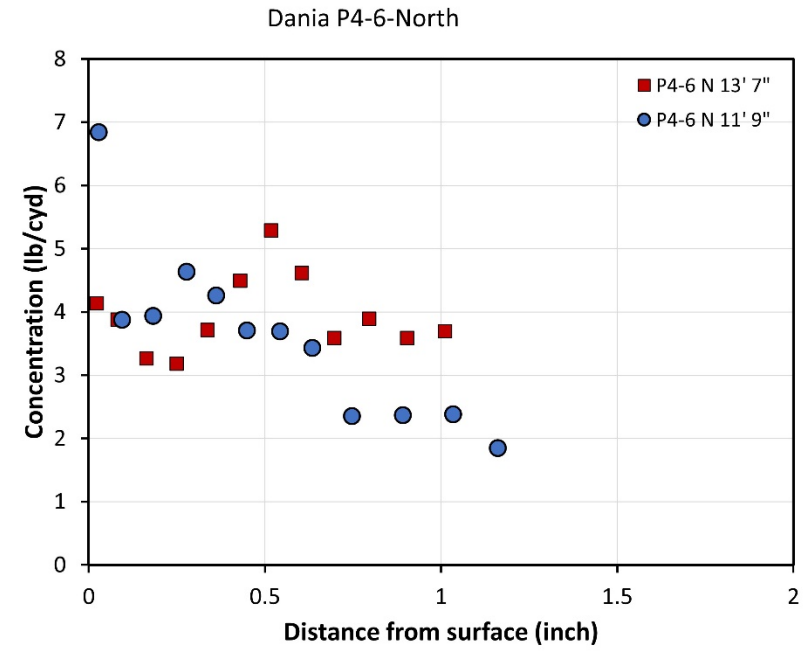

Figure 74. Profiles from cores pile 4-6 north (Bridge #860160)

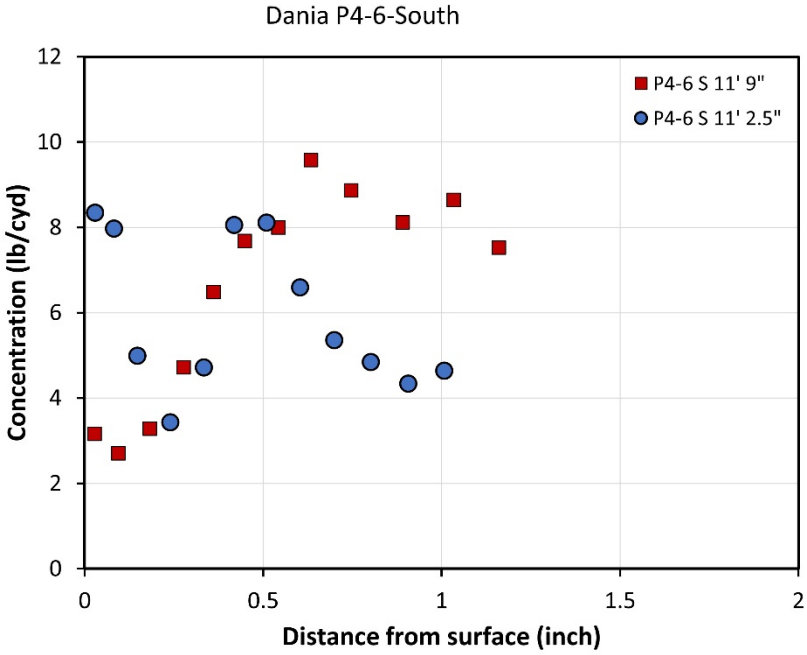

Figure 75. Profiles from cores pile 4-6 south (Bridge #860160)

3.3.3 – Profiles Bridge (#100585)

Figures 76 and 77 show the profiles obtained from cores of Bent 237 and Bent 223, respectively. Referring to the profiles in Figure 76, two of the cores from Bent 237 had cracks, and two cores were obtained at similar elevations in areas with no cracks. Higher concentrations were observed on the cores with cracks compared to the corresponding cores with no cracks. Most chloride concentration were below one pound per cubic yard. Figure 77 shows that the profiles in this figure had significant higher chloride concentrations compared to the profiles in Figure 76. The cores from Bent 223 were obtained closer to the mean high tide water mark. Note that even the profile obtained at 12 ft above MHWL showed significant more chloride penetration, than those shown in Figure 76. It is speculated that the concrete composition might be different. The diameter of the column in Bent 237 was larger than the column cored in Bent 223 (this also could affect the chloride penetration observed to some extent).

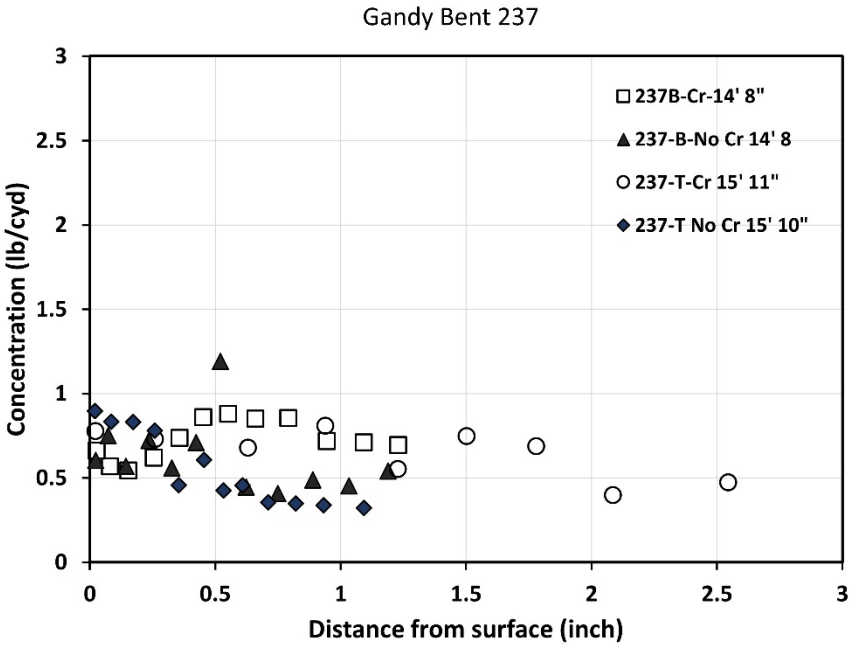

Figure 76. Profiles from cores bent 237 (Bridge #100585)

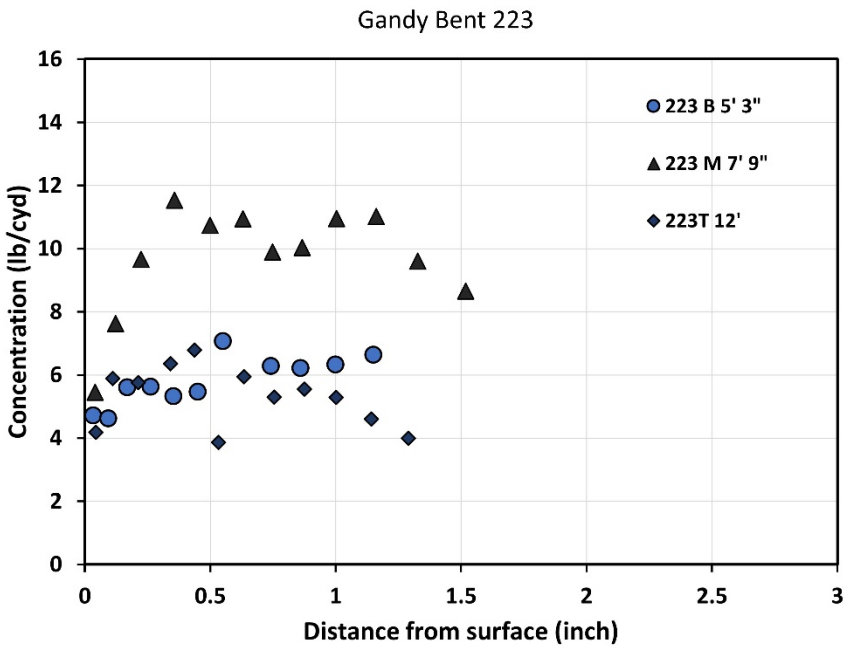

Figure 77. Profiles from cores bent 223 (Bridge #100585)

Regarding the non-conventional profiles (Figure 71 and Figure 72, cores obtained close to the top of the columns), in some cases, a minimum chloride concentration was found at 0.5" depth followed by a monotonic increase in the chloride and, in some cases, reaching a plateau (although an additional layer might have shown a concentration decrease at deeper sites).

The geometry (detailing) of the bridge, inlet geometry (local environment), wind direction, and wind speed over time might have, in some cases, enhanced turbulence and thus caused the location observed with the larger chloride concentration to vary as a function of height and time. This phenomenon might have been more prominent at the Sebastian Inlet Bridge (bridge #880005), but likely occurred also at the other two bridges visited. In the case of the bridge at Dania (bridge #860160), it is possible that inner piles wash out less and the humidity is higher in the inner piles for a longer period of time. This might have allowed corrosion to initiate and propagate at the observed spalls (Piles 2 to 5 for Bent 4), even if the pile at location six (closer to the ocean) likely had more chloride deposited over time, rain likely washed the outer piles more easily and also dried the concrete surface sooner.

Chapter 4 – Wet Candle Results

4.1 – Chloride Deposition on Wet Candles Deployed at Bridges

The exposure durations of each deployed wet candle ranged between 27 days and 49 days (but most were deployed for about a month). Figure 78 shows the chloride deposition vs. time measured at the Sebastian Inlet Bridge (bridge #880005). In most instances the chloride measured at the lower elevation was consistently higher than that measured above the bridge (wet candle setup on the bridge rail). However, there were at least four times that the values were comparable in magnitude. The maximum deposition value observed was close to 400 mg/m^{2}day. Figure 79 shows the chloride deposition vs. time measured next to Bridge #860160. The maximum deposition value observed was close to 600 mg/m^{2}day.

The average chloride deposition over the monitored period shown in the plots is as follows: at Sebastian Inlet Bridge (404 days) #880005: the top location on top of the bridge (rail) was 147.4 mg/m^{2}day and bottom setup (fishing area) was 219.5 mg/m^{2}day. The average deposition over 513 days at Bridge #860160 was 127.4 mg/m^{2}day. Although not the same height, the average deposition at the lower location on bridge #880005 was larger than the deposition observed at Bridge #860160, which suggests that the environmental conditions are more aggressive at the Sebastian Inlet compared to the bridge at Dania Beach (which is a farther distance from the ocean).

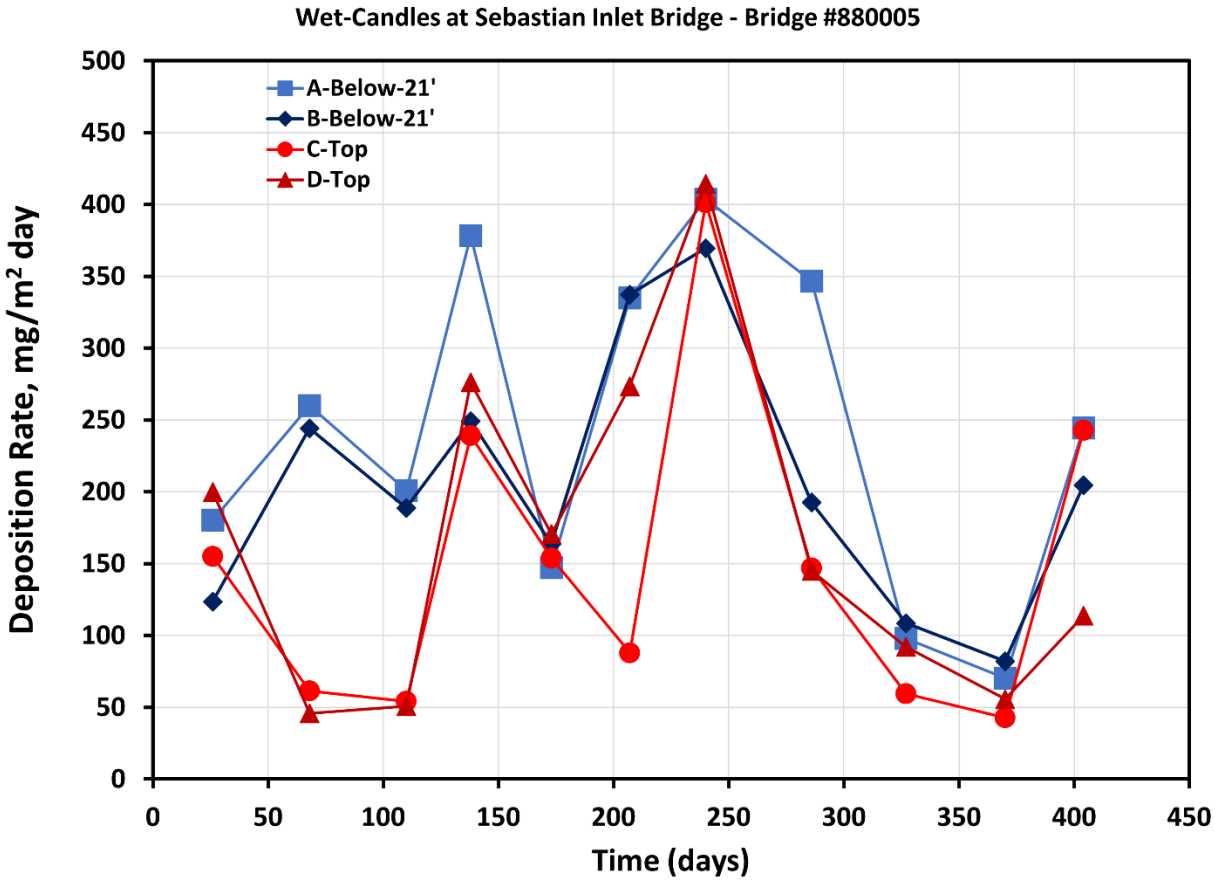

Figure 78. Chloride deposition vs. time at Sebastian Inlet Bridge

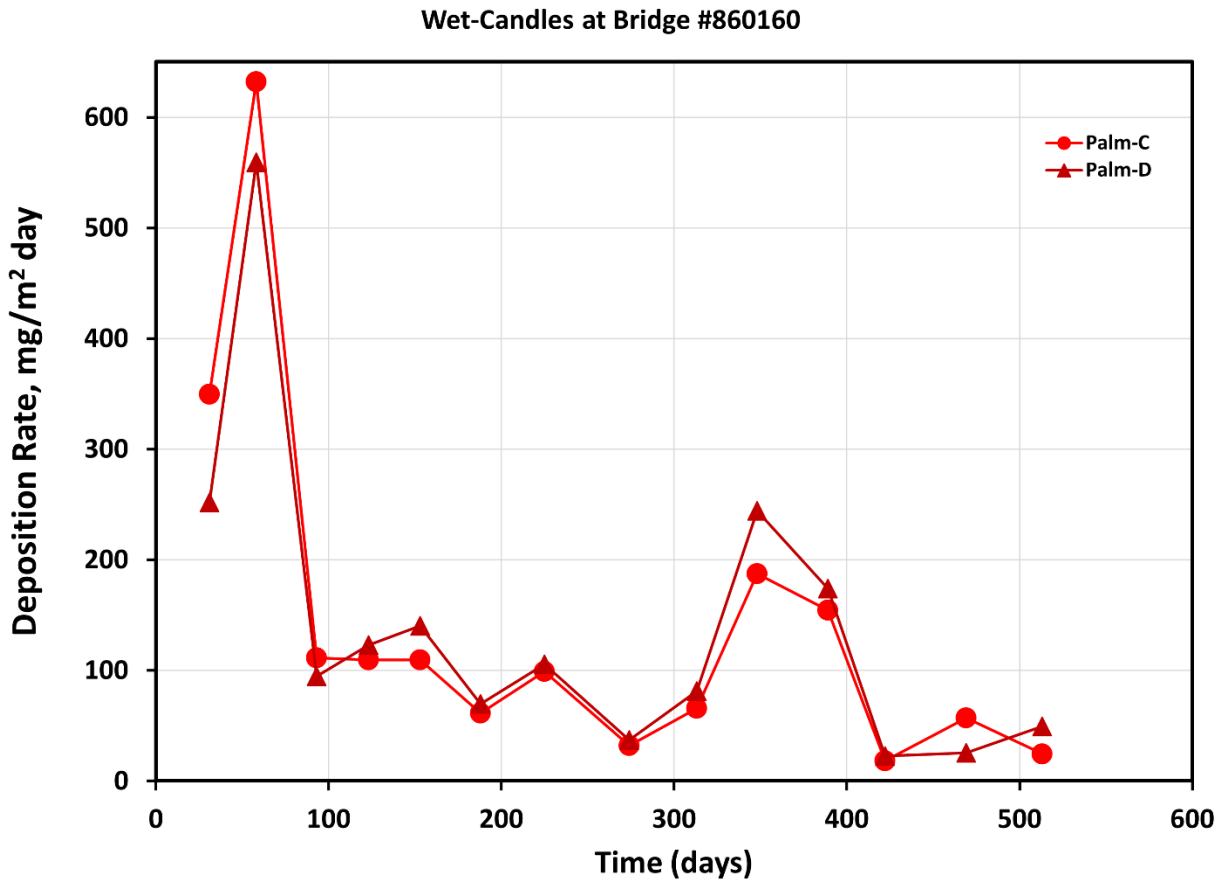

Figure 79. Chloride deposition vs. time close to Bridge #860160.

4.2 – Chloride Deposition on Wet Candles Deployed at FAU SeaTech

Figure 80 shows the chloride deposition vs. time measured on the two setups deployed on the east site at FAU SeaTech. The maximum chloride deposition was close to 1200 mg/m^{2}day. Figure 81 shows the same data but with the maximum value reduced to 600 mg/m^{2}day. At least six times, the values observed on the setup placed at the rail were of about the same magnitude with those measured at ~12 ft above MHWL, with the latter typically being larger. On the other hand, the chloride deposition values observed at the rail setup were larger at least seven times than those measured at ~12 ft above MHWL. It is possible that the wind direction and speed influenced and caused the inversion of the expected trend. There were at least five times in which a significantly larger deposition was observed on the candles deployed on the rail. Most chloride deposition values appear to be around 100 mg/m^{2}day. But there were cases in which the deposition exceeded 400 mg/m^{2}day. It is believed that with no obstacles the chloride deposition at lower elevations would be larger. It is possible that dunes at the beach, the parking lot, and palms on the beach affect how much chloride deposition is measured at the lower elevation. Another factor is the proximity to the intracoastal waterway. The average chloride deposition values observed over the initial 350 days are: on the top elevation (setup on the rail) 237.1 mg/m^{2}day and at the lower elevation 97.3 mg/m^{2}day. When including the deposition over 555 days these values are smaller, the average deposition values observed are: on the top elevation (setup on the rail) 178.1

mg/m^{2}day, and at the lower elevation 77.5 mg/m^{2}day. This suggest that during the second year the wind conditions (speed and direction) were more modest than during the first year of monitoring.

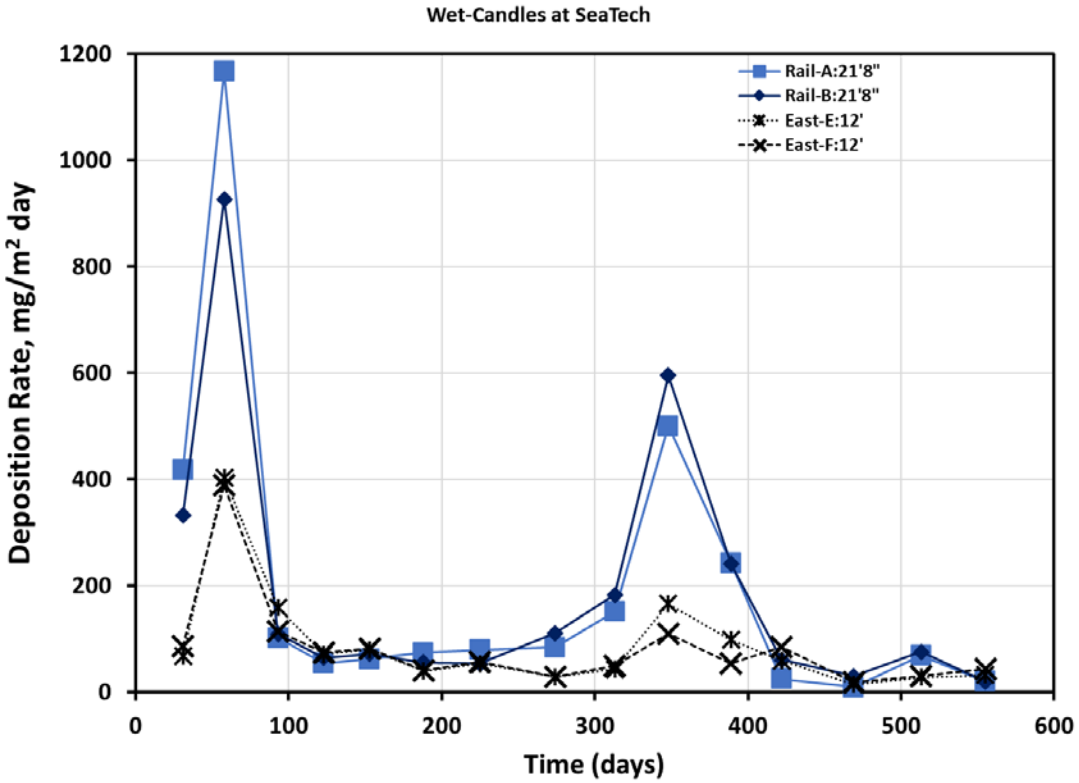

Figure 80. Chloride deposition vs. time for setup deployed at FAU SeaTech east side (full range)

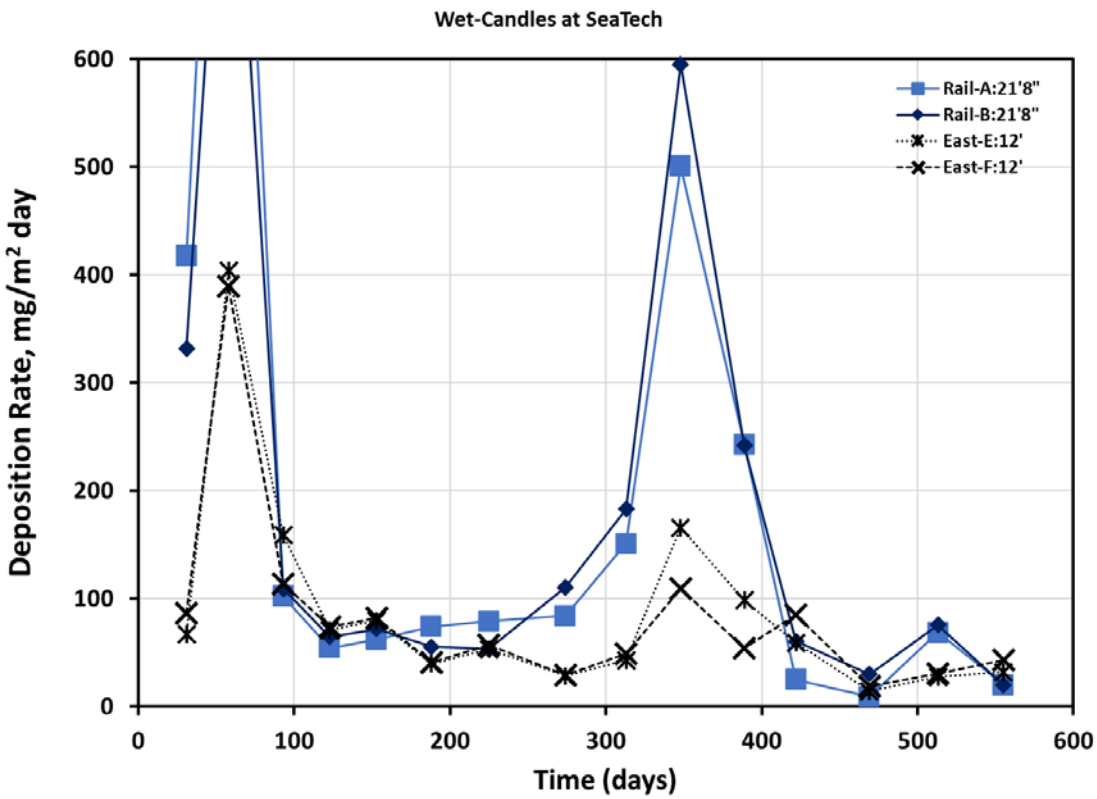

Figure 81. Chloride deposition vs. time for setups deployed at FAU SeaTech (close-up)

As a reference, the chloride deposition at a location close to Cape Canaveral has an average chloride deposition of 1000 mg/m^{2}day, whereas at Dania Beach (FAU SeaTech east site previous study), the average chloride deposition is 260 mg/m^{2}day at 100 m from the ocean (the wet candle set up from the previous investigation was at an elevation of 4 ft from the ground or about 8 ft MHWL measured with respect the marina MHWL mark).

Weather stations close to SeaTech (navy site - Jetty) and south of bridge #880005 (FAU-HBOI) were identified and the data downloaded for processing. The average wind speed was available for about five months for the site close to SeaTech. The weather station Aqua1 at FAU-HBOI was used to obtain the wind speed from January 2021 to September 2022. Figure 82 shows a plot of the monthly average wind speed for the site close to SeaTech and bridge #860160, and Figure 83 shows a plot of the monthly average wind speed for Station Aqua1 (FAU-HBOI). Lower winds appear to take place at the Aqua1 station than at the weather station at the Jetty at Dania Beach (close to bridge #860160). The data was also processed to obtain the number of hours per month that the wind average was equal or greater than 3 m/s. The instances in which this occurred were counted. The count was multiplied by the interval period and then divided by 60 minutes to obtain the number of hours per month from both stations. Table 5 and Table 6 show the number of hours per month in which the average wind speed was greater or equal to 3 m/s. The periods with larger numbers of hours exceeding 3 m/s coincided with when the measured chloride deposition was larger on the wet candles close to the corresponding bridges. This is in agreement with Meira's observations.

Meira and others have suggested that wind speeds greater or equal to 3 m/s are indicatives of higher chloride deposition. The number of recorded events were identified and listed in table form in Tables 5 and Table 6. The moths with the larger number hours are April and May 2022 for the site close to the bridge in Dania (bridge #860160), and February, April, and May for the AQUA1 station located at HBOI-FAU. The fewer hours with winds equal or greater than 3 m/s at AQUA1 station compared to the station at the jetty at Dania, can be explained by the fact that the former is located farther inland. No weather station was found in closer proximity to bridge #880005 that included wind speed and direction.

Montgomery [30] and others have correlated the wave height to the chloride deposition. Unfortunately, there are no buoys close to either bridge reported in here. The buoy mentioned in Montgomery paper is north of bridge #880005.

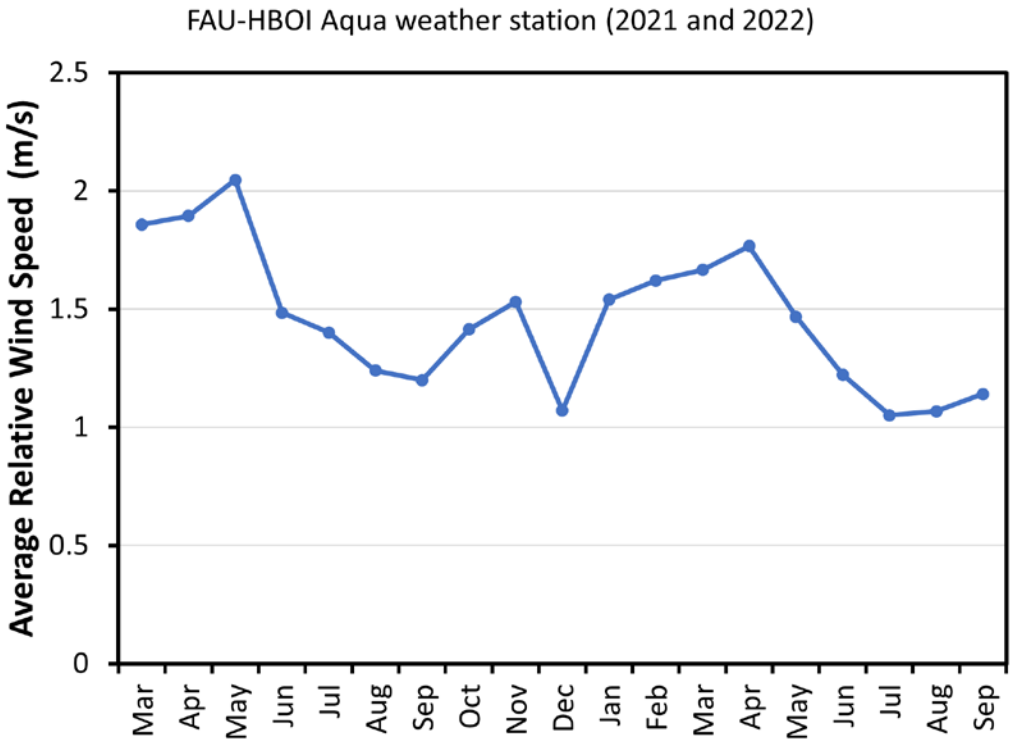

Figure 82. Average wind speed measured at aqua weather station (FAU-HBOI)

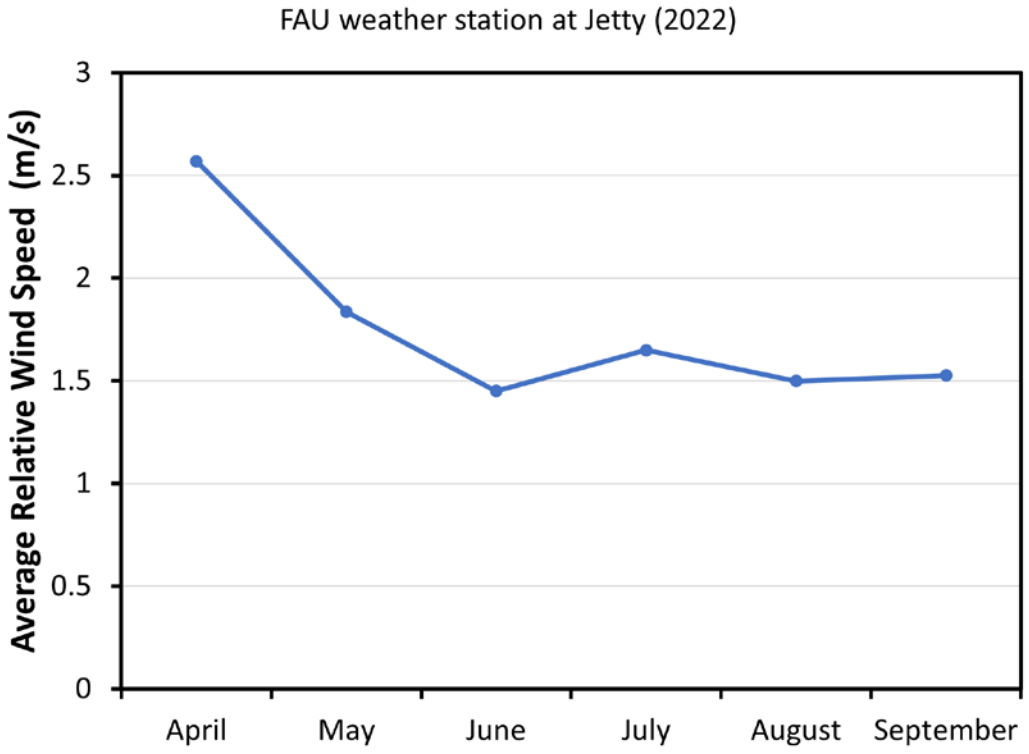

Figure 83. Average wind speed measured at Dania (navy site)

Table 5. Number of hours average wind ≥3 m/s on each month at navy site

Month	Hours/month
April 2022	456.5
May 2022	231.3
June 2022	132.0
July 2022	148.2
August 2022	105.2
September 2022	134.2

Table 6. Number of hours average wind ≥3 m/s on each month at aqua1 station (FAU-HBOI)

Month	Hours/month
March 21	123.0
April 21	122.1
May 21	164.1
June 21	62.5
July 21	42.2
August 21	35.2
September 21	29.3
October 21	57.8
November 21	72.4
December 21	32.2
January 22	82.3
February 22	76.8
March 22	93.5
April 22	108.4
May 22	60.3
June 22	32.2
July 22	17.7
August 22	18.8
September 22	39.6

Appendix C depicts the average values per month for relative humidity, temperature and wind direction obtained from the weather stations described above.

Chapter 5 – Discussion

5.1 – Diffusivity and C_{tot} Values for Samples Exposed at FAU SeaTech

This section presents the calculated chloride diffusivity values. The values presented here were obtained by fitting Fick's second law assuming that the diffusion coefficient did not change with time. The fitting took place using either a Matlab code or using USF Excel-macro (the latter has a limit of 12 layers).

The moisture content on the tested specimens likely was not as high (or at least not high all the time) as that observed on the tidal or splash zone. The relative humidity surrounding the samples is high most of the time. Moreover, the samples got wet during rain events. Sample orientation might also influence if and how much of the chloride wash out from the surface, as well as how fast the moisture leaves the sample during the dry season. The profiles presented in the results section showed that in some cases, samples with the lower w/cm ratio had chloride penetrate more when compared to those with the samples with higher w/cm (within the same composition). As a result of this observation, the calculated diffusion coefficient does not always follow the expected trend (higher D_{app} for concrete with higher w/cm, but this applies to fully immersed samples). In a number of cases, the concentration at the layers closest to the surface had a lower concentration. The table with the diffusivity values list how many layers were removed.

5.1.1 – D_{app} values for Mixes 1C1, 1C2, and 1C3 after 108 Months of Exposure

Table 7 shows the D_{app} values calculated for 1CX specimens. Four of the five 1C1 specimens had D_{app} values greater than 1×10^{-12} m^2/s, ranging from 2.2 to 15.5×10^{-12} m^2/s, with the fifth sample showing a D_{app} of 0.6×10^{-12} m^2/s. These are the samples with only OPC and a w/cm of 0.41. Mix 1C2 (20% FA) samples had one out of four samples with D_{app} greater than 1×10^{-12} m^2/s and corresponded to the sample exposed in at the east site; the other three D_{app} values ranged between 0.15 and 0.32×10^{-12} m^2/s. The two tested samples prepared with fly ash and silica fume (mix 1C3) had a D_{app} of ~ 0.32×10^{-12} m^2/s. The best fit was obtained by removing anywhere between 2 and seven layers (see column listing number of layers removed in Table 7 for details).

Table 7. D_{app} calculated on samples for mixes 1C1, 1C2 and 1C3

		# of layers removed	$m^2/s \times 10^{-12}$	In in^2/year	Assumed Co (kg/m^3)
1C1, OPC only	1A1B-H	2	0.63	0.031	0.3
	1A2B-VF	2	4.08	0.199	0.3
	1A3B-V	0	15.50	0.758	0.3
	2C1A-V	2	2.84	0.139	0.3
	2C2B-E	5	2.22	0.108	0.3
1C2, 20%FA	1E2B-FV	3	0.33	0.016	0.3
	1E4A-H	2	0.15	0.008	0.3
	2A1A-V	1 (2nd layer)	0.25	0.012	0.3
	2A1B-E	7	1.56	0.076	0.4
1C3, 20%FA+8%SF	3A1B-H	2	0.32	0.016	0.4
	3A4B-E	4	0.32	0.016	1
	3A4B-E Co=2	4	0.22	0.011	2

5.1.2 – D_{app} Values on DCL Samples Exposed for 43 Months (Samples at the East Site only)

D_{app} values were calculated using one layer removed or with all layers using the profiles obtained after approximately 43 months of exposure. The fitted D_{app} values were smaller when calculated with one layer removed for profiles of mixes DCL2, DCL4, DCL5 and DCL11, but larger for all other mixes. The calculated residual was smaller in most cases for the D_{app} values calculated with 1 layer removed. Table 8 shows the D_{app} calculated values.

Table 8. D_{app} calculated from profiles obtained after 43 months of exposure

Mix	$D_{app} \times 10^{-12}$ m^2/s	
	1 layer Removed	All layers
DCL1	0.074	0.030
DCL2	0.037	0.047
DCL3	0.080	0.063
DCL4	0.009	0.022
DCL5	0.096	0.115
DCL6	0.175	0.122
DCL7	0.023	0.006
DCL8	0.033	0.022
DCL9	0.139	0.103
DCL10	0.136	0.043
DCL10a	0.125	0.070
DCL10b	0.060	0.048
DCL11	0.047	0.060

Within a given composition group the samples with the higher w/cm had the largest D_{app} value. Although a D_{app} was calculated in all cases, the fitting was not particularly good in a few cases. Note that after 43 months of exposure, all calculated D_{app} values were less than 0.18×10^{-12} m^2/s (i.e., for all compositions).

5.1.3 – D_{app} Values of DCL Samples Exposed for 108 Months.

Table 9 shows the D_{app} in units of m^2/s on the left and on the right the D_{app} values are shown in units of in^2/year. Although the profile was calculated for all samples, no fit was possible for the profile from sample DCL-10a-F, but a fit was obtained for all other cases. In here, a brief analysis will be made with the values in m^2/s.

Table 9. D_{app} values calculated on DCL samples

	$D_{app} \times 10^{-12}$ m²/s		D_{app} in²/year	
	East	West	East	West
Mix	F group	C group	F group	C group
DCL1	0.135	0.054	0.0066	0.0026
DCL2	0.059	0.306	0.0029	0.0149
DCL3	0.814	0.134	0.0398	0.0065
DCL4	0.041	0.038	0.0020	0.0019
DCL5	0.016	0.029	0.0008	0.0014
DCL6	0.223	0.163	0.0109	0.008
DCL7	0.034	0.038	0.0017	0.0019
DCL8	0.052	0.017	0.0025	0.0008
DCL9	0.175	0.019	0.0085	0.0009
DCL10	0.088	0.217	0.0043	0.0106
DCL10a		0.138		0.0067
DCL10b	0.196	0.11	0.0096	0.0054
DCL11	0.9	0.054	0.044	0.0027

D_{app} from samples at the east site after 108 months of exposure

After 108 months of exposure, the D_{app} values for two samples exposed at the east site was close to 1×10^{-12} m²/s (0.8 for DCL3 and 0.9 for DCL11); all other D_{app} values (for those from samples exposed at east site) were less than 0.25×10^{-12} m²/s. The smallest D_{app} value was observed for DCL5-F. In general, the samples with the larger w/cm (0.47) had larger D_{app} values compared with the D_{app} of samples with similar composition and lower w/cm. In two cases the samples (DCL1-F and DCL4-F) with the lowest w/cm had larger D_{app} than the samples with intermediate w/cm (DC2-F and DCL5-F). However, all of these four D_{app} values were smaller than 0.14×10^{-12} m²/s (i.e., D_{app} values corresponding to DCL1-F, DCL2-F, DCL4-F and DCL5-F).

D_{app} from DCL samples at the west site after 108 months of exposure.

The largest D_{app} value observed was 0.3×10^{-12} m²/s (DCL2-C) on DCL-C samples exposed on the west site and with the surface facing upwards, and seven DCLX-C samples had D_{app} values smaller than 0.1×10^{-12} m²/s. In general, smaller D_{app} values were observed on the DCL-C (samples exposed at the west site) when compared to D_{app} values corresponding to the DCLX-F samples. The location farther from the ocean suggest a smaller number of spray particles reached the surface. It is possible that some of the chlorides were washout more effectively during rain events due the horizontal orientation of the samples. The solar radiation might also have been more effective in drying samples on this orientation than on samples oriented facing the ocean.

5.1.4 – C_{tot} after 28 Months and 43 Months of Exposure (DCX-F: East Site Exposure)

The C_{tot} values (were obtained by integration i.e., the area under the curve was obtained using the profiles) were obtained by multiplying the layer %cm concentration times the thickness of the layer in m. Then the values for the different layers were added. All samples milled after 43 months of exposure had a total thickness of 0.9652 cm (0.00965 m). To be able to compare, the C_{tot} values after 28 months and after 43 months, either four or five layers, were used from the 28 months concentration profiles (see the second column on Table 10, which lists the thickness corresponding to the C_{tot}). Table 10 shows the calculated C_{tot} values after 28 months and 43 months, and the column on the right displays the ratio $C_{tot43mo}/C_{tot28mo}$. In three cases, the ratio was less than 1 for samples of mixes DC3, DC8 and DC11. The largest ratio corresponded to the sample of DCL1 mix, with a ratio value of 3.2. DC5, DC6, and DC10a samples had ratios that ranged between 2.2 and 2.8, i.e., these are the samples in which chloride penetration was more significant between reported periods.

Table 10. C_{tot} after 28 and 43 months of exposure.

	thickness cm (28 mo)	$C_{tot28mo}$ %cm*m	$C_{tot43mo}$ %cm*m	Ratio
DC1	0.87	0.00645	0.02036	3.2
DC2	0.92	0.00148	0.00267	1.8
DC3	1.00	0.00354	0.00321	0.9
DC4	0.91	0.00169	0.00189	1.1
DC5	0.90	0.00123	0.00346	2.8
DC6	0.90	0.00203	0.00456	2.2
DC7	0.93	0.00131	0.00239	1.8
DC8	0.93	0.00233	0.00204	0.9
DC9	0.91	0.00149	0.00180	1.2
DC10	1.05	0.00255	0.00382	1.5
DC10a	0.95	0.00208	0.00429	2.1
DC106	0.99	0.00376	0.00551	1.5
DC11	1.10	0.00566	0.00454	0.8

5.1.5 – C_{tot} after More than 108 Months of Exposure

The amount of chlorides that penetrated the concrete of the tested samples (up to the depth measured) were obtained by integrating the profiles; i.e., the layer thickness times the concentration of a given layer (similar to what described above in the previous section). The concentration was converted to percent cementitious, and the thickness of each layer was converted to meters. These units were used to compare with values previously reported. Table 11 shows the C_{tot} values for 1CX samples (with not mortar layer), the maximum C_{tot} was observed on

samples exposed at the east site. For 1C1 sample the C_{tot} value was 0.0226, for 1C2 sample it was 0.0214 and for 1C3 it was 0.0195, which shows decreasing values as a function of composition, but of comparable magnitude. The C_{tot} values observed on samples exposed at the west property were significantly smaller, typically less than half the value observed on the samples exposed at the east site.

Table 11. C_{tot} values for 1CX samples, exposed for 110 months

Mix	Sample ID	C_{tot}	Depth (cm)
1C1 (OPC only)	1A1B-H	0.0064	1.61
	1A2B-FV	0.0123	1.45
	1A3B-V	0.0053	1.94
	2C1A-V	0.0039	1.37
	2C2B-E	0.0226	1.64
1C2 (with Fly Ash)	1E2B-FV	0.0081	1.60
	1E4A-H	0.0061	1.76
	2A1A-V	0.0065	1.39
	2A1B-E	0.0214	1.38
1C3 (with Fly Ash and Silica Fume)	3A1B-H	0.0078	1.50
	3A4B-E	0.0195	1.41

Table 12 shows the C_{tot} values calculated after integrating the profiles of DCL samples after 108 months of exposure. In most cases the C_{tot} values were greater for those exposed at the east sited when comparing corresponding mix composition for samples exposed at the west site. For example, for DC1, C_{tot}(east)=0.0099 and C_{tot}(west)=0.0055. The largest C_{tot} was observed on DCL3 sample exposed at the east site, which was 0.0449. This value was larger than the C_{tot} values observed on the 1CX samples at the east site. It is speculated that DCL3 sample was sprayed with seawater a few times (this might explain the larger C_{tot} on this sample). The smaller difference in C_{tot} value was observed for DCL5 and followed by DCL9. The C_{tot} for sample DCL10 was larger for the sample exposed at the west site. In general, the C_{tot} values observed on DCL samples was smaller than those observed on 1CX samples.

Table 12. C_{tot} value for DCL samples after 108 months of exposure

	C_{tot}	Depth (cm)			C_{tot}	Depth (cm)
DCL1F	0.0099	1.10		DCL1-C	0.0055	1.80
DCL2F	0.0060	1.10		DCL2-C	0.0064	1.10
DCL3F	0.0449	2.88		DCL3-C	0.0046	1.10
DCL4F	0.0034	1.10		DCL4-C	0.0025	1.29
DCL5F	0.0031	1.10		DCL5-C	0.0028	1.10
DCL6F	0.0047	1.10		DCL6C	0.0033	1.10
DCL7F	0.0040	1.10		DCL7-C	0.0053	1.25
DCL8F	0.0037	1.10		DCL8-C	0.0027	1.28
DCL9F	0.0029	1.10		DCL9-C	0.0023	1.45
DCL10F	0.0044	1.10		DCL10-C	0.0067	1.33
DCL10aF	0.0113	1.10		DCL10a-C	0.0053	1.08
DCL10bF	0.0101	1.10		DC 10b-C	0.0053	1.10
DCL11F	0.0068	1.10		DCL11-C	0.0036	1.69

5.2 – D_{app} Observed on Cores Obtained from the Field

5.2.1 – Previous D_{app} Values Measured in Florida Bridges at Elevations ≥9 ft above MHWL

Before this project, there were relatively few chloride profiles have been reported in Florida from bridge reinforced concrete elements at elevations >MHWL+12. Most D_{app} values obtained from Florida bridges at elevations ≥ 9 ft above MHWL were obtained from the Sunshine Skyway bridge. Table 13 lists the bridge number, the year in which the bridge was put in service, the year in which it was tested, the age, the location, the elevations, and the D_{app}. Two other bridges tested in 1992 have one location each that was cored at these heights. The D_{app} obtained at these two locations was greater than 1×10^{-12} m^2/s. [21,62]

Table 13. D_{app} measured on Florida bridges at heights ≥9 ft MHWL [21]

Bridge number	Built/In Service	Tested	Age	Location	ft (MHWL)	m (MHWL)	$D_{app} \times 10^{-12}$ m^2/s	
150189	1986	1993	7	Pier 136	9.0	2.74	**0.348**	
490031	1988	1992	4	Pier 16	9.5	2.90	**19.627**	
870607	1983	1992	9	Pier 13	9.8	3.00	**1.002**	
150189	1986	1993	7	Pier 1	10.7	3.25	**0.532**	
150189	1985	1996	11	Pier 155	18.0	5.49	0.090	C
150189	1985	1996	11	Pier 155	18.0	5.49	0.062	
150189	1985	1996	11	Pier 155	18.0	5.49	**4.700**	C
150189	1986	4/3/1997	11	Pier 155	18.0	5.49	0.057	
150189	1985	1996	11	Pier 151	19.0	5.79	0.201	C
150189	1985	1996	11	Pier 151	19.0	5.79	0.089	
150189	1985	1996	11	Pier 151	19.0	5.79	0.106	C
150189	1986	4/3/1997	11	Pier 151	19.0	5.79	0.077	
150189	1985	2011	26	T-C 44-2	26.2	8.00	**0.240**	
150189	1985	2011	26	TC 44-2	26.2	8.00	0.055	C
150189	1985	2011	26	TC 60-2	26.2	8.00	**0.747**	
150189	1985	2011	26	TC 60-2	26.2	8.00	0.083	
150189	1985	1996	11	Pier 126-1	60.0	18.29	0.049	
150189	1986	4/3/1997	11	Pier 126-1	60.0	18.29	0.052	
150189	1985	1996	11	Pier 126-1	60.0	18.29	0.226	C
150189	1985	1996	11	Pier 126-1	60.0	18.29	0.057	C
150189	1985	1996	11	Pier 126-1	60.0	18.29	0.064	C
150189	1985	1996	11	Pier 117-1	120.0	36.58	0.149	C

Note: C indicates that there was a crack where the core was obtained, TC indicates Trestle Cap

Trestle caps were cored from the SSK on pier 44 and 60 in 2011 (Figure 83). Four profiles were obtained; these profiles are shown in Figure 39. SSK1 and SSK2 cores are believed to have been obtained from the trestle cap of pier 44, SSK3 and SSK4 cores were obtained from pier 60. Two of the profiles (SSK3 and SSK4) obtained in 2011 from cores obtained at Trestle Caps show a significantly larger amount of chlorides, compared with the other two profiles.

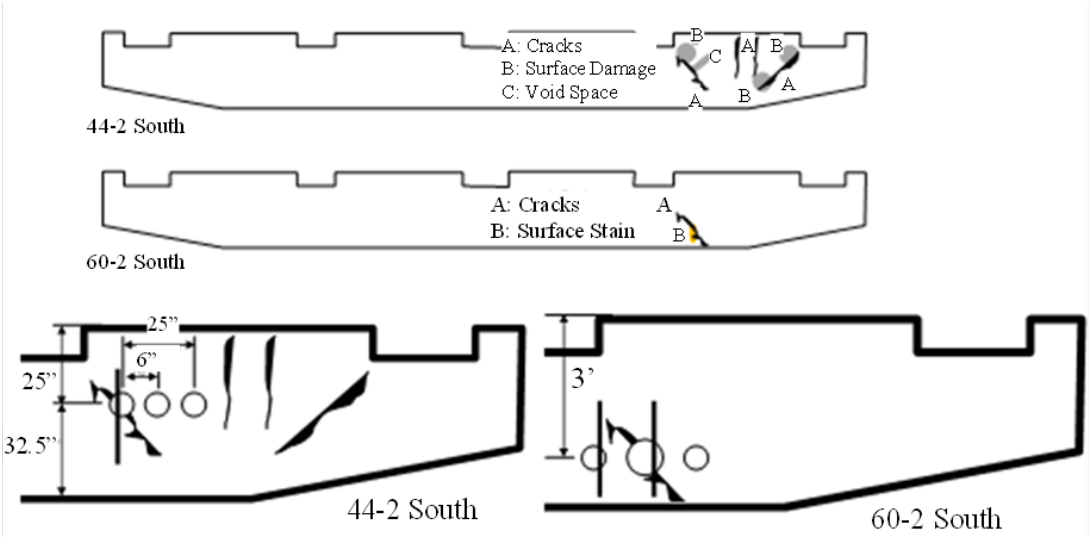

Figure 84. Location at which cores were obtained-south face of trestle caps on pier 44 and 60 SSK [21]

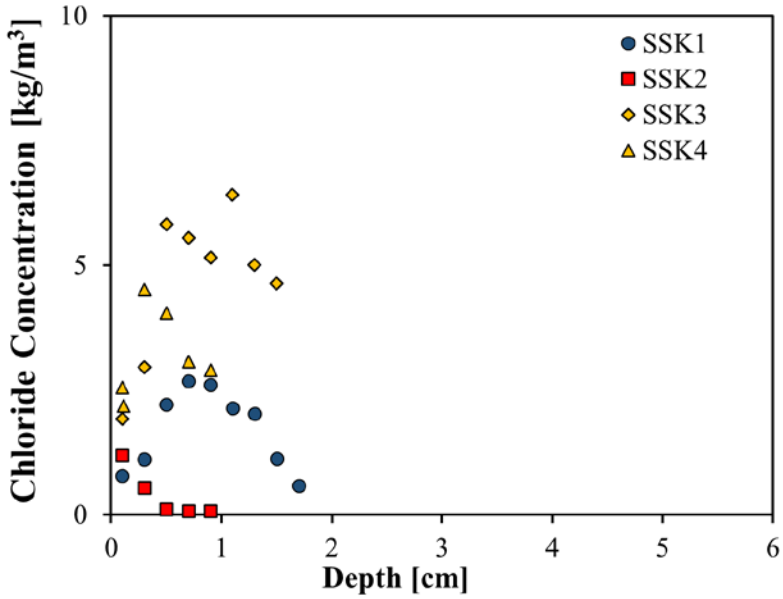

Figure 85. Chloride profiles obtained from trestle caps at SSK approx. elevation 7 to 8 m. [21]

The maximum D_{app} value on the SSK shown in Table 13 corresponded to a core taken from Pier 155 18 ft MHWL and was obtained along a crack (D_{app} 4.7 × 10^{-12} m^2/s). Four cores (values in bold) had D_{app} values > 0.23 × 10^{-12} m^2/s and were obtained from sound concrete sections from various Piers and one Trestle cap.

5.2.2 – Selected Chloride Profiles and D_{app} from Cores Obtained at Sebastian Inlet Bridge [3] in 2017

Figure 86 presents the profiles for the cores obtained at the bridge (bridge #880005) crossing the Sebastian Inlet for which D_{app} was calculated (See Table 14). The profiles obtained from beam 11-1 and beam 5-1 showed the larger chloride amounts. The chloride concentration values were obtained from a FDOT District 4 report [59]. The chloride concentration was reported from the

cores obtained by Concorr Florida Inc, during visits that took place during Sept and October 2017/ report published May 2018. Cores were taken from the columns at ~1 ft below the top of the column on selected columns, the profiles were not always included in reference [59], but the concentration at the rebar depth was included and it ranged from 4 to 7 lb/yd^3 in solid concrete, whereas for concrete delaminated or cracked the value ranged between 2 and 8 lb/ yd^3, the profile of column 2-1 solid (part of the bridge approach and possibly not in direct path of the ocean spray) showed a Cs of 5 lb/yd^3 and at the rebar depth a concentration of about 0.1 lb (the cover for this location was 3.25 inches, whereas for the other locations the cover was between 2.25 and 2.75 inches. The values in the above paragraph were taken from Figure 19 in [59]. Figure 83 shows the values in kg/m^3 and cm.

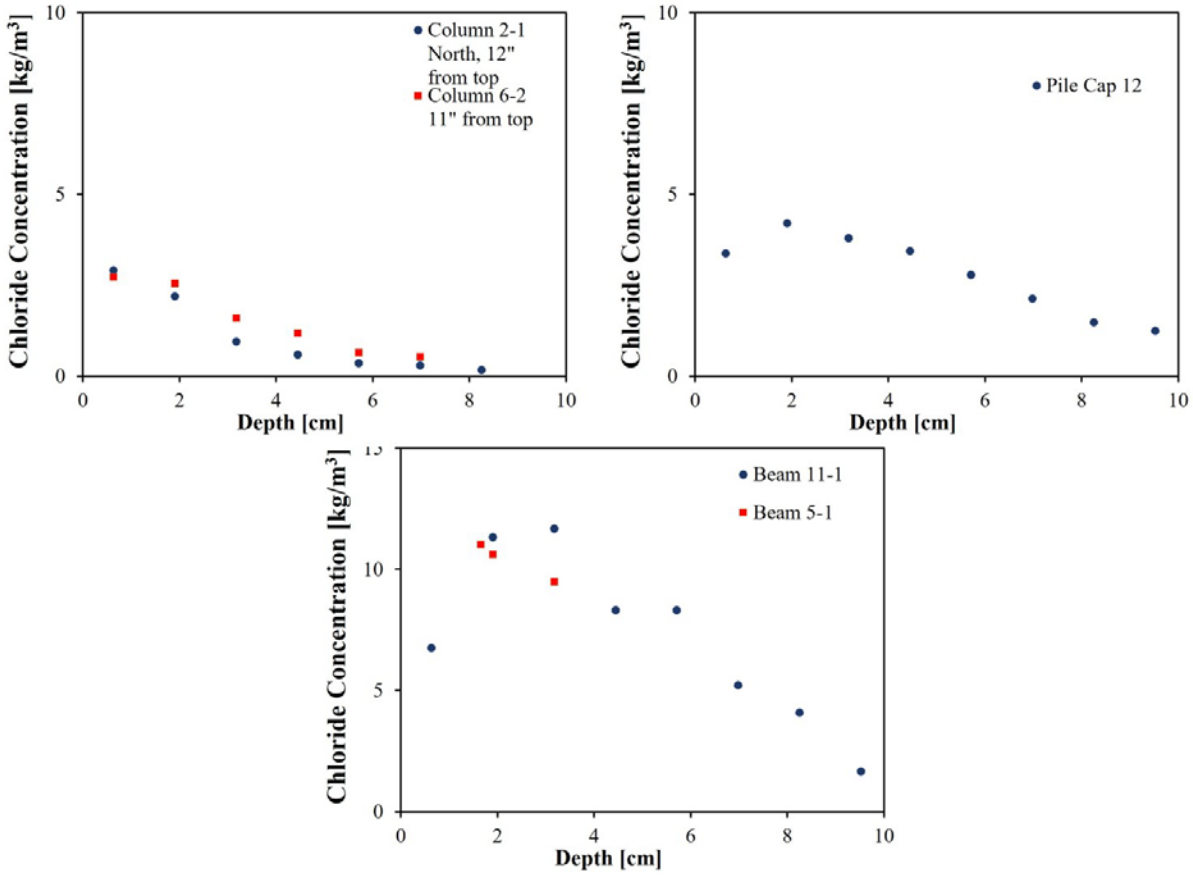

Figure 86. Chloride profiles from Sebastian Inlet bridge at indicated locations [59]

Table 14. Calculated D_{app} (bridge #880005) using profiles reported in 2018 [59]

	Element	D_{app} in^2/y	$D_{app} \times 10^{-12}$ m^2/s	Cs (fit) kg/m^3	Chloride in first layer (measured) kg/m^3
	Beam 11-1	0.072	1.475	16.06	6.7
	Beam 5-1	0.139	2.842	12.63	N/A
	Pile Cap 12*	0.094	1.923	5.41	3.38
	Column 2-1 North 12" from top	0.015	0.297	3.53	2.9
	Column 6-2 11" from top	0.032	0.664	3.24	2.7

*D_{app} of Pile Cap 12, one layer was removed when fitting to the profile.

Table 14 shows the D_{app} calculated values. Three of the D_{app} values calculated were greater than 1 × 10^{-12} m^2/s and ranged between 1.48 and 2.84 × 10^{-12} m^2/s and corresponded to cores obtained from the beams and pile cap. The other two D_{app} values were < 0.65 × 10^{-12} m^2/s and corresponded to cores obtained from the columns close to the top. The calculated Cs values tended to be greater than the concentration measured on the first layer.

5.2.3 – Cs and Concentration Measured at 1" Depth on the Cores Obtained 2021-2022

This section and the following section refer to discussing the results after the field visits that took place during fall 2021 and spring 2022. The tables in this section show the concentration measured on the first layer, labeled in the table as Cs, the concentration found at a depth of one inch, the maximum chloride concentration (C_{max}) observed for each core, and the center of mass of the layer where this concentration was observed. The depth at which C_{max} was observed varied, sometimes the center of mass of the layer was close to the surface, and in other cases, the center of mass for C_{max} was observed 0.5" to 0.75", with a few cases in which the center of mass was at a deeper layer (e.g., core C8 27 ft 8"). Table 15, Table 16, and Table 17 show the data from bridge #880005, and it is referred to by the bridge number or as Sebastian Bridge in the text. The Cs was often smaller than the C at 1 inch and C_{max}, most profiles appear to show a convection section. Table 18 shows similar values for the cores obtained from bridge #860160 (Dania Beach, FL), and Table 19 and Table 20 show corresponding values for cores obtained from bridge #100585, Gandy Bridge (Tampa Bay area).

Table 15. Bridge #880005 column 7: Cs, C at 1 inch and C_{max} (values in lb/yd^3)

Elevation at which core was obtained	Cs	C at 1 inch	C_{max}	location - center of mass inches of the corresponding layer
11'-Crack	5.07	9.18	9.27	0.45"
11'	3.29	3.58	3.76	0.07"
13'	4.19	3.01	4.19	0.03"
15'	5.35	3.29	5.68	0.07"
22'	5.37	2.83	5.37	0.02"

Table 16. Bridge #880005 column 8: Cs, C at 1 inch and C_{max} (values in lb/yd^3)

Elevation at which core was obtained	Cs	C at 1 inch	C_{max}	location - center of mass inches of the corresponding layer
12A - jacket	12.16	9.1	14.31	0.098"
12-B inner	2.98	2.05	4.37	0.32"
17'	6.78	10.38	12.79	0.72"
22'	5.15	12.53	16.52	0.47"
25'	13.09	11.65	13.09	0.025"
27' 10"	2.04	2.12	4.27	1.58"
33' 3"	4.34	3.28	4.54	0.11"

Table 17. Bridge #880005 column 10 to 13: Cs, C at 1 inch and C_{max} (values in lb/yd^3)

Column and Elevation at which core	Cs	C at 1 inch	C_{max}	location - center of mass inches
10T-25'-7"	1.42	1.38	1.82	0.39"
10B-20'-10"	1.65	1.02	2.52	0.07"
11T-25'-5"	2.95	4.68	6.79	0.57"
11B-20'-7"	3.79	4.17	5.66	0.54"
13T-28"-11"	5.51	5.32	5.51	0.035"
13B-24'-5"	2.42	5.15	5.44	1.11"

Table 18. Bridge #860160 Dania: Cs, C at 1 inch and C_{max} (values in lb/yd^3)

Elevation	Cs	C at 1 inch	C_{max}	location - center of mass inches
P3-6-East-12'10"	11.03	9.2	15.39	0.37"
P3-6-East-11'	15.33	8	15.33	0.02"
P4-6-South-11'9"	3.16	8.64	9.57	0.63"
P4-6-South-11'2.5"	8.34	4.63	8.34	0.029"
P4-6 North-13-7	4.13	3.69	5.28	0.51"
P4-6 North-11' 9"	6.84	2.38	6.84	0.04"

Table 19. Bridge #100585, Gandy bridge bent 237: Cs, C at 1 inch and C_{max} (values in lb/yd^3)

Elevation	Cs	C at 1 inch	C_{max}	location - center of mass inches
237B-C 14'-8"	0.66	0.71	0.88	0.55"
237B 14' 8"	0.6	0.47	0.74	0.073"
237T-C 15' 11"	0.78	0.81	0.81	1.00"
237T 15' 11"	0.89	0.33	0.89	0.02"

Table 20. Bridge #100585 Gandy bridge bent 223: Cs, C at 1 inch and C_{max} (values in lb/yd^3)

Elevation	Cs	C at 1 inch	C_{max}	location - center of mass (inches)
223-T-12'	4.18	5.28	6.79	0.43"
223-M-7'-9"	5.45	10.95	11.53	0.35"
223-B- 5' 3" (Crack)	4.71	6.33	7.07	0.55"

5.2.4 – Apparent Chloride Diffusivity on the Cores Obtained 2021-2022

In some cases, the fitting required the removal of several layers in order to obtain a good fit. The tables below show the core ID (profile), the number of layers removed, the fitted Cs in kg/m^3 and in lb/yd^3, the assumed Co value, the D_{app} in $m^2/s \times 10^{-12}$ and in in^2/y, the last column displays the residual that gives a sense of how good the fit was. In a few instances (four profiles), the fitting was not possible and that is indicated. In a few cases, more than one fit is included in the table for selected profiles.

Table 21. Sebastian (bridge #880005) column 7: fitted D_{app}

Elevation MHWL	Layers Removed		Cs (kg/m^3)	Cs (lb/yd^3)	Co (lb/yd^3)	D_{app} $m^2/s \times 10^{-12}$	D_{app} in^2/y	Residual
11' Crack	1		5.2	8.8	0.4	42.89	2.096	1.257
11'	0		2.3	3.8	0.6	0.32	0.016	2.278
13'	0		2.1	3.5	0.4	2.23	0.109	0.750
15'	0		3.3	5.5	1	0.13	0.006	0.259
22'	2 (5&6)		2.5	4.3	0.9	0.13	0.006	1.669

Tables 21-Table 23 show the D_{app} values for profiles of cores from the Sebastian Inlet Bridge. The largest D_{app} corresponded to C7-11' along a crack which gave a value of 2.1 in^2/y (42.9×10^{-12} m^2/s). The other D_{app} values in Column 7 were smaller than 0.11 in^2/y. This column was not partially immersed in the seawater. For Column 8, the D_{app} values ranged between 0.2 and 0.01 in^2/y, with the larger values likely corresponding to cores obtained along cracks. D_{app} was not possible to fit with the profiles of column 13, nor for the profile of core at 27' 10" in Column 8. All D_{app} values fitted for profiles of column 10 and column 11 were less than 0.05 in^2/y.

Table 22. Sebastian (Bridge #880005) column 8: fitted D_{app}

Elevation MHWL	Layers Removed	Cs (kg/m^3)	Cs (lb/yd^3)	Co (lb/yd^3)	D_{app} $m^2/s \times 10^{-12}$	D_{app} in^2/y	Residual
12' Jacket	2	9.5	16.0	0.4	0.52	0.025	0.829
12' inner	2	3.3	5.6	0.4	0.16	0.008	0.384
17'	5	7.6	12.8	0.4	4.26	0.208	1.446
17' *(Rep)*	6	8.7	14.6	0.4	1.19	0.058	0.696
22'	3	10.8	18.1	1	1.09	0.053	3.358
25'	8	9.2	15.5	1	1.07	0.052	3.738
27' 10"	Not possible to fit						
33' 3"	3 (L4-L6)	2.6	4.5	1	0.42	0.021	0.183

Table 23. Sebastian (Bridge #880005) columns 10, 11 and 13: fitted D_{app}

Column	Elevation MHWL	Layers Removed	Cs (kg/m^3)	Cs (lb/yd^3)	Co (lb/yd^3)	D_{app} $m^2/s \times 10^{-12}$	D_{app} in^2/y	Residual
10	20' 10"	0	1.2	2.0	0.674	0.12	0.006	0.531
10	25' 7"	0	1.0	1.7	0.674	0.92	0.045	0.107
11	20' 7"	5	3.6	6.1	0.674	0.99	0.048	0.235
11	25' 5"	5	5.1	8.7	0.674	0.39	0.019	0.631
13	24’ 5”	Not possible to fit						
13	28” 11”	Not possible to fit						

Table 24 shows the D_{app} values, calculated Cs obtained from the Dania Bridge (Bridge #860160) cores. Most values obtained ranged between 0.045 in^2/y and 0.005. The profile obtained from the P4-6 South face at 11’ 9” gave a value of 2.1 in^2/y when 5 layers were removed, but the D_{app} value decreased to 0.045 in^2/y when two additional layers were removed. The largest fitted Cs value was observed on P3-6 East obtained at 11’ 2.5”.

Table 24. Dania (Bridge #860160): fitted D_{app}

Pile	Elevation MHWL	Layers Removed	Cs (kg/m3)	Cs (lb/yd^3)	Co (lb/yd^3)	D_{app} m^2/s $\times 10^{-12}$	D_{app} in^2/y	Residual
P3-6E	12’ 10	0	7.6	12.9	0.674	0.609	0.029	7.5071
P3-6E	11’ 2.5”	2	9.5	16.1	0.674	0.415	0.020	4.5947
P4-6S	11' 9"	5	5.1	8.6	1.011	43.604	2.131	1.097
P4-6S_*R*	11' 9"	7	6.9	11.7	1.011	0.899	0.044	0.1846
P4-6S_B	11' 2.5"	L3to5	5.3	8.9	0.674	0.328	0.016	1.7493
P4-6N_	13' 7"	5	3.6	6.0	0.674	0.392	0.019	0.3625
P4-6N_B	11' 9"		3.3	5.6	0.674	0.151	0.007	1.6559
P4-6N_B *R*	11' 9"	L2&3	4.0	6.8	0.674	0.106	0.005	0.231

Table 25. Bridge #100585 Gandy Bridge bents 237 and 223: fitted D_{app}

Bent	Elevation MHWL	Layers Removed	Cs (kg/m3)	Cs (lb/yd^3)	Co (lb/yd^3)	D_{app} m^2/s $\times 10^{-12}$	D_{app} in^2/y	Residual
237-T	15’ 10” no crack	0	0.6	0.9	0.25	0.117	0.006	0.0161
237-T	15’ 10” crack	0	0.5	0.8	0.25	6.294	0.308	0.0311
237-B	14’ 8” no crack	0	0.4	0.7	0.25	1.439	0.070	0.1539
237-B	14’ 8” crack	0	0.5	0.8	0.25	4.290	0.210	0.0817
237-B *R*	14’ 8”	4	0.5	0.9	0.25	4.290	0.210	0.0097
223-T	12’	0	3.4	5.8	0.67	10.573	0.5178	3.0635
223-T *R*	12’	4	3.9	6.6	0.67	2.766	0.135	1.7383
223-M	7’ 9”	3	7.1	11.9	0.67	10.730	0.525	1.0702
223-B	5’ 3”	Not possible to fit						

Table 25 shows the D_{app} values obtained from fitting Gandy Bridge profiles. The D_{app} values ranged from 0.52 to 0.005 in^2/y. The D_{app} obtained from profiles of cores obtained along cracks were significantly larger. When comparing non-crack cores, the D_{app} values observed from Bent 223 were larger than those observed in Bent 237; the column in the latter bent has a larger diameter. The fitted Cs values were also larger for Bent 223, but the elevations at which the cores were obtained are significantly different. Still, it is possible that the composition of the columns might be different (either in w/cm or the amount of fly ash used).

Profiles shapes likely affected the D_{app} goodness of fit. The number of layers that showed skin effect varied, and in some cases, the layer closest to the surface had a lower concentration with an upward trend followed by a more traditional non-steady diffusion profile trend. In a few cases, the chloride concentration of the layers obtained showed an increase in chloride as the depth increased. This observation was unexpected, but even after repeating selected layers, the same trend was observed.

The profiles in Bent 60 Trestle caps from SSK (see section 5.2.1) had similar profiles as some of those observed from the Sebastian Inlet Bridge (Bridge #880005) at the higher elevations. In the sense, of low Cs value followed by an increase in concentration as a function of depth and later followed by concentration decay, the profile named SSK1 showed a more traditional profile with a significantly lower concentration. It is possible that the concrete was drier and chloride deposition was lower at this location (sound concrete).

The profiles obtained from Column 2-1 N and Column 6-2, from the Sebastian Bridge (Bridge #880005) appear to be more consistent with non-steady diffusion with higher Cs. Profiles from Beam 11-1 and Pile cap 12 cores showed profiles with skin effect, but the concentration decayed as function of depth for later layers.

The cores from Column 7 (Bridge #880005) not including the core with a crack showed D_{app} values that ranged between 2.23 to 0.12 $m^2/s \times 10^{-12}$. D_{app} from cores of Column 8 showed that most values were greater than 0.4 and smaller than 1.2 $m^2/s \times 10^{-12}$. The D_{app} value calculated for the core obtained at a height of 17' along crack was 4.26 $m^2/s \times 10^{-12}$ with 5 layers removed.

At the higher elevation obtained cores (Bridge #880005), the D_{app} measured ranged from 0.12 $m^2/s \times 10^{-12}$, two values were close to 0.4 $m^2/s \times 10^{-12}$, and in two cases, D_{app} was close to 1 $m^2/s \times 10^{-12}$, with three profiles not fitted due to complex profile trend.

The D_{app} values for Bridge #860160 ranged from 0.1 to 0.9 $m^2/s \times 10^{-12}$ (one calculated value was 43 $m^2/s \times 10^{-12}$, but with a complex profile shape)

The concrete composition appears to be significant different for the two bents (columns) cored from Bridge #100585 (Gandy Bridge). Cores from Bent 237 suggest that crack did allow for deeper and higher chloride concentration, but the maximum observed concentration was less than 1 lb/yd^3. The profile of the core obtained in a region with no crack at 15' 10" (higher location) resemble a typical non-steady diffusion, whereas the profile of core obtained at 14' 8" showed skin effect. The concentration measured at the 1-inch depth is less than 0.5 lb/yd^3 for both cores. The shape of the profiles for cores obtained in Bent 223 showed low Cs followed by increase in concentration. In all cases, there is a plateau followed by a decay for two of the profiles (7' 9" and 12').

D_{app} values measured at the Gandy Bridge (Bridge #100585) showed the largest values. For profiles for cores with cracks the D_{app} was between 4.3 and 6.3 43 $m^2/s \times 10^{-12}$, whereas D_{app} for cores with no cracks were 0.117 and 1.44 $m^2/s \times 10^{-12}$ on Bent 237. The D_{app} calculated from profiles corresponding to Bent 223 ranged between 2.7 and 10 $m^2/s \times 10^{-12}$. The concentration values observed in Bent 237 are relatively low compared to those from Bent 223. It appears that

the concrete composition is different and the concrete cored was close to the water line for those obtained from Bent 223.

For structures with supplementary cementitious materials in the concrete composition, the time to corrosion initiation will be longer than for structures built with OPC only, based on the D_{app} values observed from profiles obtained on the outdoor samples and profiles corresponding to field cores. However, given enough time, corrosion at elevations above >MHWL+12 could exceed the chloride threshold at the reinforcement depth. Besides the concrete composition and cover thickness, the structure location, the surrounding macro climate, and microclimate will influence the rate of chloride deposition and moisture levels within the concrete. Corrosion is still expected to initiate first at the splash zone. Based on the wet candle measurements it appears that chloride deposition can be significant several months on each year, but the magnitude can vary from year to year. Extreme weather events can enhance the chloride deposition on structures that are close to the ocean.

5.3 – Recommendation

The chloride deposition onto bridge structures even at high elevations (i.e., locations >MHWL+12) could be significant at locations near the coast, for sites where the wind speed (with corresponding larger breaking waves) is greater than or equal to 3 m/s for prolonged periods of time. Depending on the region topography, the ocean spray can reach the atmospheric zone and ocean aerosol particles reach elevations as high as 20 ft (or even higher) above the mean high-water line. It is recommended that the minimum concrete cover of elements at these elevations be increased to 3 inches. Regions of the structure at these heights with high chloride deposition and high moisture could eventually reach chloride concentrations at the steel reinforcement that cause corrosion to initiate. Concrete with high resistivity (low chloride diffusivity) is recommended. Joints and elements where concrete cover is known to be thin, require special attention during the service life of the structure.

Chapter 6 – Conclusions

6.1 – Summary of Monitoring Samples Exposed Outdoors at FAU SeaTech

Most D_{app} values measured on all DCL samples at the East site were smaller than 0.25×10^{-12} m^2/s. Two samples had larger D_{app} values, which were close to 1×10^{-12} m^2/s (0.8×10^{-12} m^2/s for DCL3 and 0.9×10^{-12} m^2/s for DCL11).

Seven DCL-C samples had D_{app} values smaller than 0.1×10^{-12} m^2/s, these are DCL-C samples exposed on the west site and with the surface facing upwards. The maximum Dapp value measured on these samples was close to 0.3×10^{-12} m^2/s. In general, smaller D_{app} values were observed on the DCL-C (samples exposed at the west site).

The D_{app} values calculated for most DCL samples suggest slow chloride transport into the concrete.

The D_{app} observed on samples with not mortar layer had larger D_{app} values, particularly the samples with 1C1 composition (OPC only): four of the five 1C1 specimens had D_{app} values greater than 1×10^{-12} m^2/s, ranging from 2.2 to 15.5×10^{-12} m^2/s.

6.2 – Summary of Field Component

The D_{app} was computed for most profiles, but in a few instances, the fitting was not possible (profiles of cores taken at higher elevation in Bridge #880005).

The largest D_{app} observed on Bridge #100585 was 10.7×10^{-12} m^2/s, whereas for Bridge #860160, $D_{app} \sim 0.9 \times 10^{-12}$ m^2/s.

For Bridge #880005; the D_{app} observed from profiles of lower cores on column 8 ranged between 0.5 and 4.2×10^{-12} m^2/s (several values were $\sim 1. \times 10^{-12}$ m^2/s) and from column 7, most D_{app} values were between 0.1 and 2.2×10^{-12} m^2/s (not including the 11' crack core). The D_{app} observed from profiles corresponding to cores obtained close to the top of the column ranged between 0.1 and 1×10^{-12} m^2/s, with the calculated Cs significantly smaller for those obtained close to the top of the column.

6.3 – Summary for Wet Candle

A modest chloride deposition was observed in most instances regardless of location and elevation.

Each year there were a few measurements in which the chloride deposition was high, and the height at which the maximum value was observed was not the wet candle at the lower elevation as is often expected. Turbulence and periods of high wind speed (equal to or exceeding 3 m/s) likely caused a larger chloride deposition, and the greater deposition was found at the higher elevations.

References

1. M. J. Osmolska, T. Kanstad, M. A. Hendriks, K. Hornbostel, G. Markeset, (2019) “Durability of pretensioned concrete girders in coastal climate bridges: Basis for better maintenance and future design.” *Structural Concrete*; 20: 2256–2271. https://doi.org/10.1002/suco.201900144.

2. I. S. Cole, et al., (2003) “Holistic model for atmospheric corrosion: Part 2 - Experimental measurement of deposition of marine salts in a number of long-range studies” *Corrosion Engineering, Science and Technology*, 38(4):259–266.

3. R. E. Melchers, I. Chaves, and T. Pape, (2017) “Long term durability of reinforcement in Class A and Class B concretes in Pacific Ocean marine environment”, Proceedings of Eurocorr 2017.

4. R. E. Melchers, (2015) “Field experience and the long-term durability of reinforced concrete structures”, Proceedings of Second International Conference on Performance-based and Life-cycle Structural Engineering, (PLSE 2015) pp. 9-12.

5. R. E. Melchers, T. M. Pape, I. A. Chaves, and R. J. Heywood, (2017) “Long-term durability of reinforced concrete piles from the Hornibrook Highway Bridge”, *Australian Journal of Structural Engineering*, 18(1):41-57.

6. R. E. Melchers and I. A. Chaves, (2019) “Durability of reinforced concrete bridges in marine environments”, *Structure and Infrastructure Engineering*, 16(1):169-180 https://doi.org/10.1080/15732479.2019.1604769

7. R. E. Melchers, and I.A. Chaves, (2017) “A comparative study of chlorides and longer-term reinforcement corrosion” *Materials and Corrosion*, 68(6):613–621. doi:10.1002/maco.201609310

8. M. Maage, (1997)“An historical review of Norwegian standards for durable marine concrete structures”, in Fourth CANMET/ACI International Conference on Durability of Concrete, ACI *Special Publication* 170, 835-852.

9. R. D. Browne (1986) “Practical considerations in producing durable concrete”, in Improvement of concrete durability. *Institute of Civil Engineers*, 97-130.

10. T. J. Collins, R. K. Dhir, M. J. McCarthy, and S. Caliskan (2005) “Inspection of structures in the marine environment” in *Concrete for Transportation Infrastructure*, pp. 377-384.

11. M. Nagi and D. Whiting (1994) “Corrosion of prestressed reinforcing steel in concrete bridges: state of the art”, in *ACI Special Publication 151* Concrete Bridges in Aggressive Environments, pp. 17-41.

12. T. M. Pape´ and R. E. Melchers, (2010) “The effects of corrosion on 45-year-old pre-stressed concrete bridge beams”, *Structure and Infrastructure Engineering*, 7(1-2):101-108, DOI: 10.1080/15732471003588411

13. S. Fricker, T. Vogel, H. Ungricht, & F. Hunkeler, (2010) “Acoustic monitoring of a prestressed concrete bridge and its condition survey during demolition” Final report No. 643 Research Project AGB 2005/014), Swiss Association of Road and Transportation Experts (VSS), Zurich, Switzerland.

14. W. Lukas, (1985) “Relationship between chloride content in concrete and corrosion in untensioned reinforcement on Austrian bridges and concrete road surfacings.” Betonwerk Und Fertigteil-Technik, 51(11):730–734.

15. O. E. Gjorv, (2009) “Durability design of concrete structures in severe environments”. London: Taylor & Francis.

16. M. G. Richardson, (2002) “Fundamentals of durable reinforced concrete” London: Spon Press.

17. O. O. Alao, (2014) “Refinement of air-borne chloride exposure classes for RC structures in the Cape peninsula”, M.Sc. Thesis, University of Cape Town, South Africa.

18. M. L. Gobinddass, J. Molinie, S. Richard, K. Panechou, A. Jeannot, and S. Jean-Louis, (2020), “Coastal Sea Salt Chlorine Deposition Linked to Intertropical Convergence Zone (ITCZ) Oscillation in French Guiana”, *Journal of the Atmospheric Sciences*, 77:1723-1731.

19. G. R. Meira, C. Andrade, C. Alonso, J. C. Boral, M. Padilha, (2010) “Durability of concrete structures in marine atmosphere zones – the use of chloride deposition rate on the wet candle as an environmental indicator,” *Cement and Concrete Composites*, 32:427-435.

20. G. R. Meira, C. Andrade, I. J. Padaratz, C. Alonso, and J. C. Borba Jr. (2007) “Chloride penetration into concrete structures in the marine atmosphere zone - Relationship between deposition of chlorides on the wet candle and chlorides accumulated into concrete,” *Cement and Concrete Composites*, 29:667-676.

21. F. Presuel-Moreno, W. Arias, V. Echevarria, S. Shill, Y-Y. Wu., (2014) “Diffusion vs. Concentration of Chloride Ions in Concrete”, BDK79-977-03, FDOT Final Report; Boca Raton, FL: Florida Atlantic University.

22. G. R. Meira, M. C. Andrade, I. J. Padaratz, M. C. Alonso, and J. C. Borba Jr, (2006) “Measurements and modelling of marine salt transportation and deposition in a tropical region in Brazil,” *Atmospheric Environment*, 40:5596 - 5607.

23. S. Feliu, M. Morcillo, and B. Chico, (1999) “Effect of distance from sea on atmospheric corrosion rate,” *Corrosion*, 55(9):883-891.

24. M.A. Mustafa and K.M. Yusof, (1994) “Atmospheric chloride penetration into concrete in semitropical marine environment”, *Cement and Concrete Research*, 24(4):661-670.

25. D. E. Spiel, and G. De Leeuw, (1996) "Formation and production of sea spray aerosols", *Journal of Aerosol Science*, 27:S65–S66.

26. J. Piazzola, S. Despiau, (1997) "Contribution of marine aerosols in the particle size distributions observed in Mediterranean coastal zone", *Atmospheric Environment* 31(18):2991–3009.

27. P. D. Komar and J. C. Allan, (2007) “Higher Waves Along U.S. East Coast Linked to Hurricanes”, *EOS* , Transactions American Geophysical Union 88(30):301-308.

28. J. Alcántara, B. Chico, I. Díaz, D. de la Fuente, and M. Morcillo (2015) “Airborne chloride deposit and its effect on marine atmospheric corrosion of mild steel” *Corrosion Science*, 97:74–88.

29. J. Alcántara, D. de la Fuente, B. Chico, J. Simancas, I. Díaz and M. Morcillo (2017) “Marine Atmospheric Corrosion of Carbon Steel: A Review”, *Materials*, 10, 406, 67 pages doi:10.3390/ma10040406

30. E. L. Montgomery, L. M. Calle, J. C. Curran, M. R. Kolody, (2011) “Timescale Correlation Between Marine Atmospheric Exposure and Accelerated Corrosion Testing”, Corrosion/2011 conference. OnePetro.

31. https://corrosion.ksc.nasa.gov/Coatings/AtmosphericSiteData

32. F. Corvo, N. Betancourt, A. Mendoza, (1995) The influence of airborne salinity on the atmospheric corrosion of steel, *Corrosion Science* 37(12):1889–1901.

33. K. M. A. Hossain and S. M. Easa, (2011) “Spatial distribution of Marine Salts in Coastal Region using wet candle sensors”, *IJRRAS* 7(3):228-235.

34. B. S. Phull, S. J. Pikul, and R. M. Kain (2000) "Thirty-Eight Years of Atmospheric Corrosivity Monitoring," Marine Corrosion in Tropical Environments, ASTM STP 1399, S. W. Dean, G. Hernandez-Duque Delgadillo, and J. B. Bushman, Eds., American Society for Testing and Materials, West Conshohocken, PA, pp 60-74.

35. M. Akiyama, D. M. Frangopol and M. Suzuki, (2012) “Integration of the effects of airborne chlorides into reliability-based durability design of reinforced concrete structures in a marine environment”, *Structure and Infrastructure Engineering*, 8(2):125–134.

36. G. R. Meira, W. T. A. Pinto, E. E. P. Lima, C. Andrade (2017) “Vertical distribution of marine aerosol salinity in a Brazilian coastal area – The influence of wind speed and the impact on chloride accumulation into concrete”, *Construction and Building Materials* 135:287–296.

37. Anders Daniels (1989) “Measurements of atmospheric sea salt concentrations in Hawaii using a Tala kite”, *Tellus B*: *Chemical and Physical Meteorology*, 41(2):196-206, DOI:10.3402/tellusb.v41i2.15069.

38. R. Klassen, B. Hinton, and E. Roberge, (2000) "Aerosol Model Aids Interpretation of Corrosivity Measurements in a Tropical Region of Australia," in Marine Corrosion in Tropical Environments, ASTM STP 1399, S. W. Dean, G. Hernandez-Duque Delgadillo, and J. B. Bushman, Eds., American Society for Testing and Materials, West Conshohocken, PA, pp 48-59.

39. G. Markeset (2009) Critical chloride content and its influence on service life predictions. *Materials and Corrosion*; 60(8):593–596.https://doi.org/10.1002/maco.200905288.

40. A. Blankvoll, (1997) Norwegian Road Research Laboratory, Proceedings of the International Conference on Repair of Concrete Structures from Theory to Practice in a Marine Environment, Svolvear (Norway); pp. 89–98.

41. F. L. LaQue, Marine Corrosion, ECS monograph, 1975.

42. N. D. Pham, Y. Kuriyama, N. Kasai, S. Okazaki, K. Suzuki, D. T. Nguyen, (2019) “A new analysis of wind on chloride deposition for long-term aerosol chloride deposition monitoring with weekly sampling frequency”, *Atmospheric Environment*., 198:46 - 54.

43. J. Liu, G. Ou, Q. Qiu, F. Xing, K. Tang, J. Zeng, (2018) “Atmospheric chloride deposition in field concrete at coastal region”, *Construction and Building Materials* 190:1015-1022.

44. N. D. Pham, S. Okazaki, Y. Kuriyama, N. Kasai, K. Suzuki, (2019) "Real-time aerosol chloride deposition measuring device using conductivity sensor", *Atmospheric Environment* 213:757-766.

45. R. J. Santucci, R. S. Davis & C. E. Sanders (2022) Atmospheric corrosion severity and the precision of salt deposition measurements made by the wet candle method, *Corrosion Engineering, Science and Technology*, 57(2):147-158, DOI:10.1080/1478422X.2021.2005227.

46. T.H. Muster, I.S. Cole (2005) “Attachment efficiencies of salt aerosols onto infrastructure and implications for atmospheric corrosion” *Journal of the Electrochemical Society* 152 (3):B125.

47. JIS Z 2382, (2001) Determination of Pollution for Evaluation of Corrosivity of Atmospheres, – Japanese industrial standards.

48. N Kazuhiro, D Yoshiki (1993) “Nationwide investigation on airborne sea salt (IV)” - Japan: Public Works Research Institute.

49. K. Suzuki and I. Robertson, (2011) “Atmospheric Chloride Deposition Rate for Corrosion Prediction on Oahu”, Report# UHM/CEE/11-02, Final report for Hawaii Department of Transportation.

50. H. Bian et al. (2019) “Observationally constrained analysis of sea salt aerosol in the marine atmosphere”, *Atmos. Chem. Phys.*, 19:10773–10785, https://doi.org/10.5194/acp-19-10773-2019.

51. R. Wattanapornprom, T. Ishida (2018) "Comprehensive Numerical System for Predicting Airborne Chloride Generation and Its Ingress in Concrete under Actual Environmental Conditions", *Journal of Advanced Concrete Technology*, 16:18-35.

52. H. Hilsdorf, (1995) “Concrete compressive strength, transport characteristics and durability”. In Performance criteria for concrete durability; H. Hilsdorf & J. Kropp, eds. London, UK: CRC Press, pp. 165–195.

53. T. Otha, (1991) ‘Corrosion of Reinforcing Steel in Concrete Exposed to Sea Air’, in Second International Conference on Durability of Concrete, *ACI Special Publication* 126:459-477.

54. G. R. Meira, C. Andrade, E. O. Vilar, K. D. Nery (2014) “Analysis of chloride threshold from laboratory and field experiments in marine atmosphere zone” *Construction and Building Materials* 55:289–298.

55. S. Fukuda, T. Fujiwara, M. Shoya, M. Kawakami, F. Omata, (1997) “Durability of Prestressed Concrete Bridges in the North-East District of Japan”, in Fourth CANMET/ACI International Conference on Durability of Concrete, *ACI Special Publication* 170:1447-1466.

56. C. E. T. Balestra, T. A. Reichert, W. A. Pansera G. Savaris, (2019) “Chloride profile modeling contemplating the convection zone based on concrete structures present for more than 40 years in different marine aggressive zones” *Construction and Building Materials*, 198:345-358.

57. D. Whiting and B. G. Stejskal, (1994) “Field studies of Corrosion in prestressed concrete bridges” in *ACI Special Publication* 151:73-93.

58. J. Gulikers, (2019) “Condition assessment and service life prediction of a marine concrete structure: an interesting case study”, in Concrete Solutions 2019, MATEC Web of Conferences Vol. 289, p. 08003 EDP Sciences https://doi.org/10.1051/matecconf/201928908003

59. W. Scannell, M. Duncan, (2018) “Corrosion condition evaluation of superstructure and substructure components on bridge no. 880005 in FDOT district 4” Final Report.

60. M. Morcillo, B. Chico, L. Mariaca, E. Otero, (2000) “Salinity in marine atmospheric corrosion: its dependence on the wind regime existing in the site, *Corrosion Science* 42(1):91–104.

61. H. R. Ambler, A. A. J. Bain, (1955) "Corrosion of metals in the tropics", *Journal of Applied Chemistry*, 5(9):437–467.

62. F. Presuel-Moreno, et al. (2018) “Chloride diffusivity and resistivity of cured and mature binary/ternary concrete”, FDOT Final Report; Boca Raton, FL: Florida Atlantic University.

63. ISO 9225 (2012) "Corrosion of metals and alloys — Corrosivity of atmospheres — Measurement of environmental parameters affecting corrosivity of atmospheres".

64. ASTM G140-02 (2019) “Standard Test Method for Determining Atmospheric Chloride Deposition Rate by Wet Candle Method” American Society for Testing of Materials, Annual Book of ASTM Standards.

65. FM-5-516 FDOT, (2013) “Florida Method of Test for Determining Low-Levels of Chloride in Concrete and Raw Materials,” Tallahassee, FL, USA: Florida Department of Transportation.

http://www.dot.state.fl.us/statematerialsoffice/administration/resources/library/publications/fstm/methods/fm5-516.pdf.

Appendix A: Chloride Concentration Samples Exposed at SeaTech

Chloride Titrations on DC samples exposed on the Eastern Site after approx. 108 months of exposure

Table 26. DCL1-F (after 108 months of exposure)

				DC1-F				
Layer	center of mass							
Thickness (cm)	cm	Layer	A-kg/m^3	B-kg/m^3	ave kg/m^3	A-lb/yd^3	B-lb/yd^3	ave-lb/yd^3
0.05	0.025	1	5.45	5.44	5.11	9.27	7.96	8.61
0.05	0.075	2	6.63	6.55	4.44	7.55	7.39	7.47
0.05	0.125	3	6.52	6.16	4.32	6.83	7.73	7.28
0.05	0.175	4	6.17	5.81	3.57	6.08	5.95	6.01
0.05	0.225	5	4.82	5.02	3.44	6.22	5.38	5.8
0.05	0.275	6	4.72	4.51	2.63	4.46	4.39	4.42
0.05	0.325	7	3.74	3.77	2.65	4.65	4.29	4.47
0.05	0.375	8	3.15	3.21	2.06	3.43	3.52	3.48
0.05	0.425	9	2.90	2.92	3.76	6.35	6.32	6.34
0.05	0.475	10	3.22	3.10	1.69	3.01	2.69	2.85
0.05	0.525	11	2.88	2.97	1.57	2.88	2.4	2.64
0.05	0.575	12	3.94	3.11	1.43	2.5	2.31	2.41
0.05	0.625	13	1.99	1.85	1.26	2.11	2.15	2.13
0.05	0.675	14	2.45	2.43	1.29	2.16	2.17	2.17
0.05	0.725	15	3.42	3.41	1.6	2.81	2.58	2.7
0.05	0.775	16	3.44	3.36	1.01	1.63	1.76	1.7
0.05	0.825	17	2.21	2.10	0.84	1.36	1.46	1.41
0.05	0.875	18	2.20	2.09	0.82	1.52	1.25	1.38
0.05	0.925	19	1.94	1.85	0.77	1.35	1.26	1.3
0.05	0.975	20	1.99	1.81	0.61	1.04	1.01	1.03
0.05	1.025	21	1.56	1.44	0.34	0.63	0.52	0.58
0.05	1.075	22	1.92	2.07	0.4	0.7	0.65	0.67

Table 27. DCL2-F (after 108 months of exposure)

Layer	center of mass							
Thickness (cm)	cm	Layer	A-kg/m^3	B-kg/m^3	ave kg/m^3	A-lb/yd^3	B-lb/yd^3	ave-lb/yd^3
0.05	0.025	1	5.50	4.72	5.11	9.27	7.96	8.61
0.05	0.075	2	4.48	4.39	4.44	7.55	7.39	7.47
0.05	0.125	3	4.05	4.59	4.32	6.83	7.73	7.28
0.05	0.175	4	3.61	3.53	3.57	6.08	5.95	6.01
0.05	0.225	5	3.69	3.19	3.44	6.22	5.38	5.8
0.05	0.275	6	2.65	2.60	2.63	4.46	4.39	4.42
0.05	0.325	7	2.76	2.54	2.65	4.65	4.29	4.47
0.05	0.375	8	2.04	2.09	2.06	3.43	3.52	3.48
0.05	0.425	9	3.77	3.75	3.76	6.35	6.32	6.34
0.05	0.475	10	1.79	1.60	1.69	3.01	2.69	2.85
0.05	0.525	11	1.71	1.42	1.57	2.88	2.4	2.64
0.05	0.575	12	1.48	1.37	1.43	2.5	2.31	2.41
0.05	0.625	13	1.25	1.28	1.26	2.11	2.15	2.13
0.05	0.675	14	1.28	1.29	1.29	2.16	2.17	2.17
0.05	0.725	15	1.67	1.53	1.6	2.81	2.58	2.7
0.05	0.775	16	0.97	1.05	1.01	1.63	1.76	1.7
0.05	0.825	17	0.81	0.87	0.84	1.36	1.46	1.41
0.05	0.875	18	0.90	0.74	0.82	1.52	1.25	1.38
0.05	0.925	19	0.80	0.75	0.77	1.35	1.26	1.3
0.05	0.975	20	0.62	0.60	0.61	1.04	1.01	1.03
0.05	1.025	21	0.37	0.31	0.34	0.63	0.52	0.58
0.05	1.075	22	0.41	0.39	0.4	0.7	0.65	0.67

Table 28. DCL3-F (after 108 months of exposure)

Layer	center of mass							
Thickness (cm)	cm	Layer	A- kg/m^3	B- kg/m^3	ave kg/m^3	A- lb/yd^3	B- lb/yd^3	ave- lb/yd^3
0.055	0.027	1	7.57	6.73	7.15	12.76	11.33	12.04
0.106	0.108	2	7.72	7.85	7.79	13.00	13.23	13.11
0.119	0.221	3	7.95	7.82	7.88	13.39	13.17	13.28
0.163	0.362	4	7.22	7.04	7.13	12.17	11.86	12.01
0.138	0.513	5	7.34	7.21	7.28	12.37	12.14	12.26
0.195	0.679	6	7.82	7.75	7.78	13.17	13.05	13.11
0.175	0.864	7	8.40	7.72	8.06	14.15	13.00	13.58
0.216	1.060	8	8.74	7.75	8.25	14.73	13.06	13.89
0.231	1.283	9	7.60	7.56	7.58	12.81	12.74	12.78
0.237	1.517	10	7.50	7.07	7.29	12.64	11.92	12.28
0.242	1.757	11	6.13	6.34	6.23	10.33	10.68	10.50
0.522	2.139	12	4.20	4.18	4.19	7.08	7.04	7.06
0.240	2.520	13	3.04	2.93	2.99	5.12	4.94	5.03
0.240	2.760	14	2.54	2.39	2.46	4.28	4.02	4.15

Table 29. DCL4-F (after 108 months of exposure)

Layer	center of mass							
Thickness (cm)	cm	Layer	A- kg/m^3	B- kg/m^3	ave kg/m^3	A- lb/yd^3	B- lb/yd^3	ave- lb/yd^3
0.05	0.025	1	0.85	1.09	0.97	1.43	1.83	1.63
0.05	0.075	2	1.14	1.12	1.13	1.92	1.88	1.90
0.1	0.175	3	1.93	1.95	1.94	3.26	3.28	3.27
0.1	0.275	4	1.33	1.56	1.45	2.24	2.63	2.44
0.1	0.375	5	1.27	1.21	1.24	2.14	2.03	2.08
0.1	0.475	6	0.84	0.90	0.87	1.41	1.51	1.46
0.1	0.575	7	0.79	0.80	0.80	1.33	1.35	1.34
0.1	0.675	8	0.70	0.71	0.71	1.18	1.20	1.19
0.1	0.775	9	0.59	0.55	0.57	1.00	0.92	0.96
0.1	0.875	10	0.49	1.31	0.90	0.83	2.21	1.52
0.1	0.975	11	1.97	1.99	1.98	3.33	3.35	3.34
0.1	1.075	12	1.87	1.98	1.93	3.16	3.34	3.25

Table 30. DCL5-F (after 108 months of exposure)

Layer	center of mass							
Thickness (cm)	cm	Layer	A- kg/m^3	B- kg/m^3	ave kg/m^3	A- lb/yd^3	B- lb/yd^3	ave- lb/yd^3
0.05	0.025	1	1.04	1.29	1.16	1.74	2.17	1.96
0.05	0.075	2	2.95	2.98	2.97	4.98	5.02	5.00
0.05	0.125	3	3.22	3.05	3.14	5.43	5.14	5.28
0.05	0.175	4	2.47	2.37	2.42	4.16	4.00	4.08
0.05	0.225	5	1.83	1.88	1.86	3.08	3.17	3.12
0.05	0.275	6	1.42	1.29	1.36	2.39	2.18	2.28
0.05	0.325	7	1.15	1.14	1.15	1.93	1.93	1.93
0.05	0.375	8	1.03	1.96	1.50	1.74	3.30	2.52
0.05	0.425	9	0.92	0.87	0.89	1.54	1.47	1.51
0.05	0.475	10	0.80	0.85	0.82	1.35	1.42	1.39
0.05	0.525	11	0.48	0.53	0.50	0.80	0.89	0.85
0.05	0.575	12	0.55	1.49	1.02	0.92	2.52	1.72
0.05	0.625	13	0.94	0.71	0.83	1.59	1.20	1.39
0.05	0.675	14	0.57	0.54	0.56	0.96	0.91	0.93
0.05	0.725	15	0.53	0.45	0.49	0.89	0.77	0.83
0.05	0.775	16	0.57	0.62	0.59	0.95	1.04	1.00
0.05	0.825	17	0.48	0.48	0.48	0.80	0.81	0.81
0.05	0.875	18	0.68	0.54	0.61	1.15	0.91	1.03
0.05	0.925	19	0.58	0.50	0.54	0.98	0.84	0.91
0.05	0.975	20	0.45	0.57	0.51	0.75	0.95	0.85
0.05	1.025	21	0.45	0.50	0.47	0.75	0.84	0.80
0.05	1.075	22	0.39	0.57	0.48	0.66	0.95	0.81

Table 31. DCL6-F (after 108 months of exposure)

Layer	center of mass							
Thickness (cm)	cm	Layer	A- kg/m^3	B- kg/m^3	ave kg/m^3	A- lb/yd^3	B- lb/yd^3	ave- lb/yd^3
0.05	0.025	1	2.34	1.71	2.02	3.93	2.88	3.41
0.05	0.075	2	1.35	1.43	1.39	2.28	2.42	2.35
0.1	0.175	3	2.26	2.29	2.27	3.80	3.85	3.83
0.1	0.275	4	2.28	2.39	2.33	3.85	4.02	3.93
0.1	0.375	5	2.11	2.08	2.09	3.55	3.50	3.53
0.1	0.475	6	2.05	1.77	1.91	3.46	2.98	3.22
0.1	0.575	7	1.74	1.60	1.67	2.93	2.70	2.82
0.1	0.675	8	1.33	1.34	1.34	2.24	2.25	2.25
0.1	0.775	9	1.28	1.31	1.30	2.16	2.21	2.19
0.1	0.875	10	1.13	1.12	1.12	1.90	1.89	1.89
0.1	0.975	11	1.23	1.21	1.22	2.08	2.05	2.06
0.1	1.075	12	1.31	1.40	1.35	2.21	2.36	2.28

Table 32. DCL7-F (after 108 months of exposure)

Layer	center of mass							
Thickness (cm)	cm	Layer	A- kg/m^3	B- kg/m^3	ave kg/m^3	A- lb/yd^3	B- lb/yd^3	ave- lb/yd^3
0.05	0.025	1	4.54	3.35	3.95	7.65	5.65	6.65
0.05	0.075	2	4.24	3.79	4.01	7.14	6.38	6.76
0.05	0.125	3	3.42	3.33	3.37	5.75	5.61	5.68
0.05	0.175	4	2.58	2.56	2.57	4.34	4.32	4.33
0.05	0.225	5	2.24	1.88	2.06	3.77	3.17	3.47
0.05	0.275	6	1.76	1.69	1.73	2.97	2.85	2.91
0.05	0.325	7	1.42	1.35	1.38	2.39	2.27	2.33
0.05	0.375	8	1.23	1.15	1.19	2.07	1.94	2.01
0.05	0.425	9	1.07	1.03	1.05	1.80	1.74	1.77
0.05	0.475	10	0.81	0.89	0.85	1.36	1.50	1.43
0.05	0.525	11	1.03	1.04	1.03	1.73	1.75	1.74
0.05	0.575	12	0.87	0.89	0.88	1.46	1.50	1.48
0.05	0.625	13	0.79	0.74	0.76	1.32	1.25	1.29
0.05	0.675	14	0.82	0.74	0.78	1.39	1.24	1.31
0.05	0.725	15	0.65	0.79	0.72	1.09	1.33	1.21
0.05	0.775	16	0.72	0.57	0.65	1.21	0.97	1.09
0.05	0.825	17	0.57	0.59	0.58	0.96	0.99	0.97
0.05	0.875	18	0.63	0.63	0.63	1.07	1.06	1.06
0.05	0.925	19	0.50	0.47	0.49	0.84	0.80	0.82
0.05	0.975	20	0.42	0.49	0.45	0.70	0.82	0.76
0.05	1.025	21	0.66	0.59	0.63	1.12	1.00	1.06
0.05	1.075	22	0.67	1.04	0.86	1.13	1.75	1.44

Table 33. DCL8-F (after 108 months of exposure)

Layer	center of mass							
Thickness (cm)	cm	Layer	A- kg/m^3	B- kg/m^3	ave kg/m^3	A- lb/yd^3	B- lb/yd^3	ave- lb/yd^3
0.05	0.025	1	3.05	2.85	2.95	5.14	4.79	4.97
0.05	0.075	2	3.41	3.28	3.35	5.74	5.53	5.63
0.05	0.125	3	2.85	2.70	2.78	4.80	4.55	4.68
0.05	0.175	4	2.40	2.33	2.36	4.04	3.92	3.98
0.05	0.225	5	1.97	2.02	1.99	3.31	3.40	3.35
0.05	0.275	6	1.38	1.68	1.53	2.32	2.83	2.57
0.05	0.325	7	1.31	1.16	1.24	2.21	1.96	2.09
0.05	0.375	8	1.04	1.00	1.02	1.75	1.68	1.71
0.05	0.425	9	0.89	0.84	0.86	1.50	1.41	1.45
0.05	0.475	10	0.73	0.74	0.73	1.23	1.24	1.24
0.05	0.525	11	0.78	0.90	0.84	1.32	1.51	1.41
0.05	0.575	12	0.71	0.79	0.75	1.20	1.33	1.26
0.05	0.625	13	0.82	0.84	0.83	1.38	1.42	1.40
0.05	0.675	14	0.77	0.73	0.75	1.30	1.23	1.26
0.05	0.725	15	0.78	0.73	0.75	1.31	1.23	1.27
0.05	0.775	16	1.12	0.61	0.86	1.89	1.02	1.46
0.05	0.825	17	0.67	0.60	0.63	1.13	1.01	1.07
0.05	0.875	18	0.65	0.58	0.62	1.10	0.98	1.04
0.05	0.925	19	0.56	0.63	0.60	0.94	1.06	1.00
0.05	0.975	20	0.76	0.59	0.67	1.28	0.99	1.13
0.05	1.025	21	0.92	0.84	0.88	1.54	1.41	1.47
0.05	1.075	22	0.99	0.90	0.95	1.68	1.52	1.60

Table 34. DCL9-F (after 108 months of exposure)

Layer	center of mass							
Thickness (cm)	cm	Layer	A- kg/m^3	B- kg/m^3	ave kg/m^3	A- lb/yd^3	B- lb/yd^3	ave- lb/yd^3
0.05	0.025	1	1.23	0.59	0.91	2.07	0.99	1.53
0.05	0.075	2	1.62	0.96	1.29	2.73	1.62	2.18
0.05	0.125	3	1.63	1.76	1.70	2.75	2.97	2.86
0.05	0.175	4	1.62	1.64	1.63	2.73	2.75	2.74
0.05	0.225	5	1.83	1.39	1.61	3.08	2.34	2.71
0.05	0.275	6	1.21	1.35	1.28	2.04	2.28	2.16
0.05	0.325	7	1.31	0.92	1.11	2.21	1.55	1.88
0.05	0.375	8	1.75	1.29	1.52	2.94	2.17	2.56
0.05	0.425	9	1.18	1.14	1.16	1.99	1.92	1.96
0.05	0.475	10	0.66	0.74	0.70	1.11	1.24	1.18
0.05	0.525	11	0.86	0.36	0.61	1.46	0.61	1.03
0.05	0.575	12	0.85	0.80	0.83	1.44	1.35	1.40
0.05	0.625	13	0.78	0.86	0.82	1.32	1.44	1.38
0.05	0.675	14	0.87	1.24	1.06	1.47	2.08	1.78
0.05	0.725	15	0.83	0.87	0.85	1.40	1.46	1.43
0.05	0.775	16	0.61	0.66	0.64	1.03	1.11	1.07
0.05	0.825	17	0.73	0.65	0.69	1.22	1.10	1.16
0.05	0.875	18	0.61	0.67	0.64	1.02	1.13	1.07
0.05	0.925	19	0.72	0.74	0.73	1.21	1.25	1.23
0.05	0.975	20	0.84	0.35	0.60	1.42	0.59	1.00
0.05	1.025	21	0.66	0.31	0.49	1.11	0.53	0.82
0.05	1.075	22	1.25	1.23	1.24	2.11	2.06	2.09

Table 35. DCL10-F (after 108 months of exposure)

Layer	center of mass							
Thickness (cm)	cm	Layer	A- kg/m^3	B- kg/m^3	ave kg/m^3	A- lb/yd^3	B- lb/yd^3	ave- lb/yd^3
0.05	0.025	1	4.94	2.72	3.83	8.31	4.59	6.45
0.05	0.075	2	2.44	2.61	2.53	4.11	4.39	4.25
0.05	0.125	3	2.25	2.44	2.34	3.78	4.12	3.95
0.05	0.175	4	1.91	1.83	1.87	3.22	3.09	3.16
0.05	0.225	5	2.13	1.18	1.66	3.59	1.99	2.79
0.05	0.275	6	1.45	1.49	1.47	2.44	2.50	2.47
0.05	0.325	7	1.26	1.36	1.31	2.13	2.29	2.21
0.05	0.375	8	1.17	1.26	1.21	1.98	2.12	2.05
0.05	0.425	9	1.11	1.11	1.11	1.86	1.87	1.86
0.05	0.475	10	1.08	1.03	1.05	1.82	1.73	1.77
0.05	0.525	11	1.12	1.02	1.07	1.88	1.72	1.80
0.05	0.575	12	1.00	0.98	0.99	1.69	1.65	1.67
0.05	0.625	13	1.13	1.13	1.13	1.90	1.90	1.90
0.05	0.675	14	0.90	0.85	0.88	1.52	1.44	1.48
0.05	0.725	15	0.91	0.90	0.91	1.53	1.52	1.52
0.05	0.775	16	1.60	1.23	1.42	2.69	2.08	2.39
0.05	0.825	17	1.03	1.03	1.03	1.74	1.74	1.74
0.05	0.875	18	1.12	0.96	1.04	1.88	1.62	1.75
0.05	0.925	19	0.83	0.83	0.83	1.40	1.39	1.40
0.05	0.975	20	0.93	0.91	0.92	1.56	1.53	1.55
0.05	1.025	21	0.37	0.39	0.38	0.62	0.65	0.63
0.05	1.075	22	0.35	0.38	0.37	0.58	0.65	0.62

Table 36. DCL10a-F (after 108 months of exposure)

Layer	center of mass							
Thickness (cm)	cm	Layer	A- kg/m^3	B- kg/m^3	ave kg/m^3	A- lb/yd^3	B- lb/yd^3	ave- lb/yd^3
0.05	0.025	1	2.03	1.75	1.89	3.42	2.95	3.18
0.05	0.075	2	3.97	3.70	3.84	6.70	6.23	6.46
0.05	0.125	3	4.52	4.24	4.38	7.62	7.14	7.38
0.05	0.175	4	4.22	4.07	4.14	7.10	6.86	6.98
0.05	0.225	5	3.55	3.50	3.53	5.99	5.89	5.94
0.05	0.275	6	3.39	3.35	3.37	5.72	5.65	5.68
0.05	0.325	7	4.10	3.82	3.96	6.91	6.44	6.67
0.05	0.375	8	5.20	5.30	5.25	8.76	8.93	8.84
0.05	0.425	9	3.65	3.58	3.61	6.15	6.02	6.09
0.05	0.475	10	4.45	4.51	4.48	7.50	7.59	7.54
0.05	0.525	11	4.33	4.05	4.19	7.30	6.83	7.06
0.05	0.575	12	3.73	3.69	3.71	6.29	6.22	6.25
0.05	0.675	13	3.79	3.33	3.56	6.39	5.61	6.00
0.05	0.775	14	3.85	3.54	3.70	6.48	5.97	6.22
0.05	0.875	15	3.65	3.46	3.56	6.15	5.84	5.99
0.05	0.975	16	3.73	3.69	3.71	6.28	6.22	6.25

Table 37. DCL10b-F (after 108 months of exposure)

Layer	center of mass							
Thickness (cm)	cm	Layer	A- kg/m^3	B- kg/m^3	ave kg/m^3	A- lb/yd^3	B- lb/yd^3	ave- lb/yd^3
0.05	0.025	1	4.23	3.76	3.99	7.12	6.33	6.73
0.05	0.075	2	3.80	3.57	3.68	6.41	6.01	6.21
0.05	0.125	3	4.37	4.08	4.22	7.36	6.87	7.11
0.05	0.175	4	5.44	5.35	5.39	9.17	9.01	9.09
0.05	0.225	5	7.28	5.90	6.59	12.26	9.94	11.10
0.05	0.275	6	5.30	3.84	4.57	8.93	6.47	7.70
0.05	0.325	7	2.97	3.99	3.48	4.99	6.72	5.86
0.05	0.375	8	4.55	4.53	4.54	7.66	7.64	7.65
0.05	0.425	9	3.88	4.11	4.00	6.54	6.93	6.73
0.05	0.475	10	2.84	2.77	2.80	4.78	4.66	4.72
0.05	0.525	11	3.02	3.41	3.21	5.08	5.75	5.41
0.05	0.575	12	3.08	2.48	2.78	5.18	4.17	4.68
0.05	0.625	13	2.25	2.06	2.16	3.79	3.47	3.63
0.05	0.675	14	2.33	2.60	2.47	3.93	4.39	4.16
0.05	0.725	15	2.06	2.28	2.17	3.47	3.84	3.66
0.05	0.775	16	2.25	2.28	2.27	3.79	3.85	3.82
0.05	0.825	17	2.40	2.34	2.37	4.04	3.93	3.99
0.05	0.875	18	2.20	1.93	2.07	3.71	3.25	3.48
0.05	0.925	19	2.22	2.41	2.31	3.73	4.06	3.90
0.05	0.975	20	2.03	1.76	1.90	3.43	2.96	3.19

Table 38. DCL11-F (after 108 months of exposure)

Layer	center of mass							
Thickness (cm)	cm	Layer	A- kg/m^3	B- kg/m^3	ave kg/m^3	A- lb/yd^3	B- lb/yd^3	ave- lb/yd^3
0.05	0.025	1	4.26	3.34	3.80	7.18	5.63	6.41
0.05	0.075	2	2.86	2.38	2.62	4.82	4.01	4.41
0.05	0.125	3	1.20	1.27	1.24	2.02	2.14	2.08
0.05	0.175	4	0.67	0.63	0.65	1.13	1.05	1.09
0.05	0.225	5	1.29	1.21	1.25	2.17	2.03	2.10
0.05	0.275	6	1.85	1.60	1.73	3.12	2.70	2.91
0.05	0.325	7	3.18	2.95	3.06	5.35	4.97	5.16
0.05	0.375	8	1.88	1.74	1.81	3.16	2.93	3.05
0.05	0.425	9	2.21	2.24	2.22	3.72	3.77	3.75
0.05	0.475	10	2.16	2.18	2.17	3.64	3.67	3.65
0.05	0.525	11	2.17	2.17	2.17	3.65	3.66	3.66
0.05	0.575	12	2.42	2.26	2.34	4.07	3.80	3.94
0.05	0.625	13	2.10	2.10	2.10	3.54	3.53	3.54
0.05	0.675	14	1.95	1.93	1.94	3.29	3.25	3.27
0.05	0.725	15	1.87	1.93	1.90	3.15	3.26	3.21
0.05	0.775	16	1.72	1.79	1.75	2.89	3.01	2.95
0.05	0.825	17	1.68	1.63	1.66	2.83	2.75	2.79
0.05	0.875	18	1.68	1.64	1.66	2.83	2.77	2.80
0.05	0.925	19	1.42	1.42	1.42	2.39	2.40	2.39
0.05	0.975	20	1.29	1.34	1.32	2.17	2.26	2.22
0.05	1.025	21	1.22	1.14	1.18	2.06	1.91	1.99
0.05	1.075	22	1.61	1.60	1.61	2.71	2.70	2.71

Chloride concentration results on DC samples exposed (facing up) on the west site after approx. 108 months of exposure

Table 39. DCL1-C (after 108 months of exposure)

Layer	center of mass		DC1-C					
Thickness (cm)	cm	Layer	A- kg/m^3	B- kg/m^3	ave kg/m^3	A- lb/yd^3	B- lb/yd^3	ave- lb/yd^3
0.05	0.025	1	2.19	1.97	2.08	3.70	3.31	3.50
0.05	0.075	2	4.98	4.40	4.69	8.39	7.41	7.90
0.05	0.125	3	4.69	4.60	4.64	7.90	7.75	7.82
0.05	0.175	4	4.82	4.62	4.72	8.11	7.78	7.95
0.05	0.225	5	3.54	4.14	3.84	5.97	6.97	6.47
0.05	0.275	6	2.48	2.39	2.44	4.18	4.03	4.10
0.05	0.325	7	3.07	2.68	2.88	5.17	4.52	4.84
0.05	0.375	8	2.06	2.11	2.08	3.46	3.56	3.51
0.05	0.425	9	1.69	1.52	1.61	2.85	2.57	2.71
0.05	0.475	10	1.35	1.23	1.29	2.28	2.08	2.18
0.05	0.525	11	1.23	1.10	1.16	2.07	1.85	1.96
0.05	0.575	12	0.89	0.81	0.85	1.50	1.36	1.43
0.05	0.625	13	1.19	1.35	1.27	2.00	2.27	2.14
0.05	0.675	14	0.88	0.82	0.85	1.48	1.39	1.43
0.05	0.725	15	0.66	0.54	0.60	1.10	0.91	1.01
0.05	0.775	16	0.88	0.92	0.90	1.48	1.54	1.51
0.05	0.825	17	0.56	0.52	0.54	0.95	0.87	0.91
0.05	0.875	18	0.53	0.56	0.55	0.90	0.95	0.92
0.05	0.925	19	0.49	0.52	0.50	0.82	0.87	0.85
0.05	0.975	20	0.93	1.18	1.05	1.56	1.99	1.77
0.05	1.025	21	0.73	0.66	0.70	1.24	1.12	1.18
0.05	1.075	22	0.51	0.51	0.51	0.86	0.86	0.86
0.13	1.16	23	0.56	0.54	0.55	0.94	0.90	0.92
0.13	1.29	24	0.36	0.20	0.28	0.60	0.34	0.47
0.13	1.42	25	0.30	0.32	0.31	0.50	0.53	0.52
0.18	1.58	26		0.04	0.02	0.00	0.06	0.03
0.13	1.73	27	0.09	0.22	0.16	0.15	0.37	0.26

+

Table 40. DCL2-C (after 108 months of exposure)

Layer	center of mass							
Thickness (cm)	cm	Layer	A- kg/m^3	B- kg/m^3	ave kg/m^3	A- lb/yd^3	B- lb/yd^3	ave- lb/yd^3
0.05	0.025	1	1.62	2.37	2.00	2.73	4.00	3.36
0.05	0.075	2	2.41	2.26	2.34	4.06	3.81	3.94
0.05	0.125	3	2.98	2.92	2.95	5.01	4.92	4.97
0.05	0.175	4	3.31	3.20	3.25	5.57	5.39	5.48
0.05	0.225	5	3.18	3.15	3.17	5.36	5.31	5.33
0.05	0.275	6		3.02	3.02		5.09	5.09
0.05	0.325	7	2.76	2.71	2.73	4.64	4.56	4.60
0.05	0.375	8	2.65	6.05	4.35	4.47	10.19	7.33
0.05	0.425	9	2.34	2.19	2.26	3.94	3.69	3.81
0.05	0.475	10	2.70	2.61	2.66	4.55	4.40	4.48
0.05	0.525	11	2.58	2.30	2.44	4.35	3.87	4.11
0.05	0.575	12	2.28	1.97	2.12	3.84	3.32	3.58
0.05	0.625	13	3.51	2.34	2.93	5.92	3.94	4.93
0.05	0.675	14	1.93	1.84	1.88	3.25	3.09	3.17
0.05	0.725	15	2.14	1.74	1.94	3.60	2.93	3.27
0.05	0.775	16	1.96	1.82	1.89	3.30	3.06	3.18
0.05	0.825	17	1.61	1.71	1.66	2.71	2.88	2.80
0.05	0.875	18	1.65	1.32	1.48	2.78	2.22	2.50
0.05	0.925	19	1.50	1.38	1.44	2.52	2.33	2.42
0.05	0.975	20	1.26	1.32	1.29	2.12	2.22	2.17
0.05	1.025	21	0.99	1.00	1.00	1.68	1.69	1.68
0.05	1.075	22	0.96	0.99	0.97	1.61	1.66	1.64

Table 41. DCL3-C (after 108 months of exposure)

Layer	center of mass							
Thickness (cm)	cm	Layer	A- kg/m^3	B- kg/m^3	ave kg/m^3	A- lb/yd^3	B- lb/yd^3	ave- lb/yd^3
0.05	0.025	1	3.00	2.74	2.87	5.06	4.62	4.84
0.05	0.075	2	2.97	2.95	2.96	5.00	4.97	4.99
0.05	0.125	3	2.85	2.70	2.78	4.80	4.55	4.68
0.05	0.175	4	2.44	2.37	2.41	4.11	4.00	4.05
0.05	0.225	5	2.29	1.94	2.11	3.86	3.26	3.56
0.05	0.275	6	2.16	1.89	2.02	3.64	3.18	3.41
0.05	0.325	7	1.88	1.92	1.90	3.17	3.23	3.20
0.05	0.375	8	1.88	1.96	1.92	3.17	3.30	3.24
0.05	0.425	9	1.67	1.77	1.72	2.82	2.99	2.90
0.05	0.475	10	1.78	1.65	1.72	3.01	2.78	2.89
0.05	0.525	11	1.51	1.43	1.47	2.54	2.40	2.47
0.05	0.575	12	1.46	1.39	1.43	2.46	2.35	2.40
0.05	0.625	13	1.49	1.46	1.48	2.51	2.46	2.49
0.05	0.675	14	1.25	1.33	1.29	2.11	2.24	2.18
0.05	0.725	15	1.36	1.33	1.35	2.29	2.25	2.27
0.05	0.775	16	1.16	1.15	1.16	1.95	1.94	1.95
0.05	0.825	17	0.98	1.06	1.02	1.66	1.78	1.72
0.05	0.875	18	1.04	1.03	1.03	1.75	1.73	1.74
0.05	0.925	19	0.86	0.88	0.87	1.44	1.47	1.46
0.05	0.975	20	0.77	0.88	0.82	1.30	1.48	1.39
0.05	1.025	21	0.84	0.78	0.81	1.41	1.31	1.36
0.05	1.075	22	0.86	0.83	0.84	1.44	1.39	1.42

Table 42. DCL4-C (after 108 months of exposure)

Layer	center of mass							
Thickness (cm)	cm	Layer	A- kg/m^3	B- kg/m^3	ave kg/m^3	A- lb/yd^3	B- lb/yd^3	ave- lb/yd^3
0.05	0.03	1	1.70	1.69	1.70	2.87	2.85	2.86
0.08	0.09	2	2.50	2.48	2.49	4.21	4.18	4.20
0.09	0.18	3	1.83	1.82	1.83	3.09	3.07	3.08
0.09	0.26	4	1.20	1.20	1.20	2.02	2.03	2.02
0.11	0.36	5	0.63	0.72	0.68	1.07	1.21	1.14
0.10	0.47	6	0.67	0.58	0.62	1.13	0.97	1.05
0.13	0.58	7	0.49	0.39	0.44	0.82	0.66	0.74
0.17	0.73	8	0.33	0.34	0.34	0.56	0.58	0.57
0.13	0.88	9	0.40	0.42	0.41	0.67	0.71	0.69
0.09	0.99	10	0.29	0.24	0.26	0.48	0.40	0.44
0.13	1.11	11	0.32	0.41	0.37	0.54	0.68	0.61
0.12	1.23	12	0.32	0.46	0.39	0.54	0.78	0.66

Table 43. DCL5-C (after 108 months of exposure)

Layer	center of mass							
Thickness (cm)	cm	Layer	A- kg/m^3	B- kg/m^3	ave kg/m^3	A- lb/yd^3	B- lb/yd^3	ave- lb/yd^3
0.05	0.025	1	1.64	1.66	1.65	2.77	2.80	2.78
0.05	0.075	2	1.98	2.00	1.99	3.33	3.37	3.35
0.05	0.175	3	2.08	1.98	2.03	3.50	3.33	3.42
0.05	0.275	4	1.61	1.53	1.57	2.72	2.58	2.65
0.05	0.375	5	1.08	1.03	1.05	1.82	1.73	1.78
0.05	0.475	6	0.78	0.88	0.83	1.32	1.49	1.40
0.05	0.575	7	1.39	0.75	1.07	2.35	1.26	1.80
0.05	0.675	8	0.59	0.61	0.60	1.00	1.02	1.01
0.05	0.775	9	0.56	0.55	0.56	0.94	0.93	0.94
0.05	0.875	10	0.46	0.50	0.48	0.78	0.84	0.81
0.05	0.975	11	0.38	0.39	0.39	0.64	0.66	0.65
0.05	1.075	12	0.43	0.42	0.43	0.73	0.70	0.72

Table 44. DCL6-C (after 108 months of exposure)

Layer	center of mass							
Thickness (cm)	cm	Layer	A- kg/m^3	B- kg/m^3	ave kg/m^3	A- lb/yd^3	B- lb/yd^3	ave- lb/yd^3
0.05	0.025	1	1.28	1.33	1.30	2.15	2.25	2.20
0.05	0.075	2	1.02	1.02	1.02	1.72	1.71	1.72
0.05	0.175	3	1.28	1.28	1.28	2.15	2.15	2.15
0.05	0.275	4	1.65	1.58	1.61	2.78	2.65	2.72
0.05	0.375	5	1.86	1.79	1.82	3.13	3.02	3.07
0.05	0.475	6	1.89	1.74	1.81	3.19	2.92	3.05
0.05	0.575	7	1.88	1.75	1.81	3.16	2.95	3.06
0.05	0.675	8	1.64	1.72	1.68	2.77	2.90	2.83
0.05	0.775	9	1.74	1.61	1.68	2.94	2.72	2.83
0.05	0.875	10	1.60	1.62	1.61	2.69	2.74	2.71
0.05	0.975	11	1.44	1.44	1.44	2.42	2.43	2.42
0.05	1.075	12	1.44	1.43	1.43	2.43	2.40	2.42
0.05	0.625	13	1.11	1.02	1.07	1.87	1.72	1.79
0.05	0.675	14	0.85	0.85	0.85	1.44	1.44	1.44
0.05	0.725	15	0.97	0.96	0.97	1.64	1.61	1.63
0.05	0.775	16	0.94	1.09	1.01	1.58	1.83	1.71
0.05	0.825	17	0.62	0.60	0.61	1.05	1.01	1.03
0.05	0.875	18	0.65	0.74	0.70	1.10	1.25	1.17
0.05	0.925	19	0.63	0.62	0.62	1.05	1.04	1.05
0.05	0.975	20	0.60	0.57	0.59	1.02	0.96	0.99
0.05	1.025	21	0.74	0.66	0.70	1.25	1.11	1.18
0.05	1.075	22	0.55	0.47	0.51	0.92	0.78	0.85

Table 45. DCL7-C (after 108 months of exposure)

Layer	center of mass							
Thickness (cm)	cm	Layer	A- kg/m^3	B- kg/m^3	ave kg/m^3	A- lb/yd^3	B- lb/yd^3	ave- lb/yd^3
0.07	0.03	1	4.45	4.37	4.41	7.50	7.36	7.43
0.08	0.11	2	4.32	4.46	4.39	7.29	7.51	7.40
0.12	0.21	3	2.81	2.94	2.87	4.73	4.95	4.84
0.10	0.32	4	2.16	2.97	2.57	3.64	5.01	4.32
0.10	0.41	5	1.71	1.71	1.71	2.87	2.89	2.88
0.09	0.51	6	1.53	1.45	1.49	2.58	2.43	2.50
0.11	0.61	7	1.26	0.98	1.12	2.11	1.65	1.88
0.09	0.71	8	0.90	0.93	0.92	1.52	1.57	1.55
0.11	0.81	9	0.83	0.84	0.84	1.40	1.41	1.41
0.09	0.91	10	0.78	0.69	0.74	1.32	1.17	1.24
0.15	1.03	11	0.69	0.54	0.61	1.16	0.91	1.03
0.14	1.17	12	0.51	0.40	0.46	0.87	0.68	0.77

Table 46. DCL8-C (after 108 months of exposure)

Layer	center of mass							
Thickness (cm)	cm	Layer	A- kg/m^3	B- kg/m^3	ave kg/m^3	A- lb/yd^3	B- lb/yd^3	ave- lb/yd^3
0.10	0.05	1	3.26	3.00	3.13	5.49	5.05	5.27
0.07	0.13	2	2.15	2.24	2.20	3.63	3.77	3.70
0.12	0.23	3	1.23	1.32	1.28	2.08	2.22	2.15
0.09	0.33	4	0.85	1.99	1.42	1.43	3.35	2.39
0.09	0.42	5	0.58	0.57	0.58	0.98	0.96	0.97
0.11	0.52	6	0.57	0.43	0.50	0.96	0.73	0.85
0.09	0.62	7	0.49	0.48	0.49	0.83	0.81	0.82
0.09	0.71	8	0.28	0.28	0.28	0.47	0.48	0.48
0.10	0.81	9	0.26	0.24	0.25	0.44	0.40	0.42
0.09	0.91	10	0.21	0.21	0.21	0.35	0.35	0.35
0.16	1.03	11	0.30	0.21	0.26	0.51	0.36	0.43
0.17	1.19	12	0.17	0.28	0.22	0.28	0.46	0.37

Table 47. DCL9-C (after 108 months of exposure)

Layer	center of mass							
Thickness (cm)	cm	Layer	A- kg/m^3	B- kg/m^3	ave kg/m^3	A- lb/yd^3	B- lb/yd^3	ave- lb/yd^3
0.07	0.04	1	1.65	1.95	1.80	2.78	3.29	3.04
0.09	0.12	2	1.52	1.42	1.47	2.55	2.40	2.47
0.12	0.22	3	0.93	1.06	0.99	1.57	1.78	1.68
0.14	0.34	4	0.82	0.64	0.73	1.37	1.08	1.23
0.10	0.47	5	0.61	0.54	0.58	1.03	0.92	0.97
0.17	0.60	6	0.53	0.54	0.53	0.89	0.91	0.90
0.09	0.73	7	0.58	0.39	0.48	0.98	0.65	0.82
0.13	0.85	8	0.32	0.29	0.31	0.54	0.49	0.52
0.11	0.97	9	0.36	0.55	0.45	0.60	0.93	0.76
0.14	1.09	10	0.43	0.38	0.40	0.73	0.64	0.68
0.13	1.22	11	0.30	0.26	0.28	0.50	0.44	0.47
0.16	1.37	12	0.22	0.27	0.25	0.38	0.46	0.42

Table 48. DCL10-C (after 108 months of exposure)

			DC10-C					
Layer	center of mass							
Thickness (cm)	cm	Layer	A-kg/m^3	B-kg/m^3	ave kg/m^3	A- lb/yd^3	B- lb/yd^3	ave- lb/yd^3
0.06	0.03	1	2.38	2.21	2.30	4.01	3.72	3.87
0.05	0.09	2	2.80	2.68	2.74	4.72	4.52	4.62
0.11	0.17	3	2.49	2.56	2.52	4.20	4.30	4.25
0.10	0.28	4	2.12	2.20	2.16	3.56	3.71	3.64
0.10	0.38	5	2.08	2.09	2.08	3.51	3.51	3.51
0.11	0.48	6	1.87	1.92	1.89	3.14	3.23	3.19
0.10	0.58	7	1.99	1.93	1.96	3.35	3.25	3.30
0.14	0.70	8	1.64	1.70	1.67	2.76	2.87	2.81
0.14	0.84	9	1.21	1.39	1.30	2.04	2.34	2.19
0.10	0.96	10	1.23	1.25	1.24	2.07	2.10	2.09
0.13	1.07	11	1.01	0.99	1.00	1.70	1.66	1.68
0.19	1.23	12	1.00	1.03	1.02	1.69	1.73	1.71

Table 49. DCL10a-C (after 108 months of exposure)

Layer	center of mass							
Thickness (cm)	cm	Layer	A- kg/m^3	B- kg/m^3	ave kg/m^3	A- lb/yd^3	B- lb/yd^3	ave- lb/yd^3
0.06	0.03	1	2.48	2.23	2.35	4.17	3.76	3.97
0.06	0.09	2	2.64	2.80	2.72	4.45	4.71	4.58
0.07	0.16	3	2.12	2.41	2.27	3.58	4.06	3.82
0.11	0.25	4	2.11	2.01	2.06	3.56	3.39	3.48
0.08	0.35	5	2.24	2.07	2.16	3.78	3.49	3.63
0.10	0.44	6	2.07	1.90	1.99	3.49	3.20	3.35
0.08	0.54	7	1.79	1.79	1.79	3.01	3.02	3.01
0.08	0.62	8	1.65	1.65	1.65	2.77	2.78	2.78
0.09	0.71	9	1.40	1.36	1.38	2.36	2.30	2.33
0.09	0.80	10	1.20	1.06	1.13	2.02	1.79	1.91
0.12	0.90	11	1.04	0.87	0.95	1.75	1.46	1.60
0.14	1.03	12	0.64	0.84	0.74	1.08	1.41	1.25

Table 50. DCL10b-C (after 108 months of exposure)

Layer	center of mass							
Thickness (cm)	cm	Layer	A- kg/m^3	B- kg/m^3	ave kg/m^3	A- lb/yd^3	B- lb/yd^3	ave- lb/yd^3
0.05	0.025	1	2.68	2.30	2.49	4.52	3.87	4.19
0.05	0.075	2	2.82	3.22	3.02	4.76	5.43	5.09
0.05	0.125	3	2.82	2.15	2.48	4.75	3.62	4.18
0.05	0.175	4	2.85	3.11	2.98	4.80	5.24	5.02
0.05	0.225	5	2.54	2.48	2.51	4.27	4.17	4.22
0.05	0.275	6	2.42	2.25	2.34	4.07	3.80	3.94
0.05	0.325	7	2.16	2.07	2.11	3.64	3.48	3.56
0.05	0.375	8	2.03	1.97	2.00	3.43	3.31	3.37
0.05	0.425	9	1.77	1.81	1.79	2.98	3.04	3.01
0.05	0.475	10	1.64	1.66	1.65	2.76	2.80	2.78
0.05	0.525	11	1.47	1.28	1.38	2.47	2.16	2.32
0.05	0.575	12	1.31	1.27	1.29	2.21	2.14	2.17
0.05	0.625	13	1.59	1.36	1.47	2.67	2.29	2.48
0.05	0.675	14	1.30	1.29	1.30	2.20	2.17	2.18
0.05	0.725	15	1.08	1.08	1.08	1.82	1.82	1.82
0.05	0.775	16	0.94	1.00	0.97	1.58	1.68	1.63
0.05	0.825	17	0.70	0.89	0.79	1.17	1.49	1.33
0.05	0.875	18	0.79	0.95	0.87	1.32	1.60	1.46
0.05	0.925	19	0.85	0.74	0.80	1.44	1.25	1.34
0.05	0.975	20	0.73	0.71	0.72	1.23	1.20	1.21
0.05	1.025	21	0.96	0.74	0.85	1.61	1.25	1.43
0.05	1.075	22	0.61	0.64	0.62	1.02	1.08	1.05

Table 51. DCL11-C (after 108 months of exposure)

Layer	center of mass							
Thickness (cm)	cm	Layer	A- kg/m^3	B- kg/m^3	ave kg/m^3	A- lb/yd^3	B- lb/yd^3	ave- lb/yd^3
0.07	0.03	1	0.90	1.28	1.09	1.52	2.15	1.84
0.07	0.10	2	1.51	1.51	1.51	2.54	2.54	2.54
0.14	0.21	3	1.52	1.43	1.48	2.56	2.42	2.49
0.14	0.35	4	0.93	0.71	0.82	1.56	1.19	1.38
0.13	0.48	5	0.79	0.70	0.75	1.33	1.19	1.26
0.14	0.61	6	0.66	0.55	0.61	1.11	0.93	1.02
0.13	0.75	7	0.87	0.59	0.73	1.47	0.99	1.23
0.13	0.88	8	0.49	0.47	0.48	0.83	0.78	0.81
0.13	1.01	9	0.46	0.52	0.49	0.78	0.88	0.83
0.14	1.14	10	0.43	0.42	0.42	0.72	0.71	0.72
0.18	1.30	11	0.38	0.43	0.40	0.63	0.73	0.68
0.15	1.46	12	0.33	0.29	0.31	0.56	0.49	0.52
0.15	1.61	13	0.29	0.26	0.28	0.49	0.45	0.47

Chloride concentration on older samples exposed on the Eastern site and West site after approx. 108 months of exposure

Table 52. 1A1B-H (OPC only after 108 months of exposure)

Layer	center of mass							
Thickness (cm)	cm	Layer	A- kg/m^3	B- kg/m^3	ave kg/m^3	A- lb/yd^3	B- lb/yd^3	ave- lb/yd^3
0.0735	0.03675	1	0.87	0.86	0.86	1.46	1.44	1.45
0.069	0.108	2	2.16	2.13	2.14	3.64	3.59	3.61
0.1245	0.20475	3	2.18	1.62	1.90	3.67	2.73	3.20
0.093	0.3135	4	2.10	2.07	2.08	3.53	3.49	3.51
0.1035	0.41175	5	1.78	1.68	1.73	2.99	2.83	2.91
0.131	0.529	6	1.97	1.99	1.98	3.32	3.36	3.34
0.1415	0.66525	7	1.99	1.72	1.86	3.36	2.90	3.13
0.2	0.836	8	1.61	1.67	1.64	2.71	2.82	2.76
0.1425	1.00725	9	1.40	1.35	1.38	2.37	2.27	2.32
0.126	1.1415	10	2.19	1.27	1.73	3.69	2.14	2.92
0.2015	1.30525	11	1.17	1.09	1.13	1.98	1.83	1.91
0.201	1.5065	12	0.97	0.94	0.95	1.63	1.58	1.60
0.11	5.346	13	0.73	0.73	0.73	1.23	1.23	1.23

Table 53. 1A2B-VF (OPC only after 108 months of exposure)

Layer	center of mass							
Thickness (cm)	cm	Layer	A- kg/m^3	B- kg/m^3	ave kg/m^3	A- lb/yd^3	B- lb/yd^3	ave- lb/yd^3
0.0585	0.02925	1	3.06	2.87	2.97	5.16	4.83	4.99
0.056	0.0865	2	3.48	3.22	3.35	5.87	5.42	5.64
0.1165	0.17275	3	3.42	3.27	3.34	5.76	5.51	5.63
0.1115	0.28675	4	3.37	3.32	3.35	5.68	5.60	5.64
0.116	0.4005	5	3.08	3.18	3.13	5.19	5.35	5.27
0.0985	0.50775	6	3.67	3.34	3.50	6.18	5.63	5.90
0.1955	0.65475	7	3.38	3.40	3.39	5.70	5.73	5.71
0.1645	0.83475	8	3.39	3.21	3.30	5.72	5.41	5.56
0.1595	0.99675	9	3.42	3.32	3.37	5.76	5.60	5.68
0.171	1.162	10	3.22	3.15	3.19	5.42	5.31	5.37
0.2065	1.35075	11	3.35	3.23	3.29	5.64	5.44	5.54
0.1	5.35075	13	0.99	0.86	0.93	1.67	1.45	1.56

Table 54. 1A3B-V (OPC only after 108 months of exposure)

Layer	center of mass							
Thickness (cm)	cm	Layer	A- kg/m^3	B- kg/m^3	ave kg/m^3	A- lb/yd^3	B- lb/yd^3	ave- lb/yd^3
0.0555	0.02775	1	1.64	1.41	1.52	2.76	2.38	2.57
0.0395	0.07525	2	1.61	1.30	1.45	2.70	2.19	2.45
0.111	0.1505	3	1.38	1.34	1.36	2.33	2.26	2.29
0.127	0.2695	4	1.15	1.26	1.21	1.94	2.13	2.03
0.122	0.394	5	1.23	1.19	1.21	2.06	2.01	2.03
0.0995	0.50475	6	0.92	1.04	0.98	1.55	1.76	1.65
0.156	0.6325	7	0.70	0.84	0.77	1.17	1.42	1.29
0.133	0.777	8	1.25	0.99	1.12	2.11	1.66	1.89
0.152	0.9195	9	1.02	1.06	1.04	1.71	1.79	1.75
0.126	1.0585	10	1.14	1.10	1.12	1.92	1.86	1.89
0.2605	1.25175	11	1.23	1.21	1.22	2.06	2.03	2.05
0.278	1.521	12	0.89	1.01	0.95	1.50	1.71	1.61
0.276	1.798	13	0.84	0.82	0.83	1.42	1.39	1.40
0.1	5.35	13	0.79	0.93	0.86	1.33	1.57	1.45

Table 55. 2C1A-V (OPC only after 108 months of exposure)

Layer	center of mass							
Thickness (cm)	cm	Layer	A- kg/m^3	B- kg/m^3	ave kg/m^3	A- lb/yd^3	B- lb/yd^3	ave- lb/yd^3
0.0595	0.02975	1	1.38	1.39	1.38	2.33	2.33	2.33
0.0615	0.09025	2	1.26	1.22	1.24	2.13	2.05	2.09
0.09	0.166	3	1.34	1.11	1.22	2.25	1.88	2.06
0.109	0.2655	4	1.28	1.38	1.33	2.15	2.33	2.24
0.1035	0.37175	5	1.16	1.20	1.18	1.96	2.01	1.99
0.1155	0.48125	6	1.19	1.03	1.11	2.01	1.74	1.87
0.1935	0.63575	7	1.16	1.06	1.11	1.96	1.79	1.87
0.137	0.801	8	1.09	1.10	1.10	1.84	1.86	1.85
0.164	0.9515	9	0.94	1.04	0.99	1.59	1.75	1.67
0.148	1.1075	10	1.04	1.01	1.02	1.75	1.70	1.73
0.193	1.278	11	0.94	0.88	0.91	1.58	1.49	1.54
		12						
0.1	5.278	13	0.53	0.57	0.55	0.90	0.97	0.93

Table 56. 2C2B-E (OPC only after 108 months of exposure)

Layer	center of mass							
Thickness (cm)	cm	Layer	A- kg/m^3	B- kg/m^3	ave kg/m^3	A- lb/yd^3	B- lb/yd^3	ave- lb/yd^3
0.06	0.03	1	3.27	3.06	3.16	5.50	5.16	5.33
0.05	0.09	2	4.28	4.09	4.18	7.20	6.89	7.04
0.10	0.17	3	4.84	4.60	4.72	8.15	7.75	7.95
0.12	0.28	4	4.66	4.66	4.66	7.85	7.86	7.85
0.11	0.39	5	5.07	5.20	5.14	8.55	8.76	8.66
0.11	0.50	6	5.89	5.29	5.59	9.92	8.92	9.42
0.17	0.64	7	5.85	4.85	5.35	9.86	8.17	9.01
0.15	0.80	8	5.61	5.49	5.55	9.45	9.25	9.35
0.15	0.95	9	6.54	6.10	6.32	11.01	10.28	10.65
0.15	1.10	10	5.68	5.81	5.74	9.56	9.79	9.68
0.20	1.27	11	5.83	5.55	5.69	9.81	9.35	9.58
0.25	1.50	12	5.51	5.71	5.61	9.28	9.62	9.45
0.10	5.28	13	0.53	0.57	0.55	0.90	0.97	0.93

Table 57. 1E2B-FV (OPC and 20%FA, after 108 months of exposure)

Layer	center of mass							
Thickness (cm)	cm	Layer	A- kg/m^3	B- kg/m^3	ave kg/m^3	A- lb/yd^3	B- lb/yd^3	ave- lb/yd^3
0.0525	0.02625	1	0.39	0.52	0.45	0.65	0.88	0.77
0.0515	0.07825	2	1.78	1.66	1.72	2.99	2.79	2.89
0.116	0.162	3	2.42	2.44	2.43	4.08	4.11	4.09
0.1195	0.27975	4	2.57	2.72	2.65	4.33	4.59	4.46
0.112	0.3955	5	2.95	2.88	2.92	4.97	4.86	4.91
0.114	0.5085	6	2.85	2.90	2.88	4.81	4.88	4.85
0.1405	0.63575	7	2.63	2.67	2.65	4.43	4.49	4.46
0.1255	0.76875	8	2.66	2.50	2.58	4.49	4.21	4.35
0.144	0.9035	9	2.18	2.26	2.22	3.67	3.81	3.74
0.15	1.0505	10	1.93	1.83	1.88	3.26	3.09	3.17
0.204	1.2275	11	0.78	0.89	0.83	1.31	1.50	1.41
0.2665	1.46275	12	1.31	1.26	1.28	2.21	2.12	2.16
0.11	5.346	13	1.08	1.07	1.08	1.82	1.80	1.81

Table 58. 1E4A-H (OPC and 20%FA, after 108 months of exposure)

Layer	center of mass							
Thickness (cm)	cm	Layer	A- kg/m^3	B- kg/m^3	ave kg/m^3	A- lb/yd^3	B- lb/yd^3	ave- lb/yd^3
0.05	0.025	1	2.07	2.02	2.04	3.48	3.41	3.44
0.053	0.0765	2	2.22	2.32	2.27	3.74	3.90	3.82
0.1025	0.15425	3	2.49	2.35	2.42	4.19	3.95	4.07
0.0995	0.25525	4	2.55	2.57	2.56	4.30	4.32	4.31
0.101	0.3555	5	2.02	2.11	2.06	3.41	3.55	3.48
0.1045	0.45825	6	1.98	2.00	1.99	3.34	3.36	3.35
0.1645	0.59275	7	1.85	1.74	1.79	3.11	2.93	3.02
0.136	0.743	8	1.24	1.37	1.30	2.10	2.30	2.20
0.126	0.874	9	1.06	1.17	1.11	1.79	1.96	1.88
0.148	1.011	10	0.96	1.01	0.99	1.62	1.71	1.66
0.203	1.1865	11	0.83	0.88	0.86	1.39	1.49	1.44
0.2325	1.40425	12	0.62	0.59	0.60	1.04	0.99	1.02
0.2375	1.63925	13	0.67	0.82	0.75	1.14	1.38	1.26
0.1	5.278	14	0.87	0.84	0.86	1.47	1.41	1.44

Table 59. 2A1A-V (OPC and 20%FA, after 108 months of exposure)

Layer	center of mass							
Thickness (cm)	cm	Layer	A- kg/m^3	B- kg/m^3	ave kg/m^3	A- lb/yd^3	B- lb/yd^3	ave- lb/yd^3
0.057	0.0285	1	2.90	2.76	2.83	4.89	4.65	4.77
0.069	0.0915	2	2.39	1.96	2.17	4.03	3.29	3.66
0.1095	0.18075	3	2.44	2.71	2.57	4.11	4.56	4.34
0.12	0.2955	4	2.58	2.64	2.61	4.34	4.45	4.40
0.119	0.415	5	2.40	2.20	2.30	4.05	3.70	3.88
0.1115	0.53025	6	2.03	2.10	2.06	3.41	3.53	3.47
0.1565	0.66425	7	2.26	2.11	2.18	3.80	3.55	3.68
0.141	0.813	8	1.72	1.56	1.64	2.89	2.63	2.76
0.145	0.956	9	1.39	1.29	1.34	2.34	2.18	2.26
0.1505	1.10375	10	1.36	1.10	1.23	2.30	1.86	2.08
0.2155	1.28675	11	0.85	0.86	0.85	1.43	1.44	1.44
		12						
0.11	5.346	13	0.41	0.34	0.38	0.70	0.57	0.63

Table 60. 2A1B-E (OPC and 20%FA, after 108 months of exposure)

Layer	center of mass							
Thickness (cm)	cm	Layer	A- kg/m^3	B- kg/m^3	ave kg/m^3	A- lb/yd^3	B- lb/yd^3	ave- lb/yd^3
0.0495	0.02475	1	3.35	3.01	3.18	5.65	5.07	5.36
0.0465	0.07275	2	4.29	4.20	4.24	7.22	7.08	7.15
0.099	0.1455	3	6.26	6.13	6.19	10.55	10.32	10.43
0.096	0.243	4	5.28	5.30	5.29	8.90	8.93	8.91
0.123	0.3525	5	6.22	5.72	5.97	10.48	9.64	10.06
0.146	0.487	6	6.49	6.13	6.31	10.94	10.33	10.63
0.146	0.633	7	6.52	6.50	6.51	10.98	10.95	10.97
0.1695	0.79075	8	6.55	6.65	6.60	11.04	11.20	11.12
0.138	0.9445	9	6.65	6.79	6.72	11.20	11.45	11.32
0.159	1.093	10	6.17	6.30	6.23	10.40	10.61	10.50
0.212	1.2785	11	5.89	5.80	5.85	9.92	9.78	9.85
0.1	5.2785	12	0.92	1.04	0.98	1.55	1.76	1.65

Table 61. 3A1B-H (OPC and 20%FA&8%SF, after 108 months of exposure)

Layer	center of mass							
Thickness (cm)	cm	Layer	A- kg/m3	B- kg/m3	ave kg/m3	A- lb/yd^3	B- lb/yd^3	ave- lb/yd^3
0.06	0.03	1	0.53	0.49	0.51	0.89	0.83	0.86
0.07	0.09	2	2.71	2.57	2.64	4.56	4.32	4.44
0.10	0.18	3	2.60	2.45	2.52	4.38	4.12	4.25
0.12	0.29	4	3.12	2.88	3.00	5.25	4.85	5.05
0.13	0.42	5	2.89	2.72	2.80	4.86	4.58	4.72
0.13	0.55	6	2.61	2.67	2.64	4.40	4.50	4.45
0.20	0.71	7	2.64	2.28	2.46	4.45	3.85	4.15
0.13	0.87	8	1.89	2.00	1.94	3.18	3.37	3.28
0.15	1.01	9	1.52	1.54	1.53	2.55	2.59	2.57
0.14	1.15	10	1.25	1.31	1.28	2.11	2.21	2.16
0.26	1.35	11	1.91	0.78	1.34	3.22	1.31	2.26
0.10	5.35	12	0.63	0.50	0.57	1.06	0.84	0.95

Table 62. 3A4B-E (OPC and 20%FA&8%SF, after 108 months of exposure)

Layer	center of mass							
Thickness (cm)	cm	Layer	A- kg/m^3	B- kg/m^3	ave kg/m^3	A- lb/yd^3	B- lb/yd^3	ave- lb/yd^3
0.042	0.021	1	0.42	0.38	0.40	0.71	0.65	0.68
0.0725	0.07825	2	5.49	4.86	5.18	9.25	8.19	8.72
0.1145	0.17175	3	6.18	6.10	6.14	10.41	10.27	10.34
0.1135	0.28575	4	6.57	6.83	6.70	11.06	11.51	11.28
0.1095	0.39725	5	7.08	7.01	7.04	11.93	11.81	11.87
0.1155	0.50975	6	7.10	6.75	6.93	11.97	11.38	11.67
0.1465	0.64075	7	6.36	6.23	6.29	10.71	10.49	10.60
0.121	0.7745	8	6.09	6.56	6.32	10.26	11.04	10.65
0.175	0.9225	9	5.22	5.23	5.22	8.79	8.80	8.80
0.159	1.0895	10	4.31	4.33	4.32	7.26	7.29	7.27
0.238	1.288	11	3.71	3.74	3.72	6.25	6.30	6.27
0.1	5.288	12	2.38	2.37	2.38	4.02	3.99	4.00

Appendix B: Images of the Cores Obtained During Field Visits

Sebastian Inlet Bridge- Bridge #880005, Trip 1.

Figure 87. Bent 7 east column east face, Bridge #880005.

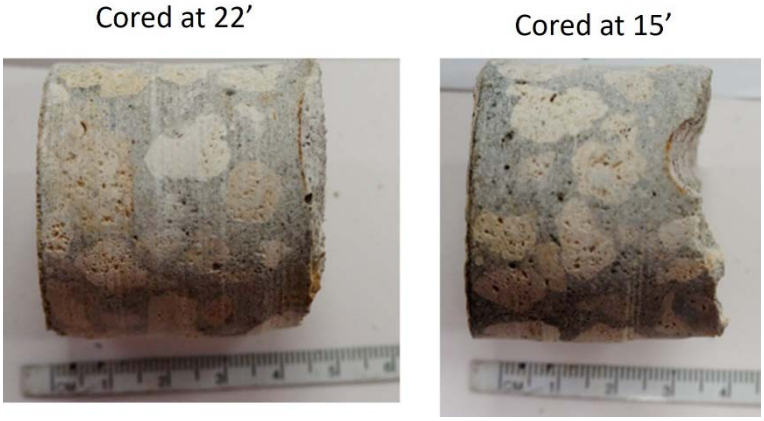

Figure 88. Bent 7 east column east face, Bridge #880005.

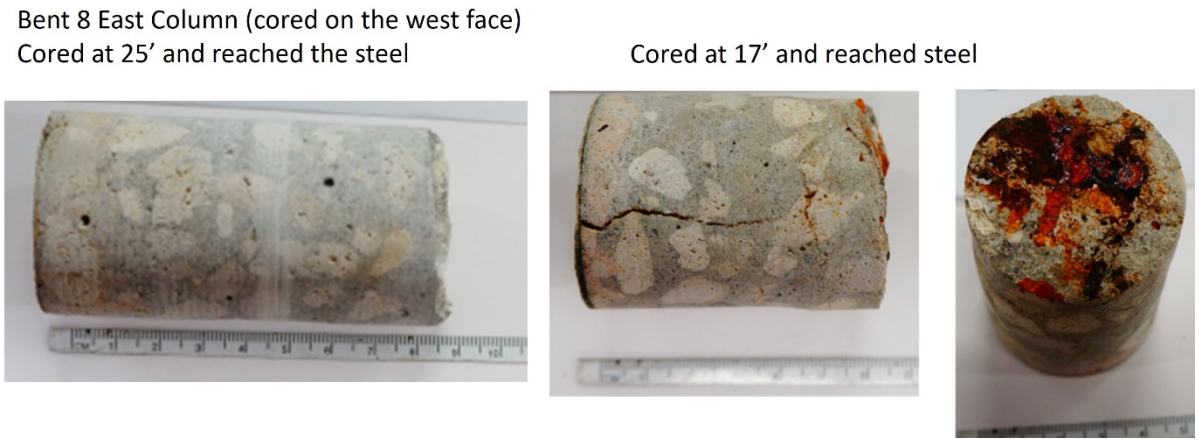

Figure 89. Bent 8 east column west face, Bridge #880005.

Cores obtained during Trip 2 to Bridge #880005

Figure 90. Bent 8 east column east face, Bridge #880005.

Figure 91. Bent 10 east column east face, Bridge #880005.

Figure 92. Bent 11 east column east face, Bridge #880005.

Figure 93. Bent 13 east column east face, Bridge #880005.

Cores obtained from Bridge #860160 Dania Beach, FL

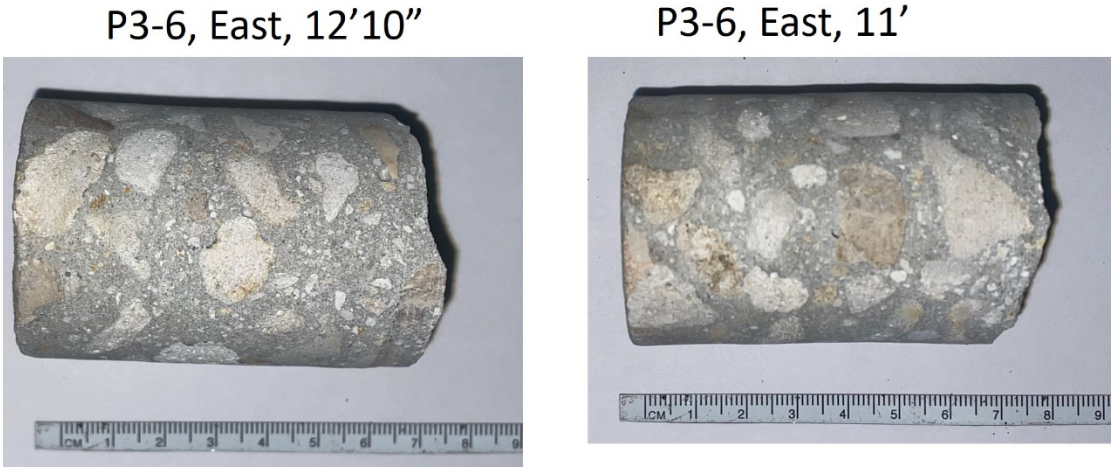

Figure 94. Cores obtained from P3-6 east face, Bridge #860160.

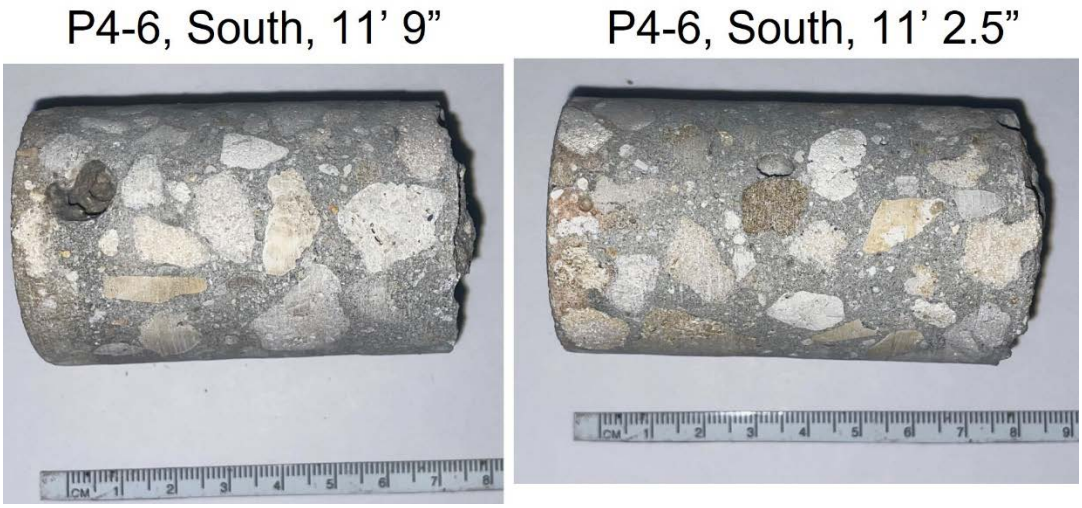

Figure 95. Cores obtained from P4-6 south face, Bridge #860160.

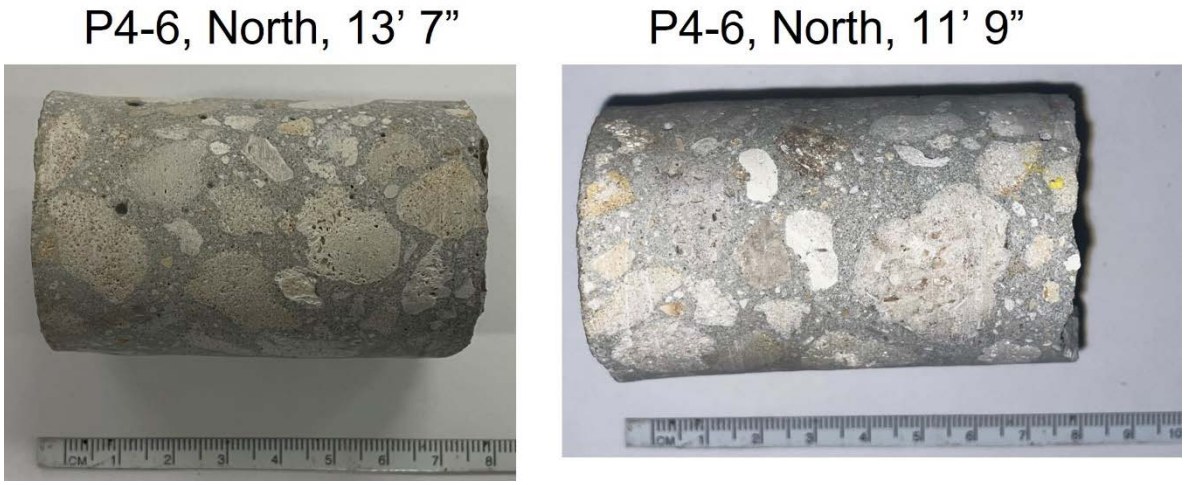

Figure 96. Cores obtained from P4-6 north face, Bridge #860160.

Gandy Bridge (#100585)

Gandy B, Bent 237 Top – Core with no crack

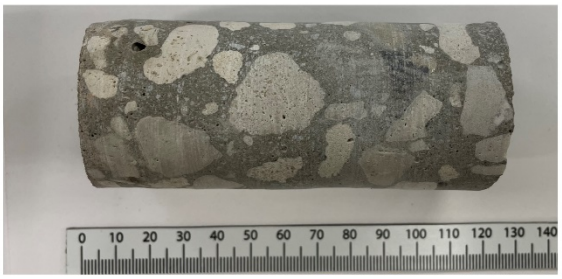

Gandy B, Bent 237 Top – Core with crack

Gandy B, Bent 237 Bottom – Core with no crack

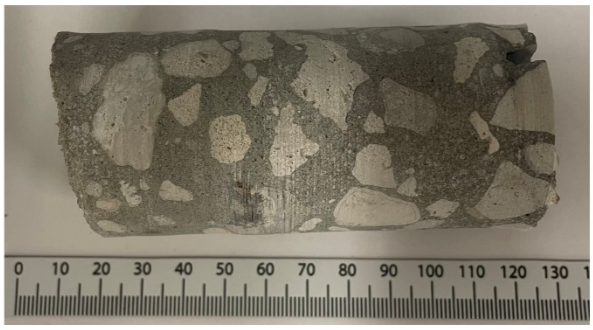

Gandy B, Bent 237 Bottom – Core with crack

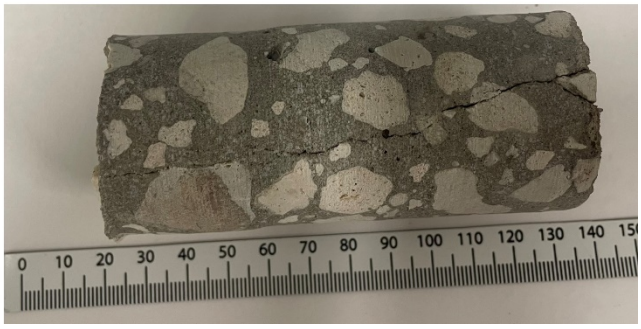

Figure 97. Cores obtained from Bent 237, Bridge #100585.

Gandy B, Bent 223 Top – Core with no crack

Gandy B, Bent 223 Middle – Core with no crack

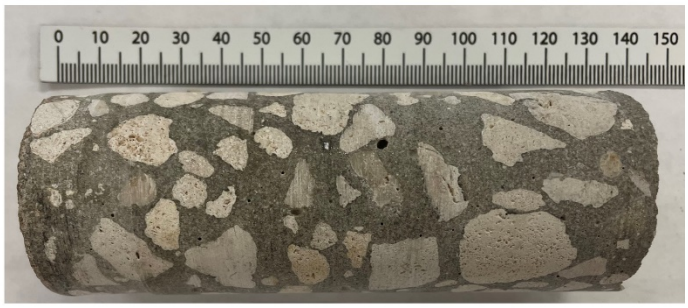

Figure 98. Cores obtained from Bent 223, Bridge #100585.

Appendix C: Weather Data Averaged per Month

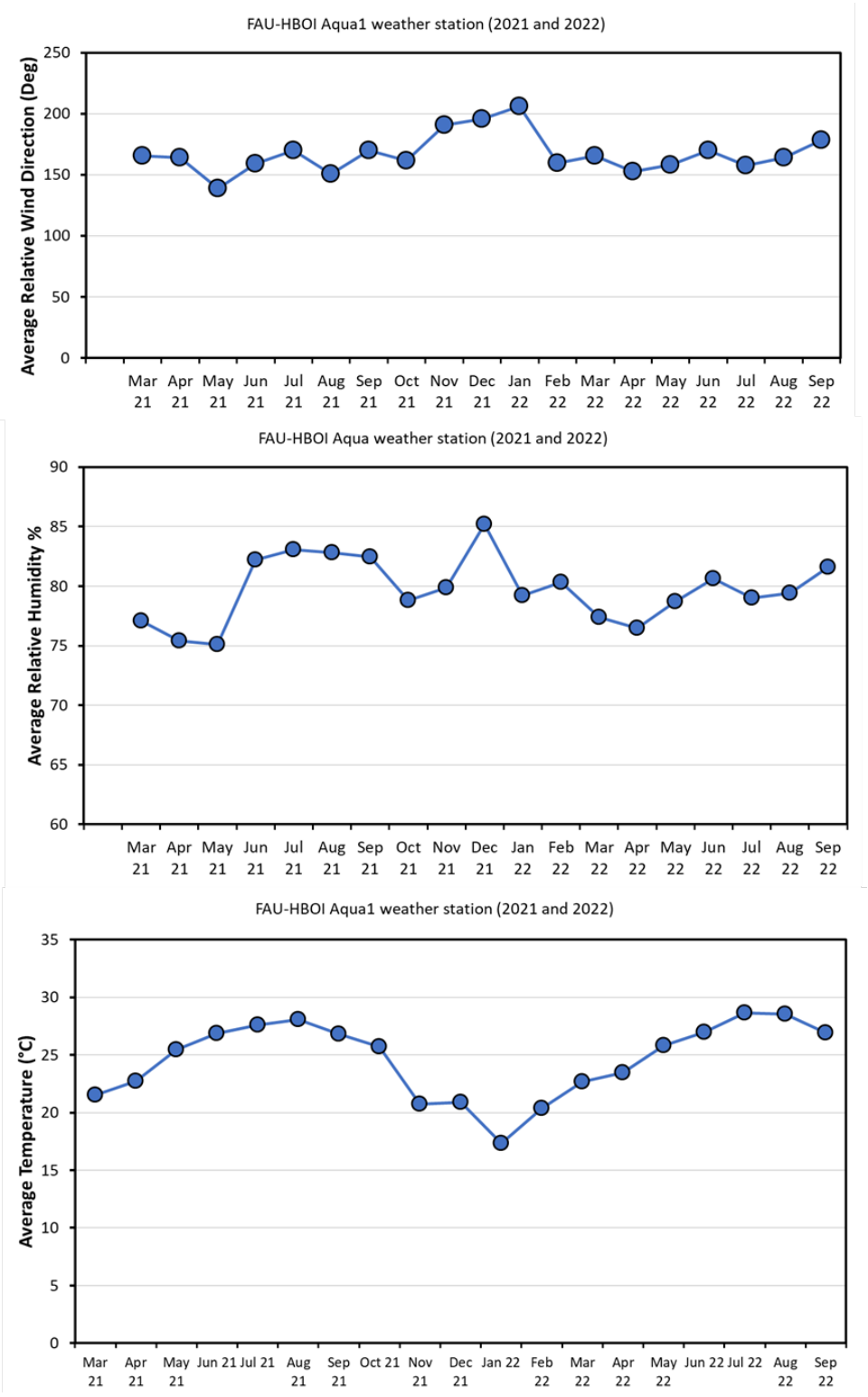

Figure 99. Wind direction, relative humidity and temperature at FAU-HBOI (south of bridge #880005).

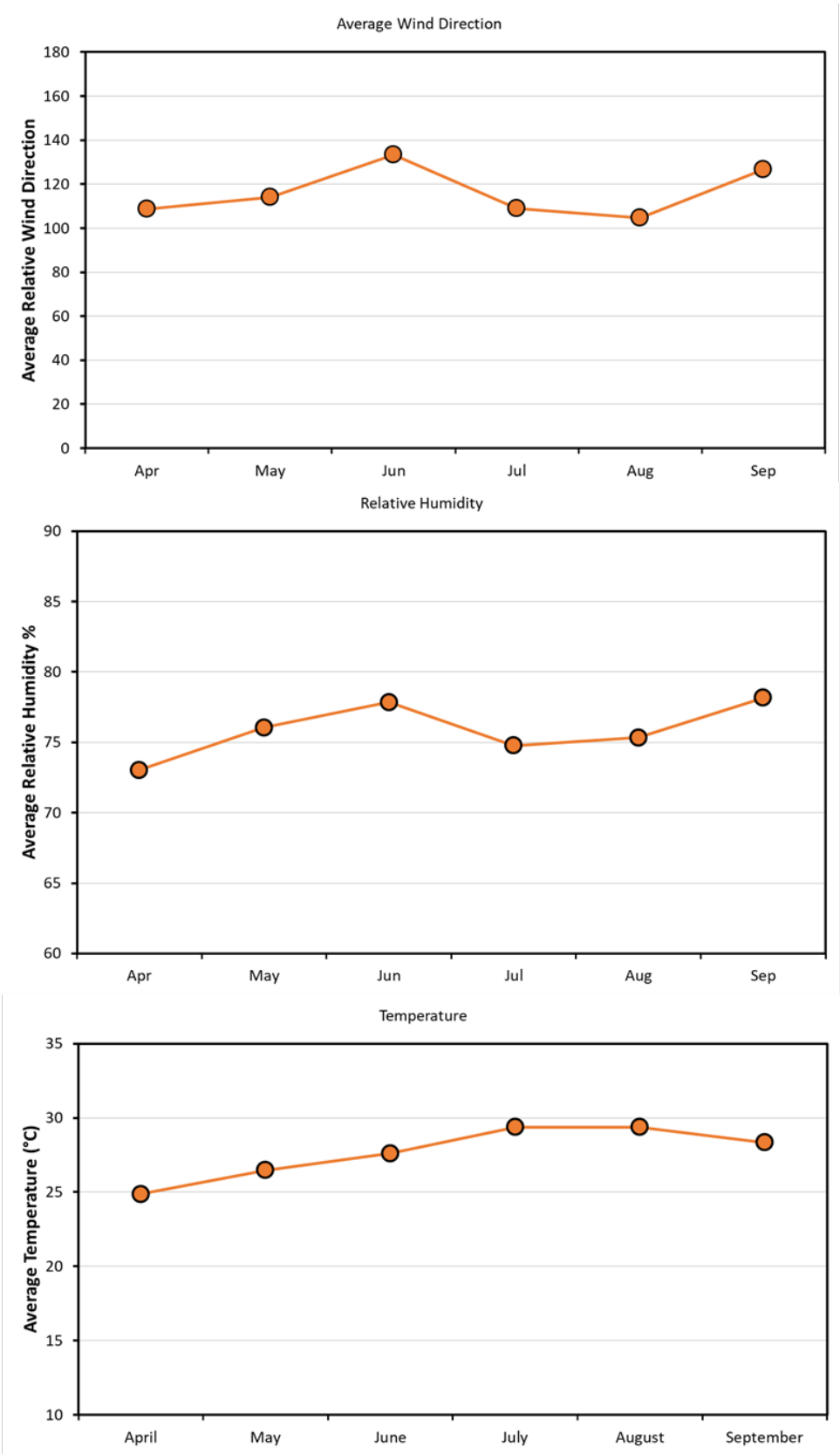

Figure 100. Wind direction, relative humidity and temperature at Dania Beach, FL (2022).